INTER- AND INTRA-KINGDOM SIGNALING IN BACTERIAL CHEMOTAXIS, BIOFILM FORMATION, AND VIRULENCE

A Dissertation

by

MANJUNATH NARAYAN HEGDE

Submitted to the Office of Graduate Studies of
Texas A&M University
in partial fulfillment of the requirements for the degree of

DOCTOR OF PHILOSOPHY

December 2011

Major Subject: Chemical Engineering

INTER- AND INTRA-KINGDOM SIGNALING IN BACTERIAL CHEMOTAXIS, BIOFILM FORMATION, AND VIRULENCE

A Dissertation

by

MANJUNATH NARAYAN HEGDE

Submitted to the Office of Graduate Studies of
Texas A&M University
in partial fulfillment of the requirements for the degree of

DOCTOR OF PHILOSOPHY

Approved by:

Co-Chairs of Committee,	Arul Jayaraman
	Thomas K. Wood
Committee Members,	Suresh Pillai
	Katy Kao
Head of Department,	Michael Pishko

December 2011

Major Subject: Chemical Engineering

ABSTRACT

Inter- and Intra-kingdom Signaling in Bacterial Chemotaxis, Biofilm Formation, and Virulence. (December 2011)

Manjunath Narayan Hegde, B. Eng., R. V. College of Engineering, Bangalore, India

Co-Chairs of Advisory Committee: Dr. Arul Jayaraman
Dr. Thomas K. Wood

Cell-cell communication between bacteria, belonging to the same species or to different species (Intra-kingdom signaling), or communication between bacteria and their animal host (Inter-kingdom signaling) is mediated through different chemical signals that are synthesized and secreted by bacteria or the host and is crucial for the survival of bacteria inside their host. The overall goal of this work was to understand the role of inter- and intra-kingdom signaling in phenotypes such as chemotaxis, colonization and biofilm formation, and virulence that are associated with infections caused by the human gastrointestinal (GI) tract pathogens. A part of our work also aimed at developing microfluidics-based models to study inter- and intra-kingdom signaling in biofilm formation, inhibition, and dispersal.

We showed that norepinephrine (NE), an important host signal produced during stress, increases human opportunistic pathogen *Pseudomonas aeruginosa* growth, motility, attachment, and virulence, and also showed that the actions of NE are mediated primarily through the LasR, and not the RhlR QS system. We investigated the molecular mechanism underlying the chemo-sensing of the intra-kingdom signal autoinducer-2 (AI-2) by pathogens *Escherichia coli* and *Salmonella typhimurium* by performing

different chemotaxis assays (capillary, microPlug and microFlow assays), and discovered that AI-2 is a potent attractant for *E. coli* and *S. typhimurium*, and that the Tsr chemoreceptor and periplasmic AI-2 binding protein LsrB are necessary for sensing AI-2, although uptake of AI-2 into the cytoplasm is not required. We concluded that LsrB, when bound to AI-2, interacts directly with the periplasmic domain of Tsr primarily at the Thr-61 and Asp-63 residues of LsrB, making LsrB the first known periplasmic-protein partner for Tsr.

We fabricated a simple user-friendly microfluidic flow cell (μBF) device that can precisely measure the effect of a wide range of concentrations of single or combinations of two or more soluble signals on bacterial biofilm formation and development. We also constructed a synthetic biofilm circuit that utilizes the Hha and BdcA dispersal proteins of *E. coli* along with a quorum sensing (QS) switch that works based on the accumulation of the signal *N*-(3-*oxo*-dodecanoyl)-*L*-homoserine lactone (3-*o*-C12HSL) and implemented it in an upgraded μBF device. We showed that a QS system may be utilized with biofilm dispersal proteins to control consortial biofilm formation by removing an existing biofilm and then removing the biofilm that displaced the first one. These types of synthetic QS circuits may be used to pattern biofilms by facilitating the re-use of platforms and to create sophisticated reactor systems that will be used to form bio-refineries.

DEDICATION

To my family and friends

who have stood by me through my ups and downs and supported me in all my decisions

ACKNOWLEDGEMENTS

Pursuit of a doctorate degree starts with a student's vision and a commitment to do good science. There is no recipe to do good science and the challenges you face during your pursuit are many. You learn to tackle those challenges as they come from experience, expert advice, inspiration, and guidance from others. Many people have brought me closer to a doctoral degree and made this Ph.D. thesis possible. It is my pleasure to thank them all.

I am eternally grateful to my research advisors, Dr. Arul Jayaraman and Dr. Thomas K. Wood, who have groomed me to become a first-rate independent researcher. Their perpetual energy and enthusiasm in research was infectious, and has always motivated to bring out the best in me. Both were always available to provide sound advice, several good ideas, and words of encouragement when I needed them the most. I also thank Dr. Suresh Pillai and Dr. Katy Kao for their time and efforts to read my dissertation and provide useful suggestions and comments.

I was delighted to interact with Dr. Mike Manson frequently in the last two years to discuss about our work related to AI-2 chemotaxis. His insights on bacterial chemotaxis are next to none. Besides, he sets an example of an excellent scientist because of his knowledge and passion for research. I owe a huge thanks to him. In addition, I would specially like to thank Dr. K. Gokulan for performing the crucial docking studies on AI-2 bound LsrB and chemoreceptor Tsr.

I am indebted to my lab buddies in the Jayaraman and the Wood group for providing a stimulating environment for intellectual development and research. I owe a huge debt

of gratitude to my colleague, Dr. Jeongyun Kim, for getting me excited about microfluidics and teaching me the basics of soft-lithography, and to Dr. Tarun Bansal for mentoring me during my early years working on my Ph.D. and ensuring that I followed good scientific practices. I also thank members of the Manson lab, Bill Cohn, Sneha Jani, Greg Whitaker, and Andrew Seely, for their help with the AI-2 chemotaxis project. I am particularly grateful to the Texas Engineering Experiment Station, National Institutes of Health, and the National Science Foundation for their support with this research.

Finally, I thank those that are dearest to me, who have loved me unconditionally, and stood by me during times of confusion and frustration. My elder sisters, Chetana and Mukta Hegde, have always believed in my abilities and are a constant source of encouragement. My brothers-in-law, Dr. Ramakrishna Hegde and Vikas B. N., have always been an inspiration. My good friends during my high school, undergraduate, and graduate studies have always helped me get through the difficult times and have provided the emotional support, entertainment, and care that I needed. Most importantly, I dedicate this doctorate degree to my parents, Narayan and Vasudha Hegde, who have made many sacrifices to give us the best education and who taught us the virtues of hard work. Particularly, my father being a science teacher himself, got me interested in science and problem solving early during my school days. My mother taught me the importance of patience and self-sacrifice in achieving success in whatever one does. Their unconditional love, unwavering trust, and constant support have materialized into who I am today.

TABLE OF CONTENTS

CHAPTER Page

CHAPTER Page

CHAPTER Page

LIST OF FIGURES

FIGURE Page

LIST OF TABLES

CHAPTER I

INTRODUCTION

1.1 Background

Bacteria are found ubiquitously in most ecological niches, either as free planktonic cells or matrix-encased, complex surface-associated communities known as biofilms (1). No better example exists in the nature than the astounding numbers of bacteria harbored by the "human superorganism"(2). The number of microbial cells in and on the human body is approximately 10-times greater than that of the human host (3). Particularly, the human distal gastrointestinal (GI) tract or gut, houses up to 1000 distinct bacterial species and an estimated excess of ~10^{14} resident microbes existing in homeostasis with the host's immune system (3). Therefore, the gut microbiome is one of the most complex microbial ecosystems, in which a diverse population of bacteria co-exists in with human cells (4).

The gut microbiome contains symbionts (or probiotics) that have known health-promoting functions, commensals, that are permanent residents that provide no benefit or cause no harm to the host (5), and pathobionts (or pathogens) that have the potential to induce pathological changes in the human host (6). Symbiotic gut bacteria supply essential nutrients, metabolize compounds in the food, defend against colonization by foodborne pathogens and by opportunistic-pathogens, and contribute to the development

---

This dissertation follows the style of *Proceedings of the National Academy of Sciences of the United States of America.*

of overall health of humans (5).

The symbiosis between bacteria and the host is disturbed when there is an unnatural shift in composition of bacteria, either by a reduction in the numbers of probiotics and/or increase in the numbers of pathogens (6). Most of the pathogens that enter the GI tract are food or waterborne. Once in the GI tract, they migrate to and colonize specific regions within the small and large intestines, leading to the onset of infections (7). For example, common foodborne pathogens such as enterohaemorrhagic *Escherichia coli* (EHEC) O157:H7, *Salmonella enterica*, and *Listeria monocytogenes* enter the gut through consumption of contaminated foods, such as raw or undercooked ground meat products and raw unpasteurized milk (8). Many incidences of pathogen outbreaks are also associated with the consumption of fruits and vegetables such as sprouts, lettuce, coleslaw, and salad which get contaminated due to contact with feces from domestic or wild animals (e.g., manure) at some stage during cultivation or handling (9). But it is not necessary that pathogens need to be food- or water-borne. In some cases, opportunistic pathogens are already resident inside the GI tract and cause infections when the right environmental conditions arise (i.e., such as when the host immune system is compromised). An example of a pathogen that opportunistically causes GI tract infections is *Pseudomonas aeruginosa* (10).

The lower and upper GI tract infections have been reported to occur through three key steps: a) recognition of the intestinal luminal environment and migration of a pathogen toward the epithelial cell lining in the gut that is covered by a layer of mucus, b) colonization and attachment of pathogens on the epithelium, and c) invasion of

pathogens or translocation of their toxins into epithelial cells (11). The seriousness of these foodborne illnesses is apparent in the health-related costs attributed with them. The United States alone spends an estimated $152 billion annually in dealing with the healthcare, workplace, and other economic costs associated with acute foodborne illnesses (12). Hence, it is important to identify environmental cues in the GI tract that help the incoming foodborne pathogen colonize specific regions in the gut and cause infections.

1.2 Motivation

Infections caused by foodborne pathogens affect millions of people and kill thousands in the United States alone. The Center for Disease Control (CDC) estimates for 2011 show that food-borne infections affect approximately 1 out of 6 Americans (or 48 million people) every year, with 128,000 hospitalizations and 3,000 deaths (13). Foodborne pathogens such as Salmonella spp., EHEC, enteropathogenic *E. coli* (EPEC), *Campylobacter spp.*, and *Staphylococcus aureus* are the most common causes of enteric infections. The symptoms of such enteric infections can range from diarrhea (sometimes bloody), cramping, abdominal pain, fever, and sometimes lead to infection in the systemic circulation and death. In United States, a significant health-related cost of ~152 billion/year, estimated after considering the sum of medical costs (hospital services, physician services, and drugs), quality-of-life losses (deaths, pain, suffering, and functional disability), and costs to others in society (e.g. costs to insurance companies that pay medical expenses) is associated with foodborne illness alone (12). Some enteric

infections, such as the ones caused by EHEC, cannot be treated by antibiotics because of the possibility of aggravating the infection due to enhanced release of the shiga toxins that are critical for the infection (14); this requires doctors to employ alternate treatment approaches such as fluid and electrolyte administration to limit the severity of symptoms (14, 15).

Other than infections caused by foodborne pathogens, severe illness also occur due to opportunistic GI pathogens that target individuals with compromised immune systems or chronic inflammation. *P. aeruginosa* is present at clinically-undetectable levels in the gut of healthy individuals (10). However, in critically-ill and immuno-compromised patients, *Pseudomonas* sp. levels have been shown to increase by as much as 100-fold (16) leading to the expression of virulence determinants (e.g., PA-I lectin/adhesin) (10) that cause infection. *P. aeruginosa* has been shown to translocate from the GI tract into the systemic circulation following shock or injury (17), and the resultant sepsis rapidly leads to mortality (18). In fact, the mere presence of *P. aeruginosa* in the gastrointestinal (GI) tract of critically-ill surgical patients has been associated with nearly 70% mortality (10).

1.3 Research importance, objectives, and novelty

Due to the close proximity of host cells and bacteria in the GI tract, a pathogen entering the GI tract is exposed to a wide range of molecules produced by both the host epithelium and commensal bacteria. It has been speculated that these molecules, in part, form an unique signature of the GI tract, which in turn, helps pathogens to identify the

microenvironment that is favorable for colonization and infection. These molecules include those used in bacterial quorum sensing or cell-cell communication and metabolites produced during normal bacterial growth. The quorum sensing signals include autoinducer-2 (AI-2) that is produced by ~55 different species of bacteria (19) including *E. coli*, *Helicobacter pylori*, *S. typhimurium*, *Streptococcus mutans*, *Vibrio cholera*, and *Vibrio harveyi*, as well as acyl homoserine lactones produced at high concentrations by numerous Gram-negative bacteria including *P. aeruginosa*, *Vibrio fischeri*, *Agrobacterium tumefaciens*, and *Rhodobacter sphaeroides* (20). Bacterial metabolites that also function as signals include indole that is produced by *E. coli*, as well as derivatives of indole such as hydroxyindoles that are produced by other GI tract bacteria from indole (21) and have been shown to affect phenotypes such as motility, adhesion to epithelial cells, and biofilm formation in *E. coli* (22-24). Eukaryotic signals produced *in situ* in the intestine of the host include hormones such as norepinephrine (NE), epinephrine, dopamine, and serotonin (25) and small molecules such as adenosine (26). Importantly, it has been shown that molecules produced by bacteria and host cells in the GI tract are recognized by host cells and bacteria, respectively (25). The abundance of these molecules and their cross-recognition by cells belonging to different kingdoms leads to a signal-centric paradigm wherein signaling molecules are thought to be a major contributor to the initiation and development of pathogen infections in the GI tract. However, the molecular basis of this interaction and its effect on the different steps involved in infections are poorly understood. Therefore, understanding the role of

signals in GI tract infections will lead to the development of approaches to control bacterial infections of the GI tract.

The overall goal of this work was to investigate the role of prokaryotic (AI-2, indole, 7-hydroxyindole, and isatin) and eukaryotic signals (NE) on specific phenotypes that promote infections - namely chemotaxis, colonization and invasion of epithelial cells, production of virulence factors, and biofilm formation. A major focus of this dissertation is on investigating the mechanism of chemotactic migration of *E. coli* and *S. typhimurium* toward AI-2. We also studied the effect of NE on phenotypes expressed by *P. aeruginosa* during gut-derived sepsis. Our work also involved developing microfluidics-based tools to study the effect of the bacterial signals indole and its derivatives on biofilm formation.

AI-2 has been reported to be a chemoattractant for *E. coli* (27) which has an AI-2 uptake system similar to that of *S. typhimurium.* However, the receptor(s) involved in AI-2 sensing have not been identified. This work is novel because this is the first study that identifies the receptor involved in the chemo-sensing of AI-2 in *E. coli* and *S. typhimurium*. Because AI-2 is produced by so many types of bacteria, this work provides a basis for understanding how planktonic (free-swimming) bacteria are possibly recruited to form mixed-species bacterial communities or biofilms. In this study, we used the non-pathogenic lab strain *E. coli* RP437 as a model strain for investigating the chemotaxis of EHEC towards GI tract molecules, since both non-pathogenic *E. coli* and EHEC possess the same five chemoreceptors Tar, Tsr, Tap, Trg, and Aer with a high degree of gene and protein sequence homology (28). Conventional methods of

studying chemotaxis such as swarm plates and capillary assays, although widely used, have numerous drawbacks that limit their use in chemotaxis investigations (29). These include difficulties in quantitation (swarm plates), variability in the cell accumulation numbers between two similar runs (capillary assays), unsuitability for studying repellent taxis (capillary assays), temporally changing concentration gradients (capillary assays), and requirements for metabolizable chemoeffectors (swarm plates). These problems are elegantly addressed by microfluidic chemotaxis models. For example, the flow-based microfluidic chemotaxis model developed in this study allows generation of temporally and spatially stable concentration gradients of chemoeffectors of any gradient strength, is equally applicable for attractants and repellents, provides quantitative data, and is more sensitive than capillary assays or swarm plates.

Although there have been several cases of *P. aeruginosa* derived sepsis reported when patients are immune-compromised or undergoing conditions of chronic stress (10), there is no direct evidence of how stress conditions promotes *P. aeruginosa* virulence and infectivity. This is the first investigation on the effect of stress hormones such as NE on *P. aeruginosa* virulence phenotypes and gene expression.

Indole has been shown to decrease biofilm formation in *E. coli* (21), but indole derivatives such as 7-hydroxyindole and isatin have differential effect on *E. coli* biofilm formation, in that the former decreases and the latter increases biofilm formation (23) . These biofilm studies were performed with only a single concentration of indole or its derivatives using traditional macroflow cells. However, it is important to know the effect of wide range of concentrations of these signals on biofilm formation or inhibition,

which would be tedious and time consuming using macroflow cells. Moreover, flow cells have the disadvantages of requiring large volumes and are not suited for high-throughput investigation, and do not facilitate spatial and temporal control of bacterial introduction and adhesion. These problems can be addressed in a microfluidic flow cell system. Micro flow cells developed previously (30-33) have several drawbacks such as disruption of fluid dynamics by biofouling of tubes used to seed bacterial cells and nutrient medium into the biofilm chamber, inability to carry out high-throughput investigations, and lack of customizable features. We developed a customizable microflow cell with eight separate microchambers for cultivating biofilms exposed to eight different concentrations of signals through a single gradient mixer. We also added a second layer of a gradient-mixer to this design to study the synthetic biofilm circuit in which we engineered cells that are able to displace an existing biofilm and then be removed on command allowing one to control consortial biofilm formation for various applications.

The specific objectives were to:

- Identify the chemoreceptor(s) in *E. coli* and *S. typhimurium* involved in AI-2 sensing and study how AI-2 interacts with the chemoreceptors to generate a chemoattractant response.
- Study the changes in gene expression and virulence phenotypes of *P. aeruginosa* on exposure to NE.
- Develop a microfluidic flow cell model for studying the interactions between two derivatives of the bacterial signal indole on biofilm formation by pathogenic *E. coli.*

- Develop a microfluidic biofilm circuit that combines the LasI/LasR QS module of *P. aeruginosa* with engineered Hha and BdcA biofilm dispersal proteins of *E. coli* to selectively remove one type of cell from an existing biofilm, and then remove the second biofilm for various engineering applications.

CHAPTER II

LITERATURE REVIEW

2.1 The human gut microbiota

The largest epithelial surface of the human body is the gastrointestinal (GI) tract, commonly known as the gut (3, 34). The upper gut consists of the esophagus, stomach, and duodenum, and the lower gut consists of the small and large intestine. Together, the organs that form the gut play dual roles in human physiology: digestion and uptake of nutrients and the more challenging task of maintaining immune homeostasis (i.e., protecting the body from potentially harmful microbes, while inducing tolerance to certain undesirable components in food, commensal micro flora, and self-antigens) (3). The gut could be considered the largest surface area of the body that is exposed to and interacts with both exogenous pathogens and intrinsic commensal microbes. The composition of the microflora in the gut is governed by age, diet, environment and phylogeny (i.e. co-evolution of the gut microbes with their host) and the ecosystem contains all three domains of life: bacteria, archaea and eukarya (fungi, yeasts and protozoa), with the largest community residing in the colon, which is a part of the large intestine (34). Although the gut is sterile during birth, microorganisms soon colonize the gut and other mucosal surfaces after birth. This colonization evolves into a highly diverse endogenous microbial population comprising over 10^{14} resident microbes, creating a symbiotic relationship that confers benefits to both microorganisms and host (3). Indeed, the human colon harbors a highly complex microbial ecosystem of about

200 grams of living cells, at concentrations of 10^{12} microbes per gram gut content, the highest recorded for any microbial habitat (35). It has been estimated that at least 1,000 different bacteria species cohabit the human gut, although some studies suggest this number may be as large as 35,000 (35).

The interactions of microbes with the host have evolved into a complex balance of host genes, gut environment, and microbes defined as the microbiome (4, 36). These microbes modulate the normal function and development of the GI tract and the overall health of humans (37). However, the gut environment can be shared by multiple pathogens that utilize the mucosa as invasion and infection sites and spread disease. It is the role of the immune system to concurrently control the responses to commensal and pathogenic organisms (37).

The importance of the microbiome and human disease is evident from the recent National Institutes of Health (NIH) initiative on the "Human Microbiome Project." This $140 million project is to focus and compare the human microbiome between individuals, and to assess how changes in the microbiome correlate with human disease, using metagenomic and genomic DNA sequencing techniques (38). A part of these studies will aim at understanding the biological and/or chemical factors produced by the gut microbiome that influence the pathogenicity of common bacterial and fungal pathogens, but the sheer complexity of the gut in terms of the abundance of eukaryotic and prokaryotic cell signals that can influence the disease-causing ability of a pathogen will make such studies particularly challenging.

2.1.1. Gut infection model

Food and water are the most common carriers of pathogens into the GI tract (7). Each kind of pathogen favors specific sites in the gut for colonization and infection (e.g., *S. typhimurium* infects the small intestine, whereas EHEC infects only the colon in the large intestine, and *P. aeruginosa* infects both the small and large intestine) (39). Infection in the gut is hypothesized to occur through three distinct steps (11) as shown in **Fig. 2.1**. **First**, the pathogen recognizes the gut environment by chemo-sensing specific favorable commensal or host-derived chemical signals and moves toward its target site. The process of sensing a chemical signal and movement toward a favorable or away from a hostile environment known as chemotaxis helps the pathogen "identify" the appropriate site for infection (40). **Second**, using different adherence factors, pathogens colonize specific sites in the gut. They can attach directly to the mucosal layer covering the epithelium or to the commensal microbes that have already colonized the site (11). Some pathogenic (e.g., Uropathogenic *E. coli* or UPEC) proliferate on the epithelial surface and form biofilms before initiating infection (41) **Third**, initiation of infection by either translocation of the pathogen into the epithelial cells (invasive type of infection), or transport of toxins from the cytoplasm of the pathogen into the host epithelial cell followed by cell death (11).

2.2 *Escherichia coli* infections

E. coli is a Gram-negative bacterium and a predominant species among facultative anaerobic bacteria of the gastrointestinal tract (11). Non-pathogenic *E. coli* and its

human host have coexisted in good health and with mutual benefit for thousands of years (34). These commensal *E. coli* strains rarely cause disease except when the host is immuno-compromised or when the normal gastrointestinal epithelial cell barrier is disrupted (42). The niche of commensal *E. coli* is the mucous layer of the mammalian colon (42). However, there are several highly adapted *E. coli* strains that have acquired specific virulence attributes, which confers an increased ability to adapt to new niches in the gut that allows them to cause a broad spectrum of disease (11). Three general clinical syndromes can result from pathogenic *E. coli* infections: enteric/diarrheal disease, urinary tract infections (UTIs) and sepsis/meningitis (11). The pathogenic *E. coli* that cause enteric disease can be classified into six categories: enteropathogenic *E. coli* (EPEC), enterohaemorrhagic *E. coli* (EHEC), enterotoxigenic *E. coli* (ETEC), enteroaggregative *E. coli* (EAEC), enteroinvasive *E. coli* (EIEC) and diffusely adherent *E. coli* (DAEC) (43). *E. coli* virulence factors can be encoded by several mobile genetic elements, including transposons (e.g., heat stable enterotoxin (ST) of ETEC), plasmids (for e.g. heat-labile enterotoxin (LT) of ETEC and invasion factors of EIEC), bacteriophage (e.g., Shiga toxin of EHEC) and pathogenicity islands (PAIs) (e.g. the locus of enterocyte effacement (LEE) of EPEC/EHEC) (11).

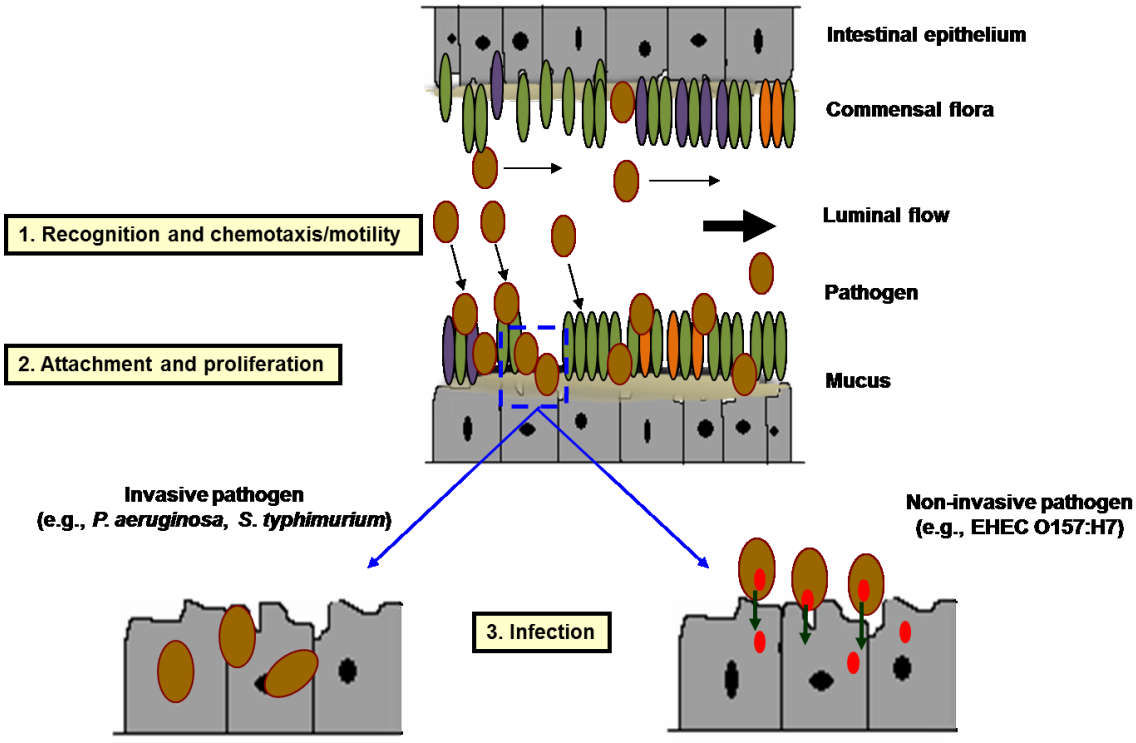

Fig. 2.1. Pathogen infection model. (1) Recognition and migration of pathogens to the epithelial cell surface (chemotaxis). (2) Proliferation, attachment, and colonization of pathogens on the commensal microbial or mucosal layer covering the epithelium. (3) Initiation of infection by translocation of the pathogen (invasive) or its toxins (non-invasive) into the epithelium.

2.2.1 *Escherichia coli* chemotaxis

Chemotaxis, or the movement toward or away from chemicals, is a universal attribute of motile cells and organisms (44). *E. coli* cells swim toward amino acids (serine and aspartic acid), sugars (maltose, ribose, galactose, glucose), dipeptides, pyrimidines and electron acceptors (oxygen, nitrate, fumarate) (45-47). Cells also swim away from potentially harmful chemicals, such as alcohols and fatty acids, but repellent responses have not been as extensively studied (48). In the absence of any stimulating

chemical gradient, *E. coli* swims in a random walk pattern produced by alternating episodes of counter-clockwise (CCW) and clockwise (CW) flagellar rotation (49). In an attractant or repellent gradient, the cells monitor chemoeffector concentration changes as they move and use that information to control the probability of the next tumbling event (50). These flagellar responses extend runs that take the cells in favorable directions (toward attractants and away from repellents), resulting in net movement toward preferred environments. *E. coli* senses chemoeffector gradients in a temporal fashion by comparing the current concentrations to those encountered over the past few seconds of travel. Out of the five chemoreceptors in *E. coli*, four (Tsr, Tar, Tap, and Trg) are transmembrane receptors. These methyl-accepting chemotaxis proteins (MCPs) or have periplasmic ligand binding sites and conserved cytoplasmic signaling domains (50) (**Fig. 2.2**) and record the cell's recent chemical past (ligand concentration) in the form of reversible methylation of specific glutamic acid residues in the cytoplasmic signaling domain of the chemoreceptors (50). Whenever the ligand bound to the periplasmic domain of the MCP's dissociates from the receptor, the flagellar motor response stops until a new ligand binds to the MCP (50). A fifth MCP-like protein, Aer, mediates aerotactic responses by monitoring redox changes in the electron transport chain (50). Aer undergoes sensory adaptation through a poorly understood, methylation-independent mechanism. The five MCP-family receptors in *E. coli* utilize a common set of cytoplasmic signaling proteins to control flagellar rotation and sensory adaptation (**Fig. 2.2**) (50). Receptor CheW and sensor kinase CheA generate receptor signals in the form

of phosphoryl groups to CheY and CheZ which control motor responses in response to chemical stimuli; CheR and CheB regulate MCP methylation state (50).

2.2.2 Methods for studying bacterial chemotaxis

There are several established qualitative and quantitative techniques for assaying bacterial chemotaxis as reviewed by Englert et al. (29). The most commonly used techniques are highlighted below.

2.2.2.1 Swim and swarm plate assays

Chemotaxis of bacteria toward a chemoeffector that can be metabolized can be measured using agar plate assays (29). For swim plate assays, motility medium containing low agar concentrations (0.25 to 0.4%) are used (29). The bacteria move in the aqueous channels inside the agar, and these channels are large enough for them swim through. As the colony grows, it metabolizes any attractants it can which causes the formation of a spatial concentration gradient in the agar. As a result, the cells migrate outward towards higher concentrations (29). By measuring the size of the sharp ring formed by cells at the edge of the steepest gradient, the strength of attraction can be measured (29). You list disadvantages for swarm plates below so only logical that you do the same for swim plates here

A variation on the swim plate method is the swarm assay. Motility medium containing higher concentrations of agar (0.5% to 0.7%) are used, and the cells swim through the aqueous layer that forms on the agar surface (51). Swarming cells typically

produce more, longer flagella (51)Both swimming and swarming assays cannot be used for measuring repellent taxis, and chemotaxis toward chemoeffectors that cannot be metabolized by the cells (29).

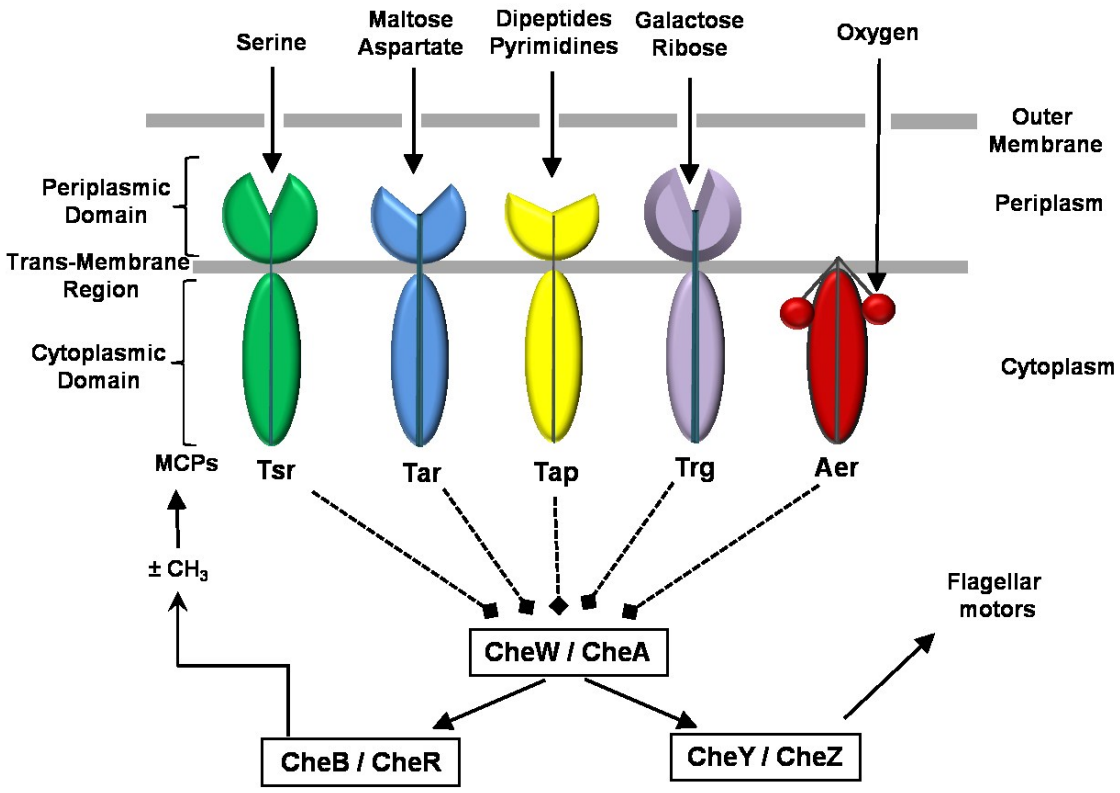

Fig. 2.2. *E. coli* chemotaxis signaling circuit. Five *E. coli* chemoreceptors Tsr, Tar, Tap, Trg, and Aer are shown along with their chemoeffector ligands serine, maltose/ aspartate, dipeptides/pyrimidines, galactose/ribose, and oxygen respectively. All five receptors employ a common set of cytoplasmic signaling proteins, CheW and CheA, which interact with cytoplasmic domain of chemoreceptor to form stable ternary complexes that generate stimulus signals in the form of phosphoryl groups. CheY and phospho-CheY signal the CCW and CW flagellar rotation, CheZ controls the phosphorylation or dephosphorylation of cheY, CheR (methyltransferase) and CheB (methylesterase) regulate the MCP methylation state.

2.2.2.2 Capillary assays

This assay was developed by Adler et al. (45) and is widely used for investigating chemotaxis. Chambers on the order of 1 cm^2 made from plastic o-rings with a 60^o cut and 1 mm in height are loaded with a suspension of highly motile bacteria in chemotaxis buffer to create a pond (**Fig. 2.3**). A 1 mm capillary is sealed at one end and filled with several mm of an attractant at the desired concentration at the other. The capillary is then inserted into the pond and incubated at the desired temperature for 30 to 45 minutes. The chemoeffector in the capillary will diffuse out into the well creating a gradient that the can be sensed by the bacteria around the opening of the capillary. The bacteria will then migrate into the capillary if the chemoeffector is an attractant. The capillary is then removed, and the contents placed into dilution buffer. Dilutions are plated on nutrient agar and colonies are counted the next day. The colony counts allow the number of cells entering the capillary to be calculated. These numbers can then be used to compare the chemotactic response and strength of response to various compounds. Although the capillary assay can be used for measuring repellant taxis, the results are not nearly as sensitive as those for attractants. Therefore, it is not ideal for use with repellents.

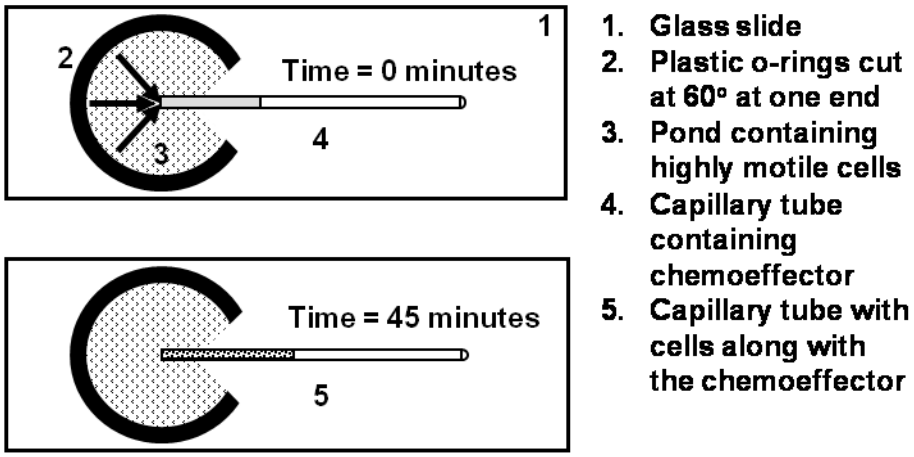

Fig. 2.3. Experimental setup for the capillary assay.

2.2.2.3 Microfluidic assays

Capillary assays are not ideal for quantifying subtle differences in migration rates or for investigating responses to complex gradients consisting of multiple chemoeffectors (29). These issues can be addressed by using microfluidics-based chemotaxis models (29). Microfluidic methods have tremendous potential for chemotaxis studies because they can be used to measure chemotaxis quantitatively (29, 52, 53). In addition, they work equally well for attractants and repellents, and they can generate highly stable gradients over any user-defined concentration range (29). Microfluidics assays are becoming increasingly popular in biological studies because of features such as small volume and large surface-to-volume ratio, laminar flow, high throughput, and compact system size for fast and accurate analysis of samples (54). Mao *et al.* (55) were the first to investigate bacterial taxis in a microfluidic flow cell, in which a concentration gradient was formed by diffusion of two parallel streams. Englert *et al.* (29, 52, 53, 56)

have developed a qualitative (microPlug assay) and a flow-based quantitative (microFlow assay) for studying chemotaxis.

2.2.3 *Escherichia coli* biofilms

Biofilms are highly-structured, matrix-enclosed bacterial communities (57). Bacterial biofilms are commonly are commonly found in the site of infection and are a common cause of persistent infections (57). Some of the common infections such as those related to dental caries, periodontitis, cystic fibrosis pneumonia, urinary catheter cystitis, contact lens, sutures, central venous catheters, and orthopedic devices are caused by single or multispecies biofilms (57). Biofilms can be up to 1,000 times more resistant to antibiotics than the planktonic cells (58). Bacteria in biofilms infect 4.3% of orthopedic and 7.4% of cardiovascular implants, and the treatment costs amount to more than $3 billion in the USA alone (58). The biofilm matrix is comprised of bacterial cells, secreted cell products, proteins, polysaccharides, DNA, and water (59, 60). Biofilm matrix formation depends on both genetic and environmental factors (59).

E. coli is a predominant species among facultative anaerobic bacteria of the gastrointestinal tract, where it thrives in an environment as multispecies biofilm (1, 61). *E. coli* biofilm formation can be affected by different molecules in different ways. AHL signals reduce biofilm formation (21), whereas AI-2 increases biofilm formation in *E. coli* (62). The internal messenger cyclic diguanylic acid (c-di-GMP) increases biofilm formation in *E. coli* (63). The eucaryotic signal furanones produced by alga *Delisea pulchra* (64, 65) decreases biofilm formation in *E. coli* by inhibiting AI-2 signaling (66).

Human stress hormones epinephrine and norepinephrine increase biofilm formation in *E. coli* O157:H7 (22) whereas bacterial signals such as indole, 7-hydroxyindole, and 5-hydroxyindole decrease biofilm formation in both pathogenic and non-pathogenic *E. coli* (21, 22, 67). Isatin increases biofilm formation in pathogenic *E. coli* and does not affect the biofilm formation in non-pathogenic *E. coli* K-12 strain (23).

2.3. *Pseudomonas aeruginosa*

P. aeruginosa is a Gram-negative bacterium frequently found in soil, aqueous habitats, plants, animals, and humans (68-70). *P. aeruginosa* contains two pathogenicity islands (PAPI-1 and PAPI-2) which harbor a shared subset of virulence genes to elicit infection in both plants and animal hosts (71, 72). *P. aeruginosa* is an opportunistic pathogen for humans and is present at clinically-undetectable levels in the normal gut (10). However, in critically-ill and immune-compromised patients, *Pseudomonas* sp. levels have been shown to increase by as much as several hundred fold (16) leading to the expression of virulence determinants (e.g., PA-I lectin/adhesin) (10) that lead to infection. *P. aeruginosa* translocates from the GI tract into the systemic circulation following shock or injury (17), and the resultant sepsis rapidly leads to mortality (18). In fact, the mere presence of *P. aeruginosa* in the gastrointestinal (GI) tract of critically-ill surgical patients has been associated with nearly 70% mortality (10). *P. aeruginosa* produces many secreted virulence determinants through the interrelated Las and Rhl quorum-sensing (QS) systems (73). In addition, the secreted *Pseudomonas* quinolone signal (PQS, 2-heptyl-3-hydroxy-4-quinolone) is also involved in the expression of

several virulence determinants (74). The regulation of PQS is not independent, but integrated with the *las* and *rhl* QS (75), as the regulator for PQS production (*pqsR,* also known as *mvfR*) is positively regulated by *lasR* and negatively regulated by *rhlR* (75).

2.3.1 Virulence factors of *Pseudomonas aeruginosa*

P. aeruginosa is notorious for its multiple virulence factors such as adhesions for biofilm formation, cyanides, elastases, hemagglutinin, motility, phenazines, pyocyanin, rhamnolipids, type III secretion, and siderophores (70, 76-80). Many of these virulence factors are regulated through QS pathways (81). These virulence factors have different effects on the physiology of the host cells; for instance, pyocyanin inhibits respiration (82), elastase disrupts blood vessels and degrades the extracellular matrices of epithelial cells (83), and rhamnolipids disrupts the cells and promote the invasion of *P. aeruginosa* (84). The tissue damages caused by the toxins of *P. aeruginosa* deteriorate the human immune system (85).

2.4 Bacterial and host signaling molecules

2.4.1 Autoinducer-2 (AI-2)

AI-2 is produced by a wide range of Gram-negative and Gram-positive bacterium such as *E. coli*, *S. typhimurium*, *V. harveyi*, *V. cholerae*, *P. gingivalis*, *Actinobacillus actinomycetemcomitans*, and *Streptococcus mutans* (19). Inside cells, AI-2 exists in multiple forms that are in equilibrium with each other (86) and is derived from the

spontaneous cyclization of the metabolite 4,5-dihydroxy-2,3-pentanedione (DPD). DPD is made from *S*-ribosylhomocysteine by LuxS (87). The form that is active in *V. harveyi* is (2*S*,4*S*)-2-methyl-2,3,3,4-tetrahydroxytetrahydrofuran borate (S-THMF borate) (88). This form of AI-2 binds to the periplasmic protein LuxP. In *E. coli* and *S. typhimurium*, a boron-free isomer of AI-2 [(2*R*,4*S*)-2-methyl-2,3,3,4-tetrahydroxytetra-hydrofuran (R-THMF)] binds to the periplasmic LsrB protein (89). LsrB is the recognition component of an ABC transporter for AI-2, and *lsrB* is in the *lsrACDBFGE* operon. LsrACD are the membrane-bound components of the ABC transporter for AI-2. Following uptake, AI-2 is phosphorylated in the cytoplasm by the LsrK kinase and then further broken down by the products of the *lsrFG* genes (90). this operon is under the control of LsrR, a repressor that is inactivated upon binding of phosphorylated AI-2. In *E. coli,* the membrane-bound YdgG (TqsA) protein has been implicated in AI-2 export from the cytoplasm (91). AI-2 is a potent chemoattractant for *E. coli* (27, 92). AI-2 also increases biofilm formation in *E. coli* (62).

2.4.2 Indole

A variety of bacteria such as *E. coli* (93), *Vibrio vulnificus* (94), *Haemophilus influenzae* (95), *Pasteurella multocida* (96), *Klebsiella oxytoca* (97), *Proteus vulgaris* (98), and *Bacteroides thetaiotaomicron* (99) produce indole from *L*-tryptophan. Nearly 80 other species have been shown to possess the tryptophan indole-lyase or tryptophanase (encoded by *tnaA*) that mediates the breakdown of tryptophan to indole, pyruvate, and ammonia. Indole is an extracellular signaling molecule produced during

the late exponential and stationary phase (100) that represses biofilm formation, motility, acid resistance (21, 22, 101, 102), and attachment of EHEC to epithelial cells (22). Indole works through QS (67) primarily at temperatures less than 37°C in *E. coli* (102). Indole increases the expression of multidrug exporter genes in *E. coli* (103) and in *S. enterica* (104). However, indole induces biofilm formation of *P. fluorescens* and *P. aeruginosa* (21).

2.4.3. Norepinephrine (NE)

NE is a catecholamine neurotransmitter (stress hormone) that is normally produced in the GI tract through the enteric nervous system (105, 106) and is important in GI-tract infections. The concentration of NE increases during early sepsis (107), and NE has been shown to stimulate the growth of several Gram-negative and -positive bacteria that are present in the intestinal lumen (108), including *P. aeruginosa* (109). Alverdy and co-workers (10) have correlated the increased NE in the luminal contents of mice after a 30% hepatectomy to increased expression of the *P. aeruginosa* virulence determinant PA-I lectin and gut-derived sepsis. The NE released in the GI tract during stress has also been reported to influence the virulence and infection of other GI tract pathogens. Bansal *et al.* (22) and others (110, 111) have shown that NE increases EHEC O157:H7 attachment and colonization to epithelial cells and colonic mucosa, respectively. NE also enhances the growth, motility, and invasiveness of *Campylobacter jejunii* (112), the expression of the K99 pilus adhesin virulence-related factor in ETEC (113), EHEC

O157:H7 virulence gene expression (22, 114), and EHEC O157:H7 chemotaxis, motility, and biofilm formation (22).

2.5. Microfluidics and its application in microbiology

Microfluidics deals with the precise control and manipulation of fluids contained in small (~10–100 μm) channels in which fluid flow is dominated by surface tension and laminar effects (54). Microfluidic based devices require smaller reagent volumes, shorter reaction times, and offer the promise of high-throughput operations (54). The current techniques used for fabricating microfluidic devices include methods such as micromachining, photolithography, soft lithography, embossing, *in situ* construction, injection molding, and laser ablation (115). Each of these techniques has advantages and disadvantages, and the most suitable method of device fabrication often depends on the specific application of the device (115). Soft lithography, which refers to the molding of a two-part polymer (elastomer and curing agent), called polydimethylsiloxane (PDMS), using photoresist masters, is faster, less expensive and a more suitable fabrication technique than glass or silicon micromachining which is used for most biological applications (116). It has features that are unique and complement conventional techniques of microfabrication: (a) It can be performed conveniently, rapidly, and inexpensively, (b) it is inert to wide range of chemicals that is found in biological systems, (c) it provides the ability to control the properties of surfaces at the molecular level, and (d) PDMS is permeable to oxygen and other gases (116).

Recently soft lithography based microfluidics devices have been used for many applications in microbiology (117). These studies can be categorized into biofilm research, pathogen detection, and nucleic acid analysis. Microfluidic based flow cell devices can be used to precisely control a biofilm environment unlike macro flow cells and has been used in several different prototypes cells (30-33). For example, Lee *et al*. (32) have used micro flow cells to study *S. epidermidis* biofilms, Cho *et al.* (33) to study the self-organization of *E. coli* colonies into biofilms, and Kim *et al.* (30) to study the effect of a gradient of antibiotics on *P. aeruginosa* biofilms. Microfluidic biochips have recently been used to monitor the response of biofilms to increased shear stress and *Candida albicans* concentrations (118). Applications related to pathogens include identification of respiratory pathogen *Bordetella pertussis* (119), a microfluidic system for saliva-based detection of infectious diseases (120), pathogenic bacteria detection in food (121), and rapid diagnosis of dengue virus infection (122). Work is also progressing on the detection of nucleic acids (DNA and RNA) using microfluidics and includes digital PCR multigene analysis of individual environmental bacteria (123) and PCR microfluidic devices for DNA amplification (124).

CHAPTER III

THE NEUROENDOCRINE HORMONE NOREPINEPHRINE INCREASES *PSEUDOMONAS AERUGINOSA* PA14 VIRULENCE THROUGH THE LAS QUORUM SENSING PATHWAY

3.1 Overview

It has been proposed that the GI tract environment containing high levels of neuroendocrine hormones is important for gut-derived *P. aeruginosa* infections. In this study, we report that the hormone norepinephrine increases *P. aeruginosa* PA14 growth, virulence factor production, invasion of HCT-8 epithelial cells, and swimming motility in a concentration-dependent manner. Transcriptome analysis of *P. aeruginosa* exposed to 500 μM, but not 50 μM, norepinephrine for 7 h showed that genes involved in the regulation of the virulence determinants pyocyanin, elastase, and the *Pseudomonas* quinolone signal (PQS, 2-heptyl-3-hydroxy-4-quinolone) were up-regulated. The production of rhamnolipids, which are also important in *P. aeruginosa* infections, was not significantly altered in suspension cultures upon exposure to 500 μM norepinephrine, but decreased on semi-solid surfaces. Swarming motility, a phenotype that is directly influenced by rhamnolipids, was also decreased upon 500 μM norepinephrine exposure. The increase in the transcriptional activation of *lasR*, but not that of *rhlR*, and the increase in the levels of PQS suggest that the effects of norepinephrine are mediated

---

primarily through the *las* quorum sensing pathway. Together, our data strongly suggests that norepinephrine can play an important role in gut-derived infections by increasing the pathogenicity of *P. aeruginosa* PA14.

3.2 Introduction

Pseudomonas aeruginosa is one of the most common opportunistic pathogens that are present at clinically-undetectable levels in the normal GI tract (10). However, in critically-ill and immuno-compromised patients, *Pseudomonas* sp. levels have been shown to increase by as much as 100-fold (16) leading to the expression of virulence determinants (e.g., PA-I lectin/adhesin) (10). *P. aeruginosa* has been shown to translocate from the GI tract into the systemic circulation following shock or injury (17), and the resultant sepsis rapidly leads to mortality (18). In fact, the mere presence of *P. aeruginosa* in the gastrointestinal (GI) tract of critically-ill surgical patients has been associated with nearly 70% mortality (10). Although the exact mechanisms underlying the increase in *P. aeruginosa* levels and their translocation during stress are largely unknown, it is becoming evident that the interaction of neuroendocrine hormones with bacteria, termed as "microbial endocrinology" (106), is important in the expression of virulence determinants during infection (10).

Norepinephrine (NE), a catecholamine neurotransmitter (stress hormone) that is normally produced in the GI tract through the enteric nervous system (105, 106), is one such molecule that is important in GI tract infections. The concentration of NE increases during early sepsis (107), and NE has been shown to stimulate the growth of several

Gram-negative and -positive bacteria that are present in the intestinal lumen (108), including *P. aeruginosa* (109). Alverdy and co-workers (10) have correlated the increased NE in the luminal contents of mice after a 30% hepatectomy to increased expression of the *P. aeruginosa* virulence determinant PA-I lectin and gut-derived sepsis. The NE released in the GI tract during stress has also been reported to influence the virulence and infection of other GI tract pathogens. We (22) and others (110, 111) have shown that NE increases *Escherichia coli* O157:H7 attachment and colonization to epithelial cells and colonic mucosa, respectively. NE has also been demonstrated to enhance growth, motility, and invasiveness of *Campylobacter jejunii* (112), the expression of the K99 pilus adhesin virulence-related factor in enterotoxigenic *E. coli* (113), *E. coli* O157:H7 virulence gene expression (22, 114), and *E. coli* O157:H7 chemotaxis, motility, and biofilm formation (22). Together, these studies indicate that NE plays an important role in the pathogenicity of different bacteria. Although these studies have shown that NE increases virulence and pathogenicity, the mechanisms through which NE impacts virulence of different bacteria are not fully understood.

P. aeruginosa controls the production of many secreted virulence determinants, including elastase, rhamnolipids, pyocyanin, exotoxin A, and catalase (73), through the interrelated *las* and *rhl* quorum sensing (QS) systems (73). In addition, the secreted *Pseudomonas* quinolone signal (PQS, 2-heptyl-3-hydroxy-4-quinolone) is also involved in the expression of the virulence determinants rhamnolipids, pyocyanin, and elastase (74). The regulation of PQS is not independent, but integrated with the *las* and *rhl* QS (75), as the regulator for PQS production (*pqsR,* also known as *mvfR*) is positively

regulated by *lasR* and negatively regulated by *rhlR* (75).

The goal of this work was to investigate the effect of 50 μM and 500 μM NE on *P. aeruginosa* virulence and gene expression. The lower concentration (50 μM) was used as representative of NE levels present in the GI tract during homeostasis, and has been used in recent studies (125) to investigate the effect of hormones on GI tract pathogens. The higher concentration (500 μM) was used as representative of supra-physiological levels of NE likely to be encountered in the GI tract during catabolic stress (105, 126). We investigated the effect of NE on the *P. aeruginosa* transcriptome, as well as on the production of different virulence factors, motility, epithelial cell attachment and invasiveness, barley seed infection, and activation of different QS systems. To our knowledge, this is the first report investigating the molecular basis of alterations in *P. aeruginosa* physiology by NE.

3.3 Results

3.3.1 Effect of NE on *P. aeruginosa* PA14 growth

The effect of NE on PA14 growth was initially determined in order to design subsequent experiments for investigating the effect of NE on the expression of genes involved in PA14 virulence determinants. Cultures of PA14 were treated with 50 μM and 500 μM NE in serum-RPMI medium, and the turbidity at 600 nm monitored. The addition of 50 μM and 500 μM NE increased the specific growth rate of PA14 by ~ 9% and 50% respectively ($0.35 \pm 0.04\ h^{-1}$ and $0.49 \pm 0.03\ h^{-1}$ with 50 μM, and 500 μM NE

respectively, compared to 0.32 ± 0.06 h^{-1} for the untreated control). The maximum turbidity at 600 nm reached in the presence of 50 μM and 500 μM NE was 1.75 ± 0.02-fold and 2.43 ± 0.07-fold greater than untreated controls (**Fig. 3.1**).

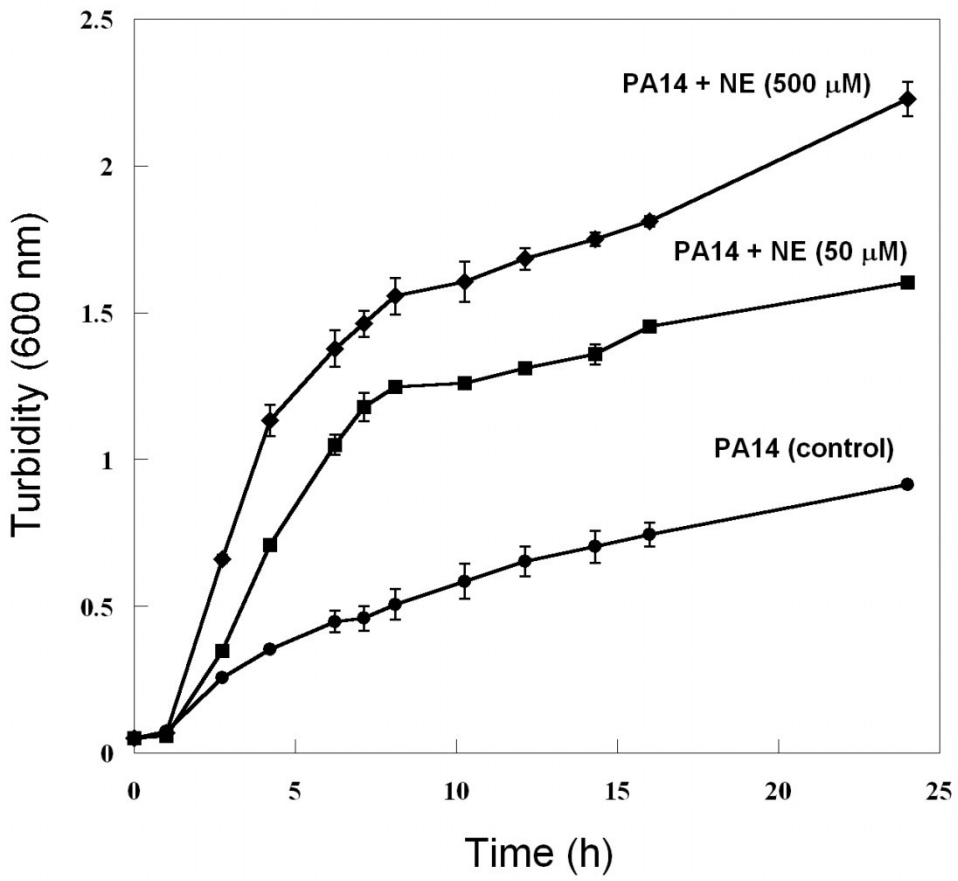

Fig. 3.1. Effect of NE on growth. *P. aeruginosa* PA14 was grown in RPMI medium at 37°C for 24 h in the presence of 50 μM and 500 μM NE. The turbidity at 600 nm was measured at different time points. Data shown are mean turbidity ± one standard deviation and are from three independent cultures.

3.3.2 Differential gene expression in planktonic cells upon exposure to NE

Whole transcriptome analysis was used to investigate the molecular basis underlying the effect of NE on PA14 gene expression, specifically its effect on the expression of genes involved in the production and regulation of virulence factors. Exposure to 50 μM NE for 7 h (corresponding to late-exponential phase of growth in **Fig. 3.1**) significantly altered the expression of 184 genes as compared to the untreated control. Of these, 128 genes were induced 4- to 209-fold, while 56 genes were repressed 4- to 42-fold (**Appendix Table I**). The genes that were increased in expression upon exposure to 50 μM NE included those of nitrate metabolism (*narGHIJK1K2*; induced 13- to 32.0-fold) that are involved in nitrate assimilation and respiration, and genes related to molybdenum cofactor synthesis (*moeA1B1CDE*; induced 5- to 209-fold) that are involved in nitrogen metabolism (127). Expression of the heme acquisition protein *HasAp* decreased by 42-fold, while genes involved in pyoverdine siderophore biosynthesis and metabolism (*pvdADEFGJLNO*) were repressed 5- to 15-fold respectively in NE exposed cultures. In addition, a few genes involved in virulence such as *toxA* (exotoxinA), *aprD* (alkaline protease), *sodM* (superoxide dismutase) were also repressed by 8-fold, 4-fold, and 12-fold respectively. However, genes involved in the production of other virulence determinants (e.g., elastase, alkaline protease, PQS, and rhamnolipids) were not significantly altered upon exposure to 50 μM NE.

Exposure of PA14 to a higher concentration of NE for 7 h significantly induced the expression of 287 genes and repressed the expression of 50 genes (**Appendix Table II**). The data showed that 34 genes were commonly expressed between PA14 exposed to 50

μM and 500 μM NE (**Appendix Table III**). The commonly-regulated genes primarily included those related to nitrogen metabolism and respiration. In addition, the expression of several QS-controlled genes associated with virulence was significantly altered in PA14 exposed to 500 μM NE (**Table 3.1**). These included the elastase synthesis genes *lasA* and *lasB*, which were induced 6.5 and 2-fold respectively, phospholipase gene *plcB* which was induced 4.0-fold, rhamnolipids synthesis related gene (*rhlG*) which was repressed 6.5-fold in the NE treated cells, and phenazine biosynthesis (pyocyanin) genes (*phzCDEF*) which were induced 2.0 to 3.3-fold. Other significantly induced virulence factor production and infection genes included those involved in flagellar synthesis (*flgD* and *flgL*; 2.3-fold and 2.1-fold), type IV fimbriae (*pilC* and *pilD*; 2.8-fold and 3-fold), PQS synthesis (*pqsABE* and *mvfR*; induced 1.9 to 4-fold), exoenzyme S regulation and production (*exsABC*; 2- to 4-fold), and exoenzyme T (*exoT,* 2-fold). Genes whose expression upon exposure to 500 μM NE included those involved in alkaline protease secretion (*aprA* and *aprE*, 2.1-fold and 2.6-fold) and the Fe (III)-pyochelin outer membrane receptor precursor gene *fptA* (2.5-fold). The fold change values obtained from qRT-PCR (**Table 3.2**) are consistent with those from whole microarray analysis.

Table 3.1. Partial list of differentially-expressed genes in suspension cells of PA14 grown in serum-RPMI medium at 37 ^{o}C for 7 h with 50 μM and 500 μM of NE. Complete data for the 50 μM and 500 μM DNA microarrays are available using GEO series accession number GSE 13326. [1]Most significant changes (greater than 4-fold for 50 μM NE array and 2-fold for 500 μM NE array) are shown in bold.

		Fold change[1]		
Locus tag	**Gene name**	**NE vs. control (50 μM)**	**NE vs. control (500 μM)**	**Description**
Quorum-sensing controlled genes				
PA0026	*plcB*	-2.3	**4.0**	phospholipase C
PA0044	*exoT*	-1.4	**2.1**	Exoenzyme T
PA0996	*pqsA*	1.0	1.9	Probable coenzyme A ligase
PA0997	*pqsB*	1.1	**2.6**	Beta-keto-acyl carrier protein synthase
PA0998	*pqsC*	1.1	1.1	Beta-keto-acyl carrier protein synthase
PA0999	*pqsD*	1.2	1.7	3-oxoacyl-[acyl-carrier-protein] synthase III
PA1000	*pqsE*	1.1	**4.3**	Quinolone signal response protein
PA1003	*mvfR*	-1.4	**3**	Transcriptional regulator MvfR
PA1130	*rhlC*	-1.3	**2.8**	Rhamnosyltransferase 2
PA1148	*toxA*	**-8.0**	1.2	Exotoxin A precursor
PA1246	*aprD*	**-4.0**	1.2	Alkaline protease secretion protein AprD
PA1247	*aprE*	**-2.1**	**-2.6**	Alkaline protease secretion protein AprE
PA1249	*aprA*	-1.4	**-2.1**	Alkaline metalloproteinase precursor
PA1710	*exsC*	-1.3	**2.1**	Exoenzyme S synthesis protein C precursor.

Table 3.1. Continued.

Locus tag	Gene name	NE vs. control (50 µM)	NE vs. control (500 µM)	Description
PA1712	*exsB*	-1.1	**3.7**	Exoenzyme S synthesis protein B
PA1712	*exsA*	-1.2	**2.1**	transcriptional regulator ExsA
PA1871	*lasA*	1.2	**6.5**	LasA protease precursor
PA1898	*qscR*	2.0	**2.5**	Quorum-sensing control repressor
PA1901	*phzC2*	1.1	**2.5**	Phenazine biosynthesis protein PhzC
PA1902	*phzD2*	1.1	**2.0**	Phenazine biosynthesis protein PhzD
PA1903	*phzE2*	1.0	**2.3**	Phenazine biosynthesis protein PhzE
PA1904	*phzF2*	-1.1	**3.3**	Probable phenazine biosynthesis protein
PA3095	*xcpZ*	1.0	**3.7**	general secretion pathway protein M
PA3097	*xcpX*	-1.1	**2.6**	general secretion pathway protein K
PA3099	*xcpV*	1.0	**2.8**	general secretion pathway protein I
PA3100	*xcpU*	-1.1	**2.8**	General secretion pathway outer membrane protein H precursor
PA3101	*xcpT*	-1.1	**2.5**	general secretion pathway protein G
PA3102	*xcpS*	1.1	**2.8**	general secretion pathway protein F
PA3103	*xcpR*	1.1	**2.0**	general secretion pathway protein E
PA3477	*rhlR*	-1.1	1.7	transcriptional regulator RhlR
PA3479	*rhlA*	-1.2	1.7	Rhamnosyltransferase chain A
PA3724	*lasB*	1.2	**2.0**	Elastase LasB
PA4209	*phzM*	-1.9	1.3	Probable phenazine-specific methyltransferase
PA4210	*phzA1*	-1.5	-1.2	Probable phenazine biosynthesis protein
PA4217	*phzS*	-2.5	1.1	Flavin-containing monooxygenase

Table 3.1. Continued.

Locus tag	Gene name	NE vs. control (50 µM)	NE vs. control (500 µM)	Description
Pyoverdine				
PA2254	*pvcA*	1.0	1.2	Pyoverdine biosynthesis protein PvcA
PA2255	*pvcB*	-1.2	1.4	Pyoverdine biosynthesis protein PvcB
PA2256	*pvcC*	1.3	1.6	Pyoverdine biosynthesis protein PvcC
PA2396	*pvdF*	**-8.6**	-1.2	Pyoverdine synthetase F
PA2397	*pvdE*	**-12.1**	-1.2	Pyoverdine biosynthesis protein pvdE
PA2398	*fpvA*	**-9.2**	1.5	Ferripyoverdine receptor
PA2399	*pvdD*	**-8.6**	**2.3**	Pyoverdine synthetase D
PA2400	*pvdJ*	**-7.5**	**1.3**	PvdJ
PA2426	*pvdS*	**-7.5**	**-2.1**	Sigma factor PvdS
PA4168	*fpvB*	**-12.1**	**2**	Second ferric pyoverdine receptor FpvB
Pyochelin				
PA4221	*fptA*	-1.9	**2.5**	Fe(III)-pyochelin outer membrane receptor precursor
PA4224	*pchG*	-1.2	-1.7	Pyochelin biosynthetic protein PchG
PA4225	*pchF*	-1.3	-1.6	Pyochelin synthetase
PA4226	*pchE*	-1.3	-1.5	Dihydroaeruginoic acid synthetase
PA4227	*pchR*	-2.5	-1.6	Transcriptional regulator PchR
PA4228	*pchD*	-1.1	-1.9	Pyochelin biosynthesis protein PchD
PA4229	*pchC*	-1.2	-1.6	Pyochelin biosynthetic protein PchC

Table 3.1. Continued.

Locus tag	Gene name	NE vs. control (50 µM)	NE vs. control (500 µM)	Description
PA4230	*pchB*	1.1	-1.5	Salicylate biosynthesis protein PchB
PA4231	*pchA*	1.0	-1.4	Salicylate biosynthesis isochorismate synthase
Motility				
PA3115	*fimV*	1.1	**2.1**	Motility protein FimV
PA4526	*pilB*	-1.3	1.7	Type 4 fimbrial biogenesis protein PilB
PA4527	*pilC*	-2.3	**2.8**	Still frameshift fimbrial biogenesis protein PilC
PA4528	*pilD*	-1.1	**3**	Type 4 prepilin peptidase PilD
PA1079	*flgD*	-1.1	**2.3**	Flagellar basal-body rod protein FlgD
PA1080	*flgE*	-1.1	1.4	Flagellar hook protein FlgE
PA1087	*flgL*	-1.1	**2.1**	Flagellar hook-associated protein type 3 FlgL
PA1099	*fleR*	-1.1	**4.3**	Two-component response regulator

Table 3.2. Gene name and its corresponding primer sequence used for qRT-PCR; relative change in expression of the genes determined by microarray (50 µM NE and 500 µM NE) and qRT-PCR at 7 h. Significant changes in gene expression (greater than 4-fold for 50 µM NE array and 2-fold for 500 µM NE array) are shown with an asterisk.

PA#	Gene	Forward primer (5'-3')	Reverse primer (5'-3')	Fold change (50 µM NE vs. no NE) 7 h		Fold change (500 µM NE vs. no NE) 7 h	
				Microarray	qRT-PCR	Microarray	qRT-PCR
PA0026	*plcB*	ACTACACCTCGTACTGGCACTT	TTCAGCTCGCGGTTGTAGAGAT	-2.3	-3.4	4.0*	7.1*
PA1430	*lasR*	TAAGGACAGCCAGGACTACGAGAA	TGGTAGATGGACGGTTCCCAGAAA	1.2	1.3	1.0	1.5
PA1871	*lasA*	ACCCGAAAGTGTTGTTGACCCT	TTCCTCGAAACCGTAGTAGCGT	1.2	-1.4	6.5 *	4.7 *
PA2426	*pvdS*	ATGTGGTCCAGGATGCGTTCTT	TATTTCTGTTCGAGCGCCTGCT	-7.5*	-9.8*	-2.1*	-3.4*
PA3477	*rhlR*	AATTTGCTCAGCGTGCTTTCCGTG	TGGGTCAGCAACTCGATCATGCAA	-1.1	-1.5	1.7	1.3
PA4527	*pilC*	TTTCCATGCGCACCACCAATGT	ATCGGCTCCATCAACGTTGTCA	-2.3	-2.8	2.8 *	1.7
PA0393	*proC*	CAGGCCGGGCAGTTGCTGTC	GGTCAGGCGCGAGGCTGTCT	-	-	-	-

3.3.3. Effect of NE on production of *P. aeruginosa* PA14 virulence factors

The levels of five virulence factors - pyocyanin, elastase, rhamnolipid, PQS, and pyoverdine - were determined in PA14 cultures exposed to 50 μM and 500 μM of NE. The production of pyocyanin increased 2.1 ± 0.2-fold and 3.9 ± 0.2-fold after 16 h and 24 h of exposure to 50 μM NE (**Fig. 3.2A**), but did not change significantly at earlier time points. Similarly, exposure to 500 μM NE increased pyocyanin 3.2 ± 0.9-fold, 4.9 ± 0.5-fold, and 6.4 ± 0.4-fold at 12 h, 16 h, and 24 h, respectively (**Fig. 3.2A**). NE exposure increased elastase production by 3.4 ± 0.3-fold at 16 h and by 6.2 ± 1.4 fold at 24 h upon exposure to 500 μM NE; however, elastase levels did not increase with 50 μM NE (**Fig. 3.2B**). The levels of PQS increased by 9.7 ± 0.5-fold after 24 h exposure to 500 μM NE but not with 50 μM NE (**Fig. 3.2C**). Rhamnolipid levels were only marginally increased upon exposure to both 50 μM and 500 μM NE (1.7 ± 0.1/1.8 ± 0.1-fold at 16 h and 1.2 ± 0.4/1.3 ± 0.4-fold at 24 h) (**Fig. 3.2D**). The levels of pyoverdine were not altered with either concentration of NE for up to 24 h (not shown).

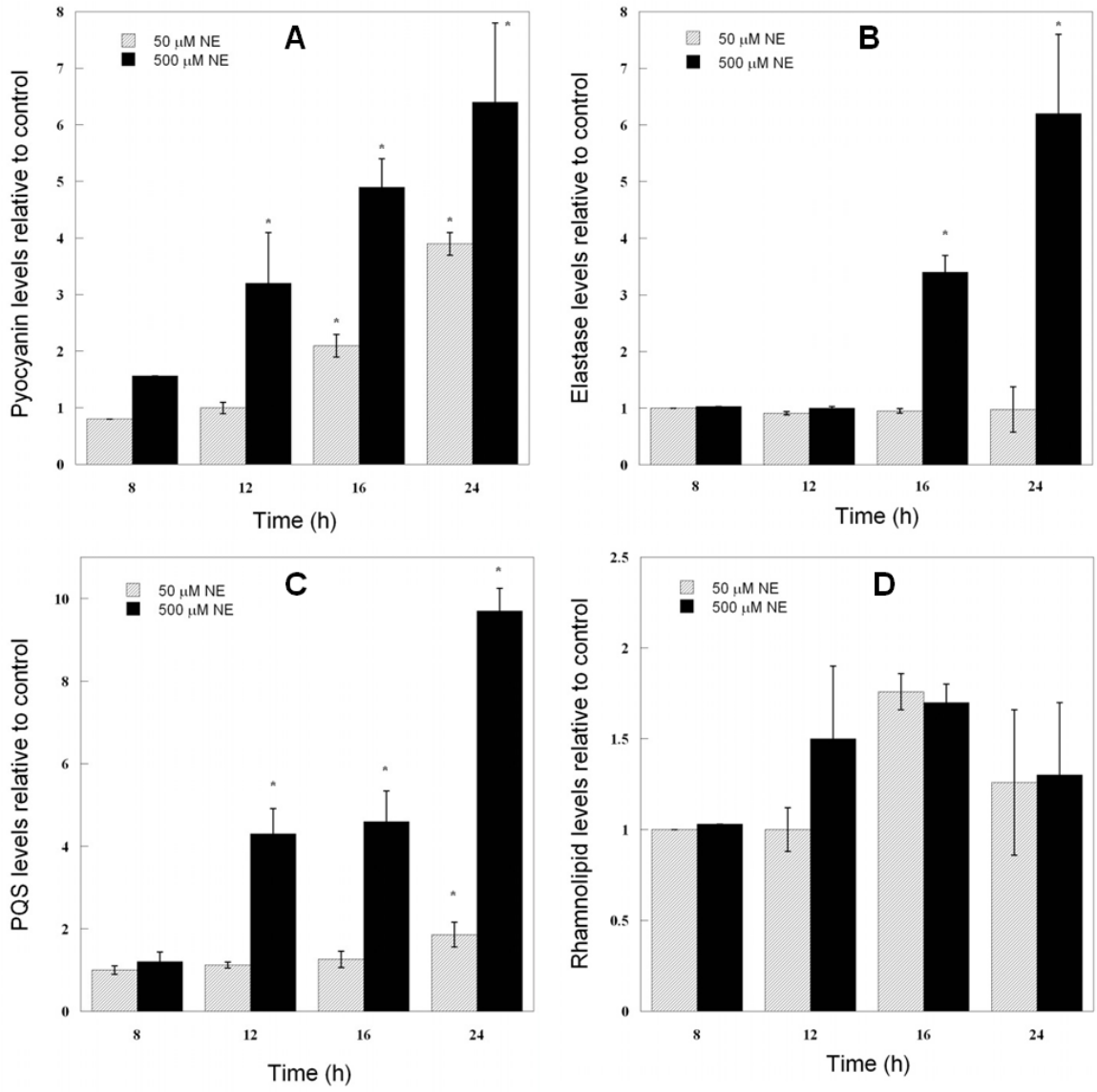

Fig. 3.2. Virulence factor production in the presence of NE. Changes in the levels of (A) pyocyanin, (B) elastase, (C) PQS, and (D) rhamnolipid in *P. aeruginosa* PA14 in the presence of 50 μM and 500 μM NE. Virulence factors were measured in triplicate after 8, 12, 16, and 24 hours of exposure to NE and normalized to the cell density of the culture. Data shown are from three independent experiments. Error bars indicate mean fold change ± one standard deviation. *****: statistical significance at $p < 0.05$ for NE treated cultures relative to untreated control.

We investigated the effect of increased virulence factor levels on attachment and invasion of the HCT-8 human enterocyte cell line. The extent of PA14 adhesion to HCT-8 cells in the presence of 50 μM and 500 μM NE increased by 1.6 ± 0.3-fold and 2.9 ± 0.4-fold, respectively (**Fig. 3.3A**). Similarly, invasion of HCT-8 cells was also increased by 1.5 ± 0.2-fold and 4.2 ± 0.5-fold upon exposure to 50 μM and 500 μM NE. Together with the increase in PA14 virulence factor levels, our data strongly indicate increased PA14 virulence and infectivity upon exposure to NE (especially at 500 μM NE).

Since PA14 can infect both plant and animal hosts (71), we also investigated the effect of increased virulence factor levels on infection using a barley seed infection model (128). Germination of barley seeds in the presence of PA14 was reduced to 51 ± 4% ($p < 0.005$) of the untreated control which is in good agreement with our prior work (128). The addition of 50 μM and 500 μM NE further reduced germination further to 20 ± 7% and 9 ± 4% of the control ($p < 0.01$) (**Fig. 3.3B**); hence, 50 μM and 500 μM NE increased *P. aeruginosa* virulence by 2.6 ± 0.9-fold and 6 ± 3fold, respectively. Nearly 100% germination of barley seeds was observed in negative controls and seeds treated only with 50 μM or 500 μM NE (**Fig. 3.3B**). These results further confirm that exposure to NE increased PA14 virulence.

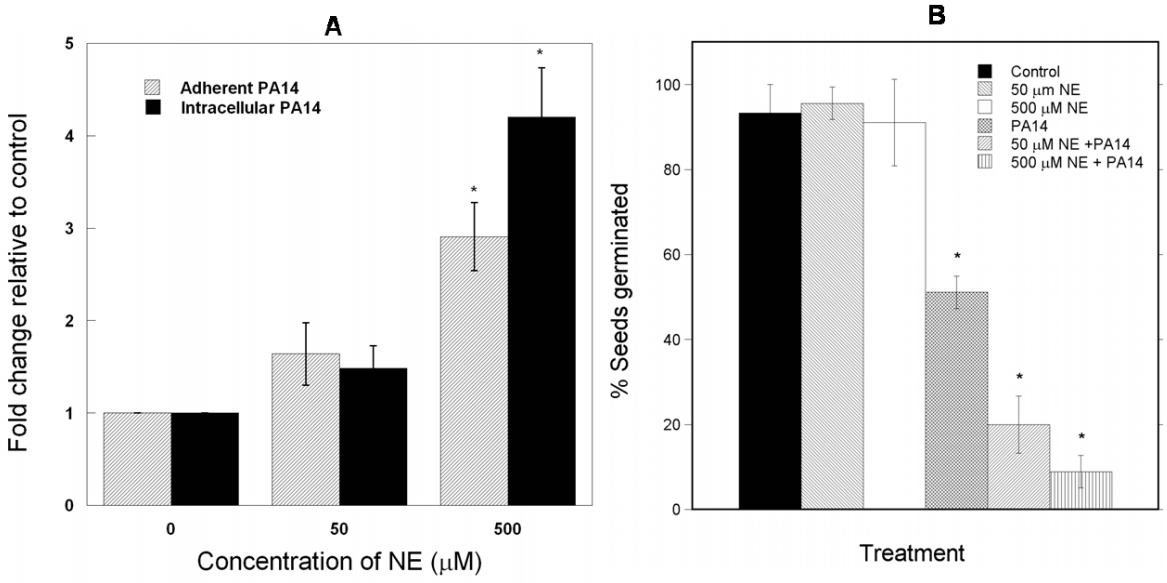

Fig. 3.3. Epithelial cell attachment and invasion and barley seed infection in the presence of NE. Relative changes in *P. aeruginosa* PA14 (A) attachment and invasion to HCT-8 cells, and (B) barley seed germination, after exposure to 50 μM or 500 μM NE. For the attachment and invasion assays, cell counts (mean ± one standard deviation) are from duplicate LB agar plates and generated from nine HCT-8 cell culture wells and 3 independent experiments. '*' indicate statistical significance determined using the Student t-test at $p < 0.05$. For the barley seed germination assay, the percentage of barley seeds germinated was calculated. Data are the average of three independent experiments, and one standard deviation is shown. '*' indicate statistical significance determined using the Student t-test at $p< 0.001$.

3.3.4 Effect of NE on *P. aeruginosa* PA14 swimming and swarming motility

Since motility is directly related to infection (129), we investigated the effect of NE PA14 swimming and swarming motility. The swimming motility of PA14 in serum-free RPMI with 0.5% agar supplemented with 10 μM $FeCl_3$ (i.e., the same base medium used for microarray and virulence factor experiments) increased in the presence of NE in a concentration dependent manner (**Fig. 3.4**). Swimming motility was increased by 30% and 60% upon exposure to 50 μM and 500 μM NE. Interestingly, an extracellular product zone was detected in control and 50 μM NE plates outside the swimming

motility halo, but was absent in the 500 μM plates. The constituent of this clear zone was abiotic as it did not grow on plates, and was identified as rhamnolipid using methylene blue staining (130). The diameter of this secreted rhamnolipid zone was only slightly less than control with 50 μM NE but was virtually abolished at 500 μM (**Fig. 3.4**), suggesting that NE suppressed PA14 rhamnolipid production when growing on agar surfaces.

Since rhamnolipids contribute to *P. aeruginosa* swarming (130), we also investigated the effect of NE on PA14 swarming motility. **Figs. 3.5A-C** show that exposure to 500 μM NE completely inhibited PA14 swarming motility; however, no effect was observed with 50 μM NE. Since an increase in intracellular iron levels has been shown to decrease rhamnolipid production (131), we investigated whether the NE-mediated decrease in swarming motility is due to an increase in intracellular iron levels. **Fig. 3.5D** shows that increasing iron concentration in the swarming agar from 10 μM to 100 μM completely inhibited swarming motility similar to that observed with 500 μM NE.

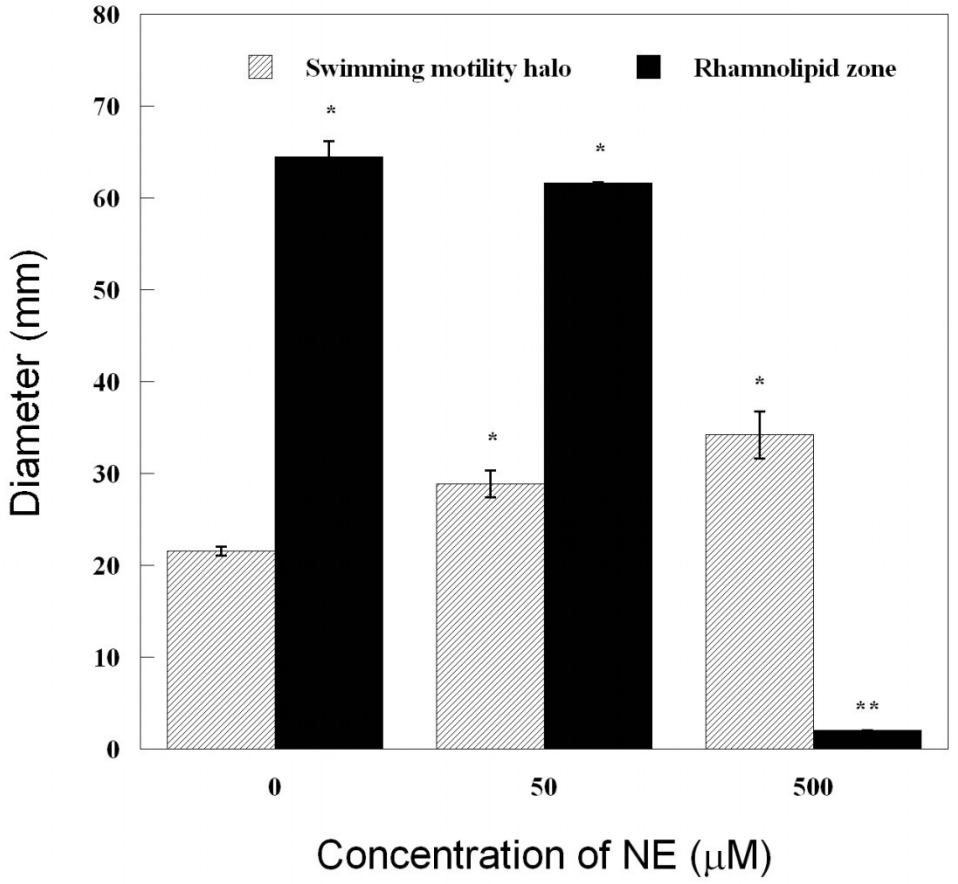

Fig. 3.4. Changes in swimming motility upon exposure to NE. Changes in *P. aeruginosa* PA14 swimming motility upon exposure to NE. PA14 was spotted onto RPMI 0.3% motility agar medium supplemented with 10 μM $FeCl_3$ containing 50 μM or 500 μM of NE. The swimming halo diameter and the clear rhamnolipid zone diameter were measured after 24 h at 37^{o}C. Error bars indicate mean halo diameter or rhamnolipid zone diameter ± one standard deviation. Data shown are from three independent cultures. *****: statistical significance at $p < 0.05$ for NE treated cultures relative to control. ******: diameter of the rhamnolipid zone with 500 μM outside the motility halo was negligible and could not be accurately measured.

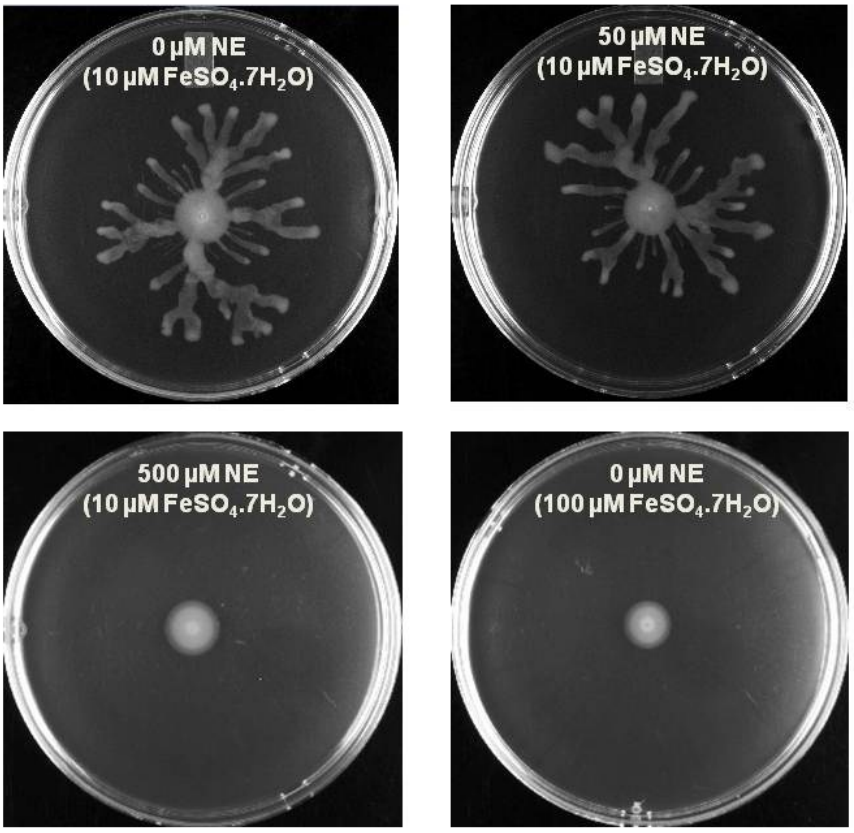

Fig. 3.5. Changes in swarming motility upon exposure to NE or excess iron. *P. aeruginosa* PA14 was spotted onto 0.5% BM2 motility agar containing 10 µM $FeSO_4.7H_2O$ and (A) 0 µM, (B) 50 µM, or (C) 500 µM NE. (D) 100 µM of $FeSO_4.7H_2O$. Representative images from three independent experiments are shown

3.3.5 NE enhances activity of *las*, but not *rhl*, quorum sensing

We hypothesized that the effects of NE at a concentration of 500 µM are mediated primarily through the *las*, but not the *rhl*, quorum sensing (QS) system. Therefore, we determined the transcriptional activation of *lasR* and *rhlR* (i.e., the response regulators of the *las* and *rhl* QS systems) with NE using a promoter::*lacZ* reporter fusion (132) during

the mid to late-exponential growth phase (i.e., after 4, 5.5, 6.5, and 7.5 hours of growth in the presence of NE). PA14 with the *plasR::lacZ* reporter plasmid showed a 3.2 ± 0.8-fold increase in β-galactosidase activity in the presence of 500 μM NE after 7.5 hours (**Fig. 3.6**), but did not demonstrate an increase in the presence of 50 μM NE. Although detectable β-galactosidase was observed at earlier time points (4 h, 5.5 h, and 6.5 h), the changes in activity observed with NE were not statistically significant from the control. On the other hand, PA14 with the *prhlR::lacZ* reporter did not show any change in β-galactosidase activity in the presence of NE (50 μM and 500 μM) compared to the untreated control at any of the time points. These results suggested that NE increases the activity of *las*, but not the *rhl*, QS pathway.

3.4 Discussion

It has been proposed that *P. aeruginosa* in the GI tract lumen can respond to specific environmental cues (e.g., high concentration of hormones) to express different virulence determinants and initiate infection (133). This hypothesis is supported by the fact that neuroendocrine hormones play an important role in gut-derived sepsis (134), and have been reported to spill over into circulation (105) and the lumen (135). In addition, intestinal levels of tyrosine hydroxylase, the rate-limiting enzyme in NE biosynthesis, has been shown to be increase 2 h after the onset of sepsis, and has been speculated to contribute to the increase in gut-derived NE during sepsis (136). Although plasma levels of circulating catecholamines have been found to be in the nanomolar range during sepsis (105), It should be noted that such plasma levels reflect spillover from tissue sites

located throughout the body, and do not accurately reflect the local concentration at any particular tissue site. For example, Kopin et al., (137) have estimated that concentration of NE at the receptor site during non-septic conditions was at least three-fold higher than that detected in the plasma. In fact, the plasma concentrations of hormones may underestimate the local concentration of NE in the GI tract by orders of magnitude (138) as the mesenteric organs contribute to approximately half of the NE produced in the body (126). Therefore, although the concentrations of NE (50 μM and 500 μM) used in this study do not reflect reported actual plasma concentrations, they are representative of the concentration range reported in the GI tract during normal and catabolic stress (133, 139) and are consistent with concentrations used in previous studies (112, 125, 140-142).

The increase in PA14 WT growth rate with 50 μM and 500 μM NE is consistent with *in vitro* studies showing that NE stimulates the growth of several bacterial pathogens, including *E. coli* and *P. aeruginosa* (109, 143), in serum-based (i.e., transferrin-containing) nutritionally-minimal growth media. It has been proposed that NE enhances pathogen growth by providing access to iron needed for growth (144) through production of siderophores (145). Although pyocyanin synthesis genes are up-regulated on exposure to 500 μM NE, interestingly, genes involved in the production of other major *P. aeruginosa* siderophores such as pyoverdine and pyochelin (146) were down-regulated upon NE exposure. Since several of these genes are regulated by the transcription factor Fur and repressed under conditions of iron abundance (147), our data suggest that PA14 preferentially utilizes pyocyanin for iron acquisition from a minimal nutrient environment (145) such as that seen in the GI tract, and the increase in iron

levels leads to down-regulation of other siderophore genes.

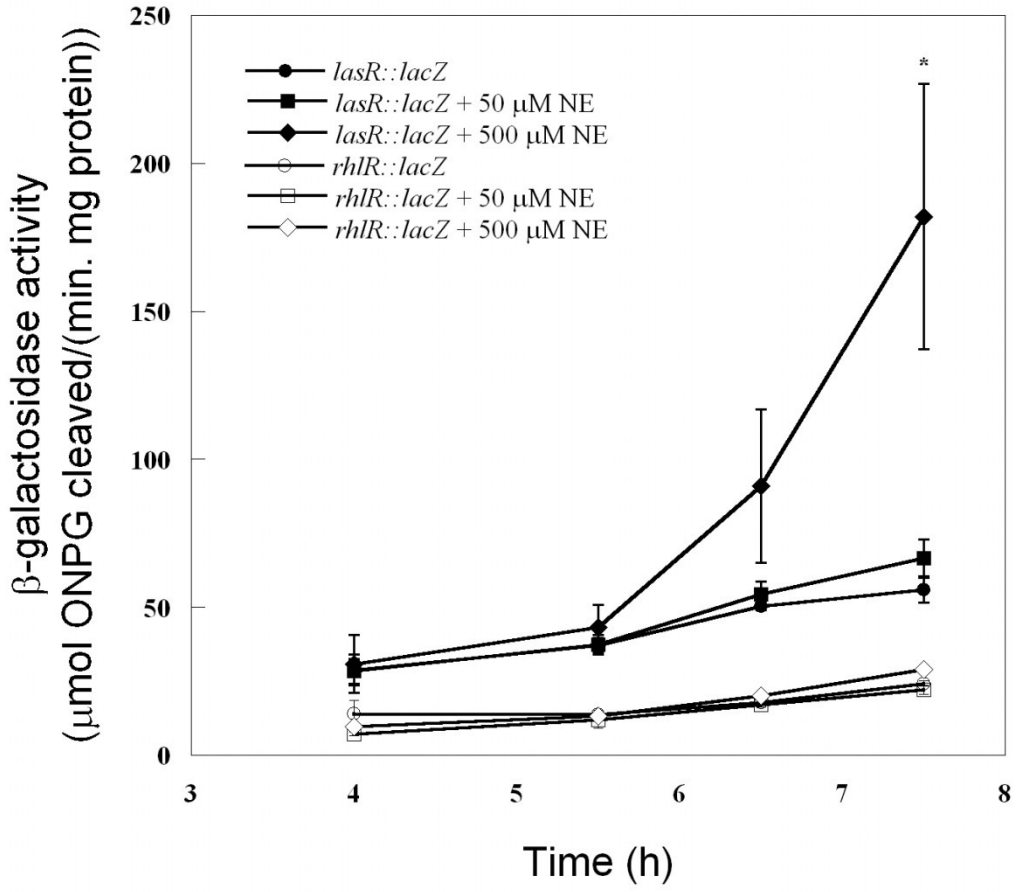

Fig. 3.6. Effect of NE on quorum sensing pathways. Changes in *lasR* and *rhlR* expression were measured using the β-galactosidase activity assay. PA14 cultures containing plasmids with *lasR::lacZ* and *rhlR::lacZ* transcriptional fusions respectively were grown with 50 μM and 500 μM NE. The β-galactosidase activity in one mL culture aliquots was determined and normalized to the cell density. The β-galactosidase activity of PA14 cultures observed in plasmids with only *lacZ* (i.e., no *lasR* or *rhlR* fusion) was negligible. Data shown are from three independent experiments and represent mean β-galactosidase activity ± one standard deviation. '*' indicate statistical significance determined using the Student t-test at $p < 0.05$

The increase in the production of the *P. aeruginosa* virulence factors such as pyocyanin and elastase suggests that the pathogen may opportunistically utilize host hormones to facilitate infection. Our data suggest pyocyanin may play a dual role in *P. aeruginosa* infections. Apart from stimulating PA14 growth through rapid acquisition of iron in minimal environments, pyocyanin is also likely involved in virulence as our data show pyocyanin levels increasing even after 24 h of exposure to NE (i.e., when the pathogen is no longer growing). The growth-independent production of pyocyanin likely increases the susceptibility of host cells to infection as pyocyanin has also been shown to cause oxidative stress in epithelial cells (148) and apoptosis in neutrophils (149). Similarly, the increase in the levels of elastase, which is involved in degradation of elastin and collagen in host tissues during infection (150), and PQS, which inhibits human T cell proliferation and acts as an immune modulator (151, 152), also reinforce the idea that the NE-mediated increase in virulence factor levels could contribute to *P. aeruginosa* infections. The concordance between virulence factor production and attachment/invasion of epithelial cells supports the idea that PA14 could utilize NE during colonization and infection of the GI tract. The increase in infection with the barley seed germination assay, a valid model for *P. aeruginosa* PA14 virulence as this strain contains a common set of virulence genes to elicit soft rot disease in lettuce and *Arabidopsis* plants, as well as in mice (72), further strengthens the hypothesis that high concentrations of NE increases PA14 virulence.

Since NE is produced *in situ* in the GI tract (105, 106, 141), it is likely that pathogens in the GI tract encounter either low luminal concentrations of NE under

normal conditions, or short-lived bursts of higher NE concentrations during acute stress. The observation that sustained exposure (> 8 h) to 500 μM, but not 50 μM, of NE is needed to cause an increase in pyocyanin, elastase, and PQS levels is significant in the context of gut-derived *P. aeruginosa* infections as it suggests that acute exposure to hormones is not likely to lead to *P. aeruginosa* infection.

The fact that NE significantly increased the levels of only pyocyanin (6.4-fold), elastase (6.2-fold), and PQS (9.7-fold), but not rhamnolipids (30%) and pyoverdine (unchanged), in suspension cultures at 24 h, argues that the increase in virulence factor levels is due to a NE-specific effect and not merely due to the increased cell density upon NE exposure. Four lines of evidence suggest that the *las* QS pathway is involved in mediating the effects of NE in PA14. First, the increase in expression of *lasA* and *lasB*, the up-regulation of *lasR* promoter activity, and increased production of elastase, strongly suggest the involvement of the *las* QS system. Second, the increase in the expression of other *las* QS-controlled *P. aeruginosa* virulence factor genes (phospholipase C) and in the expression of type II secretion genes (*xcpRSTUVXZ*) (153) that is involved in secreting elastase and phospholipase and is itself controlled by *las* QS (153), is also indicative of the *las* QS being activated upon exposure to NE. Third, the 2-fold increase in the expression of the global response regulator *gacA*, which positively regulates *lasR* and the production of extracellular virulence factors such as pyocyanin, cyanide, and exoenzyme lipase (154), in the presence of 500 μM NE suggests that NE may be acting through *gacA* to increase the *las* QS activity. Fourth, the increase in the levels of PQS also suggests increased *las* QS activity, as the expression of *mvfR* (up-

regulated 3-fold in our study), the regulator of PQS production, has been shown to be up-regulated by *lasR* but down-regulated by *rhlR* (75). The activation of *P. aeruginosa* QS by host hormones is also consistent with other studies showing that eukaryotic hormones such as epinephrine can influence *E. coli* O157:H7 quorum sensing (155).

It was surprising to note that while rhamnolipid levels were slightly increased or unchanged (16 h and 24 h data points, respectively in **Fig. 3.2D**) upon exposure to 500 μM NE in suspension cultures, they were significantly decreased on motility agar plates after 24 h. It is possible that the effect of NE on rhamnolipid production depends on the culture format in which PA14 is grown (i.e., in suspension or on semi-solid surfaces). Overhage *et al.* (156) recently reported that ~ 7.5% of the *P. aeruginosa* PAO1 genome, including genes involved in the type III secretion system, extracellular proteases, and siderophore synthesis, are differentially expressed under swarming conditions compared to suspension cells or biofilms. Since colonization on a semi-solid surface closely mimics the *in vivo* scenario where a mucus layer covers epithelial cells, it is possible that the NE-mediated decrease in rhamnolipid production is significant in the context of PA14 virulence *in vivo*. Since colonization of epithelial cells is necessary for the infection process, the decrease in swarming motility observed with 500 μM NE could contribute, in part, to increased colonization and subsequent invasion. Further work is required to completely understand differences between *P. aeruginosa* pathogenesis in surface-associated and planktonic cultures.

3.5 Summary

We have shown that NE at a concentration of 500 μM, but not 50 μM, increases *P. aeruginosa* PA14 growth, motility, attachment, and virulence, all of which are integral to infection. Our data also show that the actions of NE are mediated primarily through the *las*, and not the *rhl* QS system. We propose that *P. aeruginosa* can utilize NE for colonization of the GI tract to initiate infection that eventually leads to gut-derived sepsis.

3.6 Materials and methods

3.6.1 Bacterial strains, mammalian cell line and materials

P. aeruginosa PA14 wild type (157) was used for all the experiments. *E. coli* DH5α transformed with plasmids pLP170, pPCS1001, and pPCS1002 containing the *lacZ*, *plasR::lacZ*, and *prhlR::lacZ* transcriptional fusions respectively, was kindly provided by Dr. Barbara Iglewski (132). PA14 was grown at 37^{o}C in RPMI 1640 medium (MP Biomedicals, Solon, Ohio) supplemented with 10% heat-inactivated horse serum (Hyclone, Logan, Utah) in all experiments unless indicated otherwise. *L*-(-)-Norepinephrine-(+)-bitartrate (NE) was obtained from EMD Biosciences, La Jolla, CA. The human ileo-cecal colorectal adenocarcinoma line, HCT-8 (ATCC, Mansasses, VA), derived from enterocytes at the junction of the large and small bowel, was grown at 37^{o}C in a 5% CO_2 humidified environment using RPMI 1640 medium supplemented with 10% horse serum (HS) as the growth medium. Elastin-Congo Red obtained from MP Biomedicals was used for the elastase assay. Carbenicellin and gentamicin was obtained

from Fisher Scientific (Fair Lawn, NJ) and MP Biomedicals, respectively.

3.6.2 Growth rate measurement

For growth rate measurements, a single colony of PA14 was grown overnight in Luria-Bertani (LB) broth, and re-inoculated in serum-RPMI medium in the presence of 50 μM and 500 μM NE to an initial turbidity of ~ 0.05 at 600 nm. The turbidity of the cultures at 600 nm was monitored every hour and the growth rate of the exponentially growing cultures was calculated. Growth curves were obtained in triplicate using three independent cultures, and the statistical significance of specific growth rate was determined using the unpaired Student's t-test.

3.6.3 Total RNA isolation and microarray analysis

PA14 was grown overnight in LB to turbidity at 600 nm of ~5.0 and diluted in 100 mL of serum-RPMI medium to an initial turbidity at 600 nm of 0.05. Different concentrations of NE (50 μM or 500 μM) were added and the cultures grown for 7 hours until late exponential phase (turbidity at 600 nm of ~0.5, 1.1 and 1.5 with 0 μM, 50 μM and 500 μM NE, respectively). Cell pellets were prepared and RNA was isolated as described previously (158).

The *P. aeruginosa* Genome Array (Affymetrix, P/N 510596) containing 5,500 of the 5,570 open reading frames of *P. aeruginosa* PA01, was used to analyze changes in the PA14 transcriptome. cDNA synthesis, fragmentation and hybridizations were as described previously (159). Hybridization was performed for 16 h at 50°C, and the total

cell intensity was scaled to an average value of 500. The probe array images were inspected for any image artifact. Background values, noise values and scaling factors of all the arrays were examined and were comparable. The intensities of polyadenosine RNA control were used to monitor the labeling process. For each binary microarray comparison of differential genes expression, if the gene with the larger transcription rate did not have a consistent transcription rate based on the 13 probe pairs (*p*-value less than 0.05), these genes were discarded. A gene was considered differentially expressed when the *p*-value for comparing two chips was lower than 0.05 (to assure that the change in gene expression was statistically significant and that false positives arise less than 5%), and the expression ratio (between cells treated with NE and control) was greater than 4.0 for 50 μM NE array and 2.0 for 500 μM NE array (based on the standard deviation of fold-change values) (160). Gene functions were obtained from http://www.pseudomonas.com/download.jsp . The expression data have been deposited in the NCBI Gene Expression Omnibus (161) and are accessible through Accession No. GSE# 13326.

3.6.4 Quantitative Reverse-Transcription Polymerase Chain Reaction (RT-PCR)

Quantitative RT-PCR was performed using a Bio-Rad iCycler (Bio-Rad, CA) real-time PCR unit. Approximately 20 ng of total RNA from control or NE-treated PA14 was used for each reverse transcription reaction. Gene sequences were downloaded from http://www.pseudomonas.com/search.jsp and gene-specific primers were used for *plcB*, *lasR*, *lasA*, *pvdS*, *rhlR*, *pilC*, and *proC* (housekeeping control) (**Table 3.2**). Threshold

cycle numbers were calculated using the MyiQ software (Bio-Rad), and PCR products were verified using agarose electrophoresis. RT-PCR experiments were performed thrice (i.e., three experimental replicates) using the same RNA sample used for the microarray analysis.

3.6.5 Virulence factor assays

PA14 cells were grown in serum-RPMI with 50 μM or 500 μM NE for 8, 12, 16, and 24 h. At each time point, pyocyanin was extracted from the cell-free culture supernatant into the aqueous phase as described previously (162). The pyocyanin concentration was normalized to the cell density (turbidity at 600 nm). The PA14 *phzM* mutant was used as the negative control.

Elastase activity in PA14 cultures exposed to 50 μM or 500 μM NE was determined as described previously (163). The elastase activity was normalized with the cell density (turbidity at 600 nm) to determine elastase activity per cell. The PA14 *lasI* mutant was used as the negative control for elastase production.

PQS was extracted from control and NE-treated PA14 cultures as described previously (164), and measured using a thin layer chromatography (TLC) assay (165). Synthetic PQS (Syntech Solution, San Diego, CA) was used as a standard, and the PA14 *pqsA* mutant was used as the negative control. PQS levels were determined by imaging the TLC plate using a VersaDoc 3000 imaging system (BioRad, Hercules, CA, USA).

The pyoverdine concentration was determined by measuring the absorbance of the culture supernatant at 405 nm and normalizing with the cell density (turbidity at 600 nm)

as described previously (166). The PA14 *pvdF* mutant was used as the negative control for pyoveridin production.

The rhamnolipid assay was adapted from Ohman et al. (163). PA14 cells were grown in serum-RPMI with and without 50 μM and 500 μM NE. After 8 h, 12 h, 14 h, and 24 h, 1 mL of the cell suspension was centrifuged at 10,000×g for 2 min, and rhamnolipids were extracted into the aqueous phase as described previously (164). The absorbance of the aqueous layer was recorded using the orcinol colorimetric assay at 495 nm and normalized by the cell density (turbidity at 600 nm). The PA14 *rhlR* mutant was used as the negative control for rhamnolipid production. All virulence factor assays were performed in triplicates using three independent cultures.

3.6.6 Swimming and swarming motility

The swimming motility assay was adapted from Bearson and Bearson (167). Briefly, a single colony of PA14 was grown overnight in LB and sub-cultured at 1:100 in LB medium, and grown to a turbidity of ~ 1.0 at 37^{o}C. NE (50 μM and 500 μM) were added to 0.3% agar (Difco Laboratories, Detroit, MI) in serum-free RPMI medium. Serum was not included in the plates because of difficulties in preparing serum-RPMI agar plates. Instead, 10 μM $FeCl_3$ (Acros Organics, NJ) was added to the medium as Bearson and Bearson (167) have shown that iron is required for observing NE-mediated changes in phenotype (e.g., swimming motility) in the absence of serum-derived iron. The size of the motility halos were measured after 24 hours. Five motility plates were used for each concentration of NE, and the experiment was repeated with three independent cultures

(total of 15 plates per NE concentration). The diameter of the transparent zone surrounding the motility halo in PA14 control plates was determined by adding 50 µL of methylene blue (Fisher Scientific, Fair Lawn, NJ) to the edge of the clear zone and by tracing the dye till it covered the border of the entire zone (130).

Swarming motility was performed as described previously (156). Briefly, fresh BM2 swarm agar plates containing 10 µM $FeSO_4.7H_2O$ and supplemented with 0.1% casamino acids (Difco Laboratories, Detroit, MI) and 0.5% bacto-agar (Difco Laboratories, Detroit, MI) were used. PA14 were grown overnight in LB, re-inoculated at 1:100 in LB medium, and grown to a turbidity of ~ 1.0 at 37^{o}C. NE (50 µM and 500 µM) were added to the BM2 swarm agar plates, and the swarming motility pattern was observed after 24 hours. The concentration of iron source in BM2 agar was increased to 100 µM and 1 mM $FeSO_4.7H_2O$ and swarming motility pattern of PA14 was observed after 24 h. Motility agar plates were freshly prepared and dried for 3 h prior to the experiment. Five motility plates per NE concentration were used, and the experiment was repeated with three independent cultures (total of 15 plates per NE concentration).

3.6.7 Epithelial cell attachment and invasion assay

Adhesion of PA14 on epithelial cells and its invasion into epithelial cells was determined as described by Bansal *et al.* (22) and Fleiszig *et al.* (168), respectively. Low passage HCT-8 cells were seeded into standard 24-well tissue culture plates (Corning Inc., Corning, NY) and grown to ~ 80% confluency. HCT-8 cell monolayers were washed twice with sterile phosphate buffered saline (PBS) to remove unattached cells,

and the growth medium was replaced with antibiotic-free medium containing 10% heat-inactivated HS. PA14 (turbidity at 600 nm of ~ 0.8) and NE (50 μM or 500 μM) were added to wells and incubated for 3 hours. Loosely attached PA14 were removed by washing the wells thrice with sterile PBS.

For the adhesion assay, HCT-8 cells were lysed in the wells with 0.1% Triton X-100 and the cell suspension vigorously mixed prior to enumeration of bacteria. For the invasion assay, fresh RPMI medium with 200 μg/ml gentamicin (a concentration which completely killed PA14 suspension cells) was added to each well after removal of loosely attached PA14 cells. After a 2 h incubation to kill attached (extracellular) *P. aeruginosa*, HCT-8 cells were washed once with PBS and lysed with 0.1% Triton X-100. Bacterial counts for both the adhesion and invasion assays were enumerated by plating the appropriate dilutions of the lysate on LB agar plates. Colonies were counted after 24 h incubation at 37^{o}C. The experiment was repeated thrice with independent HCT-8 cultures.

3.6.8 Barley seed pathogenicity

The barley seed pathogenicity assay (128) was used to assess *P. aeruginosa* virulence. Briefly, an overnight culture of *P. aeruginosa* PA14 was re-inoculated in LB medium at 37°C and grown to turbidity at 600 nm of ~1. The cells were washed once with sterilized distilled water and twice with sterile Hoagland solution (169), and then re-suspended to turbidity at 600 nm of 1.00 ± 0.03. Fifteen sterilized barley seeds were placed in beakers containing 10 mL of Hoagland solution with the appropriate

concentration of NE and/or PA14 at 25°C with gentle shaking (200 rpm). After 3 days, the number of germinated seeds was counted in each beaker. The experiment was performed with two independent cultures in triplicate (total 90 seeds per condition).

3.6.9 β-galactosidase reporter assay

PA14 with the reporter plasmids pLP170 (control with promoterless *lac*Z), pPCS1001 (*plasR::lac*Z) and pPCS1002 (*prhlR::lac*Z) (132) were introduced into PA14 by electroporation. PA14 reporter strains were grown overnight in LB supplemented with 100 μg/mL carbenicellin, and re-inoculated in two flasks containing 25 mL of serum-RPMI medium at 1:100 dilution. NE (50 μM and 500 μM) was added into the flasks and the culture was assayed for β-galactosidase activity at 25 ^{o}C at 4 h, 5.5 h, 6.5 h and 7.5 as previously described (170). The PA14 cells resuspended in ice-cold TEP buffer (50 mM Tris-HCl [pH 7.4], 5 mM EDTA, 1 mM phenylmethylsulfonyl fluoride) were sonicated for 30 s twice with an interval of 15 s to disrupt the cell membrane. Significant differences between experimental groups were determined using the Student's t-test at a level of significance of $p < 0.05$ or lower.

CHAPTER IV

CHEMOTAXIS TO THE GENERAL QUORUM-SENSING SIGNAL AI-2 REQUIRES THE TSR CHEMORECEPTOR AND THE PERIPLASMIC LSRB AI-2-BINDING PROTEIN

4.1 Overview

Autoinducer-2 (AI-2) is a quorum-sensing autoinducer made by Gram-positive and Gram-negative bacteria. In *Salmonella enterica* serovar Typhimurium, AI-2 binds to the periplasmic binding protein LsrB as (2*R*,4*S*)-methyl-2,3,3,4-tetrahydroxytetrahydrofuran (*R*-THMF). LsrB is the recognition component of an ABC transporter used for AI-2 uptake. Several different chemotaxis assays demonstrate that AI-2 is a potent attractant for *Escherichia coli* and *S. typhimurium*. The Tsr chemoreceptor and LsrB are necessary for sensing AI-2, although uptake of AI-2 into the cytoplasm is not. We conclude that Thr-61 and Asp-63 of LsrB, when bound to AI-2, interact directly with the periplasmic domain of Tsr, making LsrB the first known periplasmic-protein partner for Tsr. Chemotaxis toward a bacterial-cell-density signal like AI-2 may be an important virulence factor within the gastrointestinal (GI) tract and could help free-swimming, planktonic bacteria colonize developing biofilms.

---

*Reprinted in part with permission from "Chemotaxis to the quorum-sensing signal AI-2 requires the Tsr chemoreceptor and the periplasmic LsrB AI-2-binding protein" by Manjunath Hegde, Derek L. Englert, Shanna Schrock, Bill Cohn, Christian Vogt, Thomas K. Wood, Michael D. Manson, and Arul Jayaraman, 2011, *Journal of Bacteriology,* 193(3):768-773. Copyright by American Society for Microbiology

4.2 Introduction

Many functions in bacteria are regulated by population density, including formation of biofilms and production of virulence factors (171). Assessment of population density, known as quorum sensing, relies on the ability of cells to determine the concentration of compounds known as autoinducers (AIs). As the cell density increases, the AI accumulates to a concentration that triggers a quorum-sensing response. Autoinducers typically activate the expression of certain genes and repress the expression of others. The genes whose expression is induced typically include those responsible for production of the autoinducer, resulting in a positive feedback loop. In several well-studied systems, the cell densities required to accumulate enough AI for good induction are 10^8 per ml or higher.

AIs are of two basic types: species-specific and general (86). Species-specific AI-1s are usually acyl homoserine lactones in Gram-negative bacteria and modified peptides in Gram-positive bacteria. Induction of bacterial luciferase in the bioluminescent marine species *Vibrio fischeri*, the sole colonizer of the light organ of the Hawaiian bobtail squid, requires an AI-1 specific to that organism (172). The marine bacterium *Vibrio harveyi*, which colonizes the surface of dead organic matter, requires both a specific AI-1 and a general autoinducer, called AI-2 (173), for full induction of bioluminescence. AI-2 is derived from the spontaneous cyclization of the metabolite 4,5-dihydroxy-2,3-pentanedione (DPD). DPD is made from *S*-ribosylhomocysteine by the enzyme LuxS (87). *S*-ribosylhomocysteine is an intermediate in the breakdown of *S*-

adenosylhomocysteine, the product remaining after methyl-group donation by *S*-adenosylmethionine.

AI-2 is produced by a wide range of Gram-negative and Gram-positive bacteria and exists in multiple forms that are in equilibrium with each other (86). The form that is active in *V. harveyi* is (2*S*,4*S*)-2-methyl-2,3,3,4-tetrahydroxytetrahydrofuran borate (S-THMF borate) (88). This form of AI-2 binds to the periplasmic protein LuxP. In *S. typhimurium*, a boron-free isomer of AI-2 [(2*R*,4*S*)-2-methyl-2,3,3,4-tetrahydroxytetra-hydrofuran (R-THMF)] (**Fig. 4.1A**) binds to the periplasmic LsrB protein (89). LsrB is the recognition component of an ABC transporter for AI-2, and the *lsrB* gene is in the *lsrACDBFGE* operon. LsrACD are the membrane-bound components of the ABC transporter for AI-2. Following uptake, AI-2 is phosphorylated in the cytoplasm by the LsrK kinase and then further broken down by the products of the *lsrFG* genes (90). This operon is under the control of LsrR, a repressor that is inactivated upon binding of phosphorylated AI-2. Thus, AI-2 induces its own uptake and destruction, and auto-stimulation by self-produced AI-2 is transient (90). The production and possible fates of AI-2 in *S. typhimurium* are shown in **Fig. 4.1B**. *E. coli* also contains an Lsr uptake system similar to that of *S. typhimurium*. In *E. coli,* the membrane-bound YdgG (TqsA) protein has been implicated in AI-2 export from the cytoplasm (91).

Prior work has shown that AI-2 is a chemoattractant for *E. coli* (174, 175). However, the receptor(s) involved in AI-2 sensing has/have not been identified. In this study, we investigated the molecular mechanism underlying AI-2 chemotaxis in *E. coli* and show that the same system probably operates in *S. typhimurium*.

Fig. 4.1. Structure of AI-2 and post-production processing (**A**) Structure of AI-2. Although AI-2 exists in multiple forms that are in equilibrium with each other, only the R-THMF form of AI-2 that was found bound to LsrB in *S. typhimurium* (89) is shown. (**B**) Production, transport, sensing, and metabolism of AI-2. AI-2 is produced inside the cells in several steps during the degradation of *S*-adenosylhomocysteine (SAH). The last step in AI-2 (solid red pentagon) production is catalyzed by LuxS. AI-2 is secreted, most likely by TqsA (91), to the periplasm. It presumably passes freely in and out of the periplasmic space through porins in the outer membrane and equilibrates with the external environment. When AI-2 accumulates to a high enough level, it binds to the LsrB protein in the periplasm. LsrB-AI-2 may interact directly with the ligand-binding domain of the Tsr chemoreceptor to evoke an attractant response by inhibiting (red X) the activity of the CheA kinase and thus lowering the cytoplasmic concentration of the tumble regulator, phospho-CheY. LsrB associated with AI-2 can also bind to LsrACD, an ABC transporter that imports AI-2 into the cytoplasm, where it is phosphorylated by the LsrK kinase (89). Phospho-AI-2 binds to the LsrR repressor to induce transcription of the *lsrACDBFGE* operon. LsrF and LsrG together break down phospho-AI-2 into an unknown product (open red pentagon).

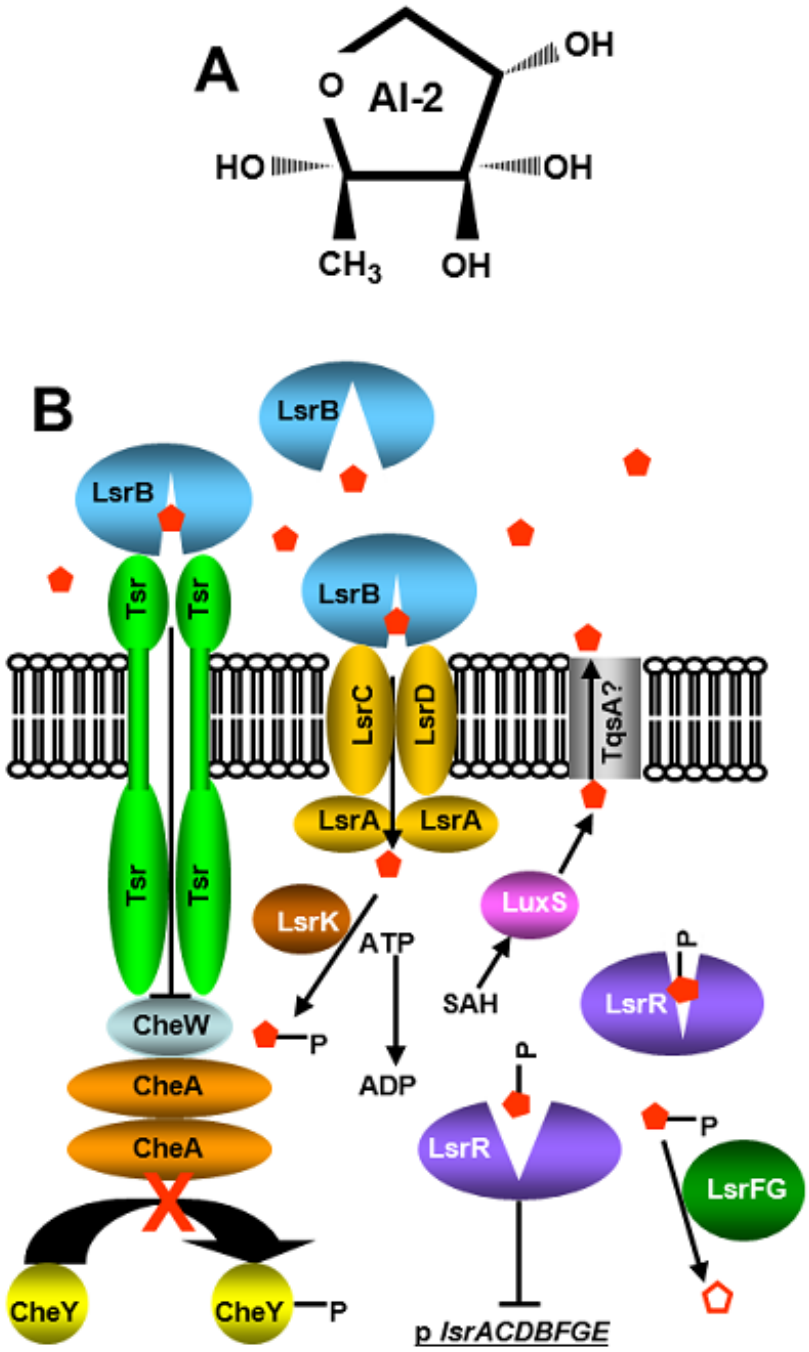
A
O
AI-2
OH
HO
OH
CH3
OH
B
LsrB
LsrB
LsrB
Tsr
Tsr
Tsr
Tsr
LsrC
LsrD
TqsA?
LsrA
LsrA
LsrK
ATP
ADP
P
LuxS
SAH
LsrR
P
CheW
CheA
CheA
CheY
CheY
P
LsrR
P
P
LsrFG
p lsrACDBFGE

4.3 Results

4.3.1 *Escherichia coli* chemotaxis toward AI-2 is mediated through Tsr and LsrB

The microPlug (μPlug) assay (176), a modified plug-in-pond assay, provides a qualitative but highly visual representation of chemotaxis (**Fig. 4.2**). The responses of *E. coli* strain CV1 and its isogenic *tsr* and *lsrB* mutant derivatives are shown in **Fig. 4.3**. In the absence of AI-2 in the plug, CV1 cells distributed themselves randomly (**Fig. 4.3A**). However, when CV1 cells were exposed to plugs containing 200 μM *L*-serine or 200 μM AI-2, they exhibited strong attractant responses, shown by the accumulation of bacteria at the agarose plug-liquid interface (**Fig. 4.3B** and **C**). Strain CV5 (CV1 Δ*tsr*), which lacks the *L*-serine receptor Tsr, did not respond to *L*-serine (**Fig. 4.3D**) and gave a severely attenuated response to AI-2 (**Fig. 4.3E**). Strain CV12 (CV1 Δ*tar-tap* Δ*trg*), which has Tsr as its only functional receptor (other than Aer), responded to both *L*-serine and AI-2 (data not shown), although the accumulation was somewhat decreased relative to that of strain CV1. Thus, Tsr is both necessary and sufficient for good AI-2 chemotaxis in *E. coli* K-12, although there may be a small residual response in cells lacking Tsr.

Because AI-2 is known to bind to the periplasmic protein LsrB, we also looked at the responses of MJ101 (CV1 *lsrB*ΩKan^r) cells. These cells responded like strain CV1 to *L*-serine (**Fig. 4.3F**) but showed no accumulation around plugs containing 200 μM AI-2 (**Fig. 4.3G**). In contrast, MJ102 (CV1 *lsrC*ΩKan^r) cells, which should still produce LsrB

but not be able to take up AI-2 into the cytoplasm, accumulated around plugs containing 200 μM *L*-serine (data not shown) and 200 μM AI-2 (**Fig. 4.3H**). The accumulation to AI-2 was somewhat weaker than that of strain CV1, perhaps because of a polar effect of the *lsrC*ΩKan^r insertion on the downstream *lsrB* gene in the *lsrACDBFGE* operon (177). MJ101 cells containing plasmid pCA24N-$P_{T5\text{-}lac}$*::lsrB*, which encodes wild-type *E. coli* LsrB, accumulated around AI-2-containing plugs about as well as MJ102 cells (data not shown) when 1 mM isopropyl β-D-1-thiogalactopyranoside (IPTG) was added to induce LsrB synthesis.

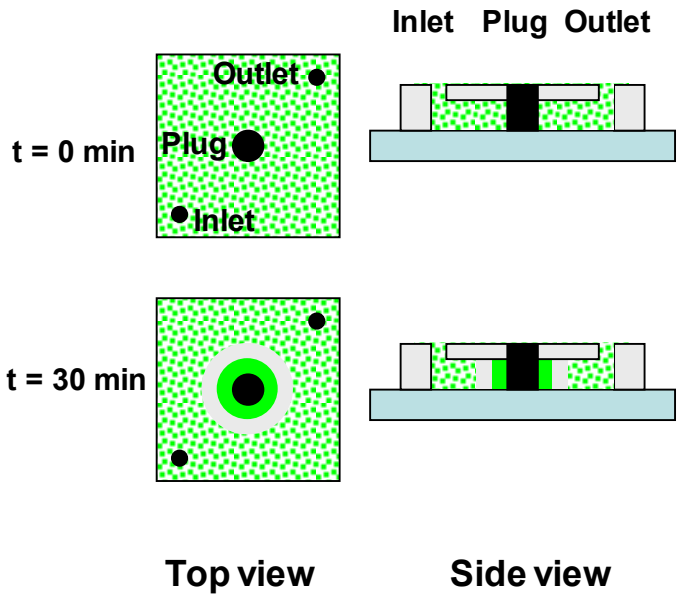

Fig. 4.2. Schematic of the modified μPlug assay. Both top and side views of the chamber are shown. GFP-labeled bacteria suspended in CB were introduced at the inlet, and the outlet allowed escape of air. The agarose plug contained CB plus *L*-serine or AI-2 at the desired concentration. The plug was visualized by addition of 5% bromophenol blue to provide optical contrast. Gradients in the bacterial suspension form by diffusion of attractant out of the plug. Gradients develop rapidly and are relatively steep. The cartoon shows the distribution of GFP-labeled cells when they are first introduced (t = 0 min) and at the end of the experiment (t = 30 min)**.**

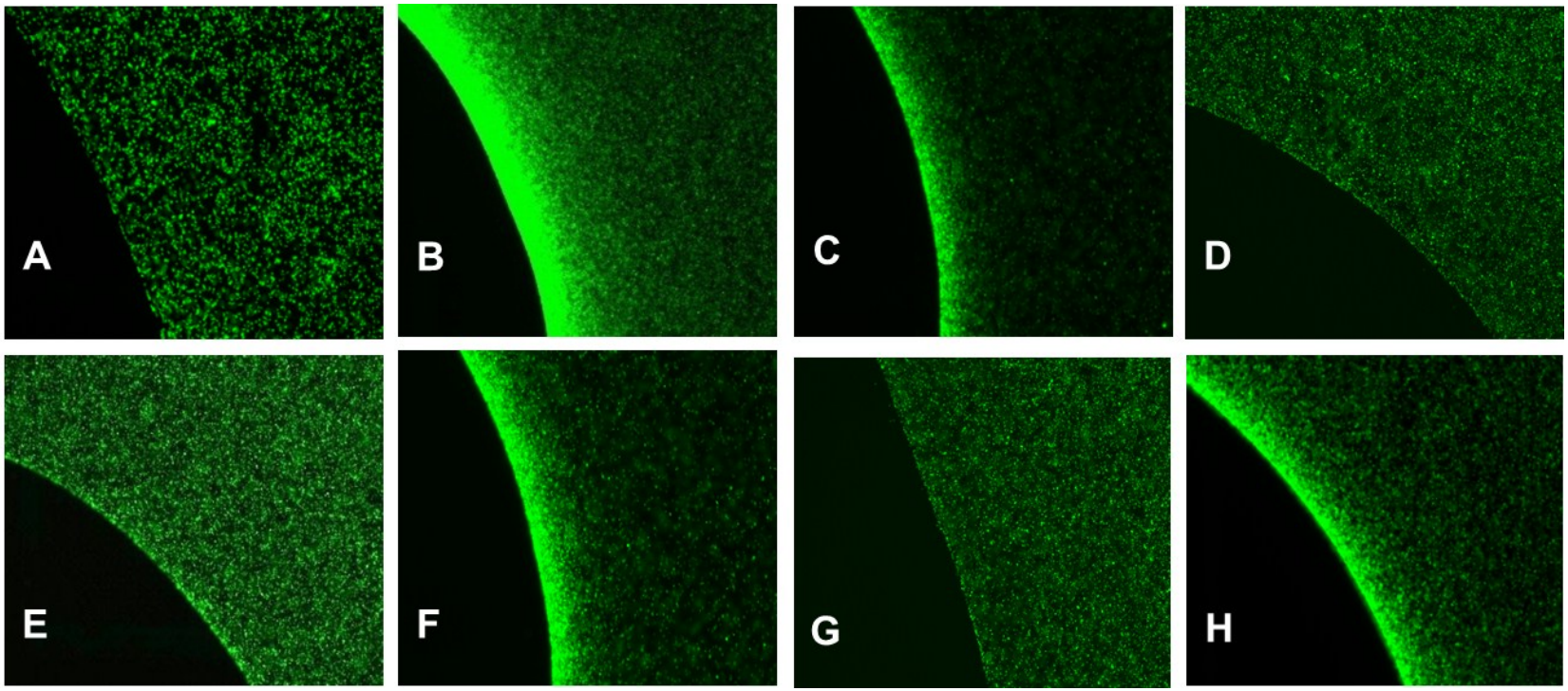

Fig. 4.3. Chemotactic responses to *L*-serine and AI-2 in the μPlug assays. Panels A-H show the results of μ (**A**) Distribution of wild-type (CV1) cells in the absence of any attractant in the plug. (**B**) Distribution of wild-type (CV1) cells with 200 μM *L*-serine in the plug. (**C**) wild-type (CV1) cells with 200 μM AI-2 in the plug. (**D**) Δ*tsr* (CV5) cells with 200 μM *L*-serine in the plug. (**E**) Δ*tsr* (CV5) cells with 200 μM AI-2 in the plug. (**F**) *lsrB*ΩKan^r (MJ101) cells with 200 μM *L*-serine in the plug. (**G**) *lsrB*ΩKan^r (MJ101) cells with 200 μM AI-2 in the plug. (**H**) Distribution of *lsrC*ΩKan^r (MJ102) cells with 200 μM AI-2 in the plug.

To quantify the response to AI-2 and to compare it to the response to *L*-serine, we performed capillary assays (178). As expected from the μPlug assay results, CV1 and CV12 cells accumulated in capillaries containing either *L*-serine or AI-2 (**Fig. 4.4A**), with the CV1 strain giving a stronger response, whereas CV5 (Δ*tsr*) cells did not accumulate in capillaries containing either compound. MJ101 cells (*lsrB*ΩKan^r) responded to *L*-serine but not to AI-2, whereas MJ102 cells (*lsrC*ΩKan^r) responded to both (**Fig. 4.4B**). Thus, the conclusions from the μPlug assay were confirmed.

By plotting the data from the capillary assay on a log/log plot, we could extrapolate back to a threshold concentration for both compounds in each strain (179). With *L*-serine, the extrapolated detection thresholds for strains CV1, CV12, and MJ101 are all in the range of 2-4 X 10^{-12} M (**Fig. 4.4C**). The result is quite different with AI-2, because strains CV1 and CV12 have extrapolated detection thresholds of ~5 X 10^{-12} and 2 X 10^{-11} M (**Fig. 4.4D)**, respectively, but the extrapolated detection threshold for the LsrC$^-$ strain MJ102 is at least 100-fold lower at ~2 X 10^{-14} M (**Fig. 4.4D).** This is the result expected if the periplasmic AI-2 concentration in MJ102 cells is higher than in CV1 cells, because in the latter strain AI-2 is being cleared from the periplasm by transport into the cell. The same phenomenon has been seen with cells containing maltose-binding protein in the absence of a functional maltose transport system (180).

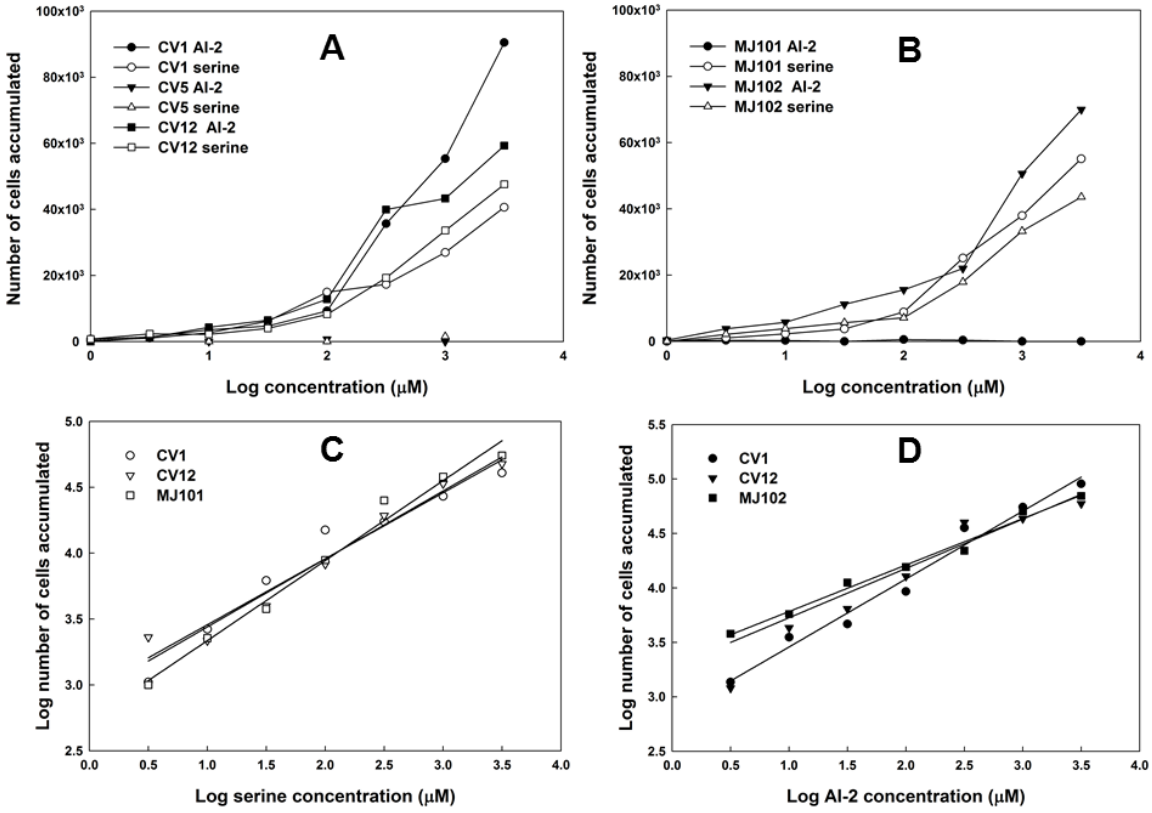

Fig. 4.4. Responses of cells to *L*-serine and AI-2 in the capillary assay. Background accumulations in buffer-only capillaries were in the range of 500-1000 cells. (**A**) Normalized (buffer-only control subtracted) values of CV1 (wt) cells, CV5 (Δ*tsr*) cells, and CV12 (Δ*tar-tap* Δ *trg*) cells exposed to capillaries containing *L*-serine (open symbols) or AI-2 (closed symbols). (**B**) Normalized values of CV1 cells, MJ101 (*lsrB*ΩKan^r) cells, and MJ102 (*lsrC*ΩKan^r) cells exposed to capillaries containing *L*-serine (open symbols) or AI-2 (closed symbols). (**C**) The data for the responses of the CV1, CV12, and MJ101 cells to *L*-serine plotted on a log-log scale. The straight lines are linear regressions can be extrapolated back to a threshold value. The extrapolated threshold concentrations, as predicted by Weber's law, are 1.7 x 10^{-12} for strain CV12 and 3.5 x 10^{-12} M for strain CV1 and MJ101. The regression lines for CV12 and MJ101 are identical. (**D**) The data for the responses of CV1, CV12, and MJ102 cells to AI-2 plotted on a log-log scale. The linear regressions can be extrapolated back to a threshold value. The extrapolated threshold concentrations are 1.6 x 10^{-11} for strain CV1, 4.6 x 10^{-12} M for strain CV12, and 2.5 x 10^{-14} M for strain MJ102.

To test the relative sensitivity of cells to *L*-serine and AI-2 in an independent assay, we employed the μFlow device (176, 181). The gradients were created in two ways. In the first scenario, a linear gradient was generated across the 1050 μm width of the microfluidic observation chamber by utilizing two input channels delivering 0 and 200 μM chemoeffector, respectively. In the second scenario, a non-linear gradient was generated by using five input channels to deliver 0, 0, 2, 20, and 200 μM chemoeffector, respectively. The configurations of the device and the resulting gradients are shown in **Fig. 4.5**. The concentration at the entry point for the cells was 100 μM in the linear gradient and 2 μM in the non-linear gradient, and the cells were pre-equilibrated with these concentrations prior to their introduction into the observation chamber. The distribution profiles of fluorescently labeled CV1 cells in *L*-serine and AI-2 are shown in **Fig. 4.6**. For each set of conditions, the chemotaxis migration coefficients (CMC values; (181, 182)) were calculated and are shown in **Fig. 4.6**. CV1 cells responded to non-linear and linear gradients of AI-2 (**Fig. 4.6D** and **F**) with similar CMC values (0.24 and 0.25), but they responded significantly only to the non-linear gradient of *L*-serine, in which the gradient is very steep at the point at which the cells enter the chamber (compare **Fig. 4.6C** and **E**). Even in the non-linear gradient, the CMC value for *L*-serine was only 0.13, about 50% that of the CMC value for AI-2. These results are consistent with the idea that chemotaxis to AI-2 is more sensitive at higher chemoeffector concentrations than is chemotaxis to *L*-serine.

We also tested the MJ102/pCA24N-$P_{T5\text{-}lac}$*::lsrB* strain in a non-linear AI-2 gradient in the μFlow device (data not shown). It gave a CMC value of 0.18, lower than the value

for CV1 cells in non-linear AI-2 gradients but higher than that for CV1 cells in non-linear gradients of *L*-serine. At present, we have no way of measuring periplasmic levels of LsrB, but the somewhat attenuated response of MJ102/pCA24N-$P_{T5\text{-}lac}$*::lsrB* cells relative to wild-type cells could reflect a decreased level of LsrB in the complemented strain.

4.3.2 Tsr and LsrB are required for AI-2 chemotaxis in *S. typhimurium*

We asked whether the pathogenic strain 14028 of *S. typhimurium* was also attracted to AI-2. The parental strain swam toward plugs containing 200 μM *L*-serine or AI-2 (**Fig. 4.7A and B**), whereas a Δ*tsr* derivative of strain 14028 responded neither to *L*-serine nor AI-2 (**Fig. 4.7C and D**), indicating that Tsr is required for AI-2 chemotaxis in *S. typhimurium*. *S. typhimurium* strain MET259 (14028 *lsrB::mudJ*) (183), which lacks LsrB, also did not respond to AI-2 in the μPlug assay (**Fig. Fig. 4.7E**), whereas *S. typhimurium* strain MET235 (183) (14028 *lsrC::mudJ*) cells lacking LsrC did (**Fig. 4.7F**). Again, the response of strain MET235 to AI-2 might be attenuated by polarity of the *lsrC::mudJ* insert on *lsrB* expression. We conclude that AI-2 chemotaxis in *S. typhimurium* is also mediated through Tsr and LsrB. Accumulations around the plug were consistently lower with *S. typhimurium* than with *E. coli*, perhaps because the higher swimming speed of *S. typhimurium* minimized accumulation.

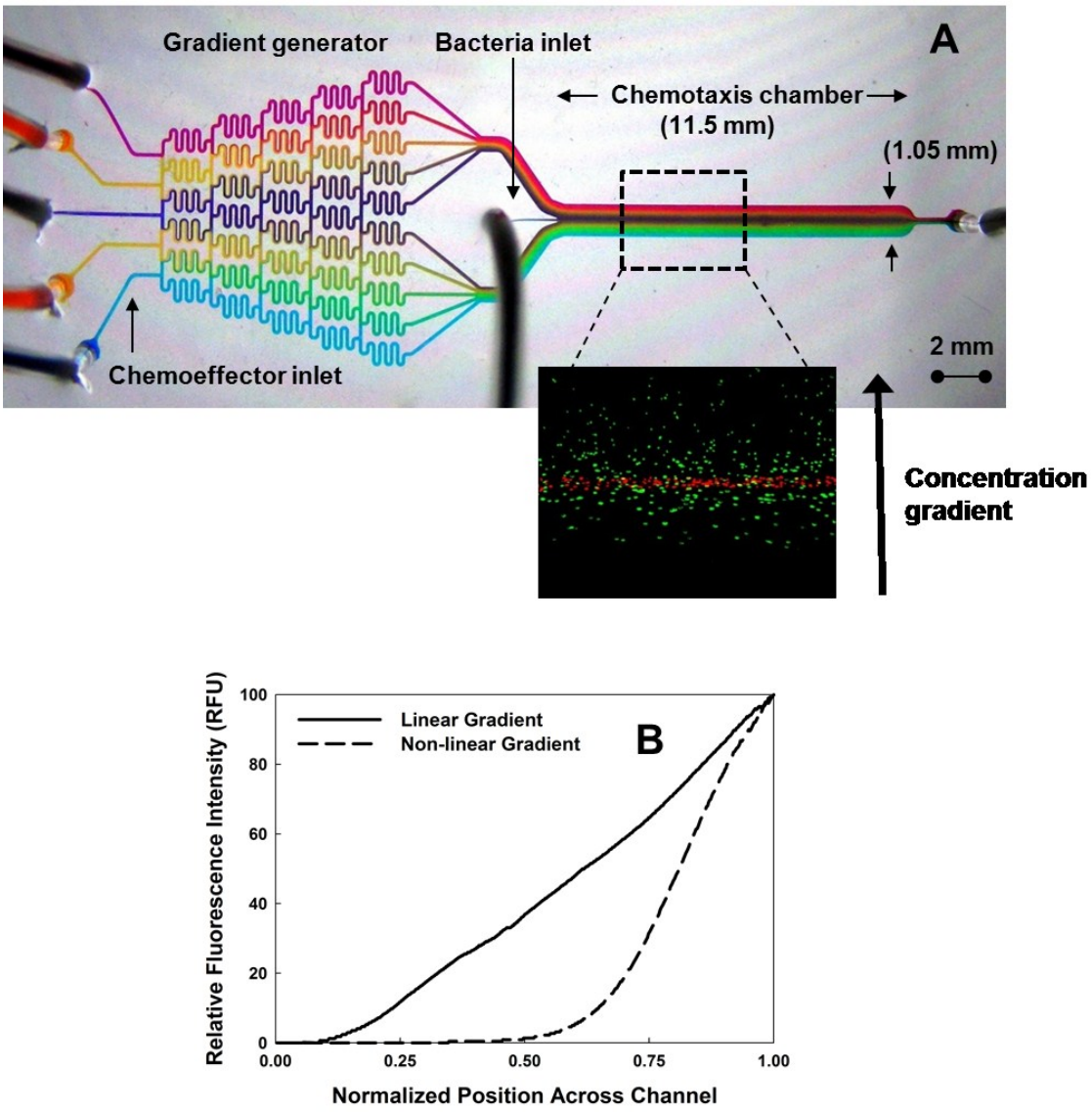

Fig. 4.5. The µFlow device (***A***) Schematic representation of the µFlow chemotaxis device. The device consists of a gradient-mixing module with five inlets and a chemotaxis observation chamber (20 x 1050 x 11500 µm). The bacterial inlet is 50 µm. For visualization, a gradient made from dyes of five different colors is shown. Inset shows a representative snapshot of cells moving up a concentration gradient. (***B***) Formation of concentration gradients in the µFlow device. Linear (black line; generated using two inputs) and non-linear (red line; generated using five inputs) concentration gradients of 0 – 100 ng/mL of fluorescein isothiocyanate (FITC) were established in the chemotaxis observation chamber. Fluorescence images were acquired after 30 min, and the fluorescence intensity was determined at 16 µm intervals using Matlab.

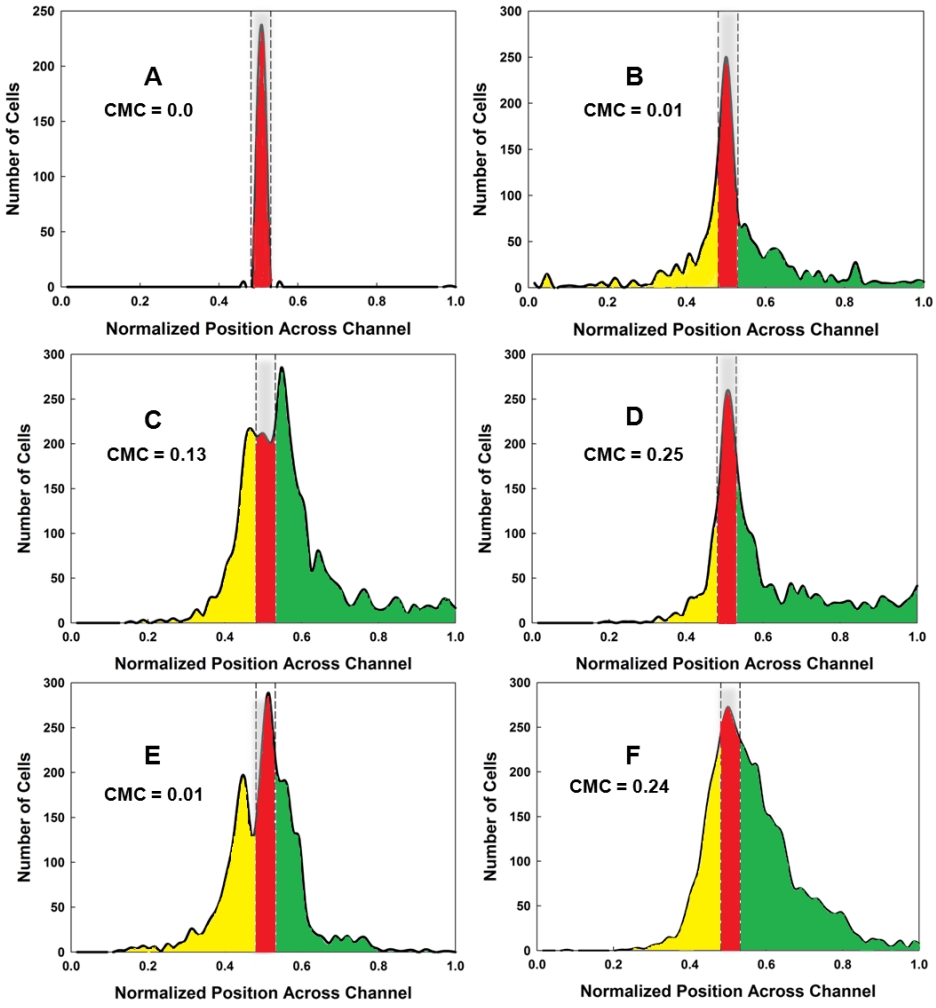

Fig. 4.6. Assays of chemotactic behavior in the μFlow device. (A) Typical distribution of RFP-labeled dead cells, shown in red. The distribution of cells from one run is shown; it is typical for that found for RFP-labeled dead cells in all runs. The area occupied by dead cells is delineated by the gray bar enclosed in dashed lines. (B) Typical distribution of CV1 (wt) GFP-labeled cells in the absence of a chemoeffector gradient. The distribution of cells moving in the up-gradient direction beyond the "dead" zone is highlighted in green, and the distribution of cells moving in the down-gradient direction is highlighted in yellow. GFP-labeled cells remaining in the region occupied by dead cells (highlighted in red) were not included in the calculation of CMC values. (C) Typical distribution of CV1 cells in a 0-200 μM non-linear gradient of *L*-serine. (D) Typical distribution of CV1 cells in a 0-200 μM non-linear gradient of AI-2. (E) Typical distribution of CV1 cells in a 0-200 μM linear gradient of *L*-serine. (F) Typical distribution of CV1 cells in a 0-200 μM linear gradient of AI-2. All assays were run a minimum of three times. CMC values are indicated on the graphs.

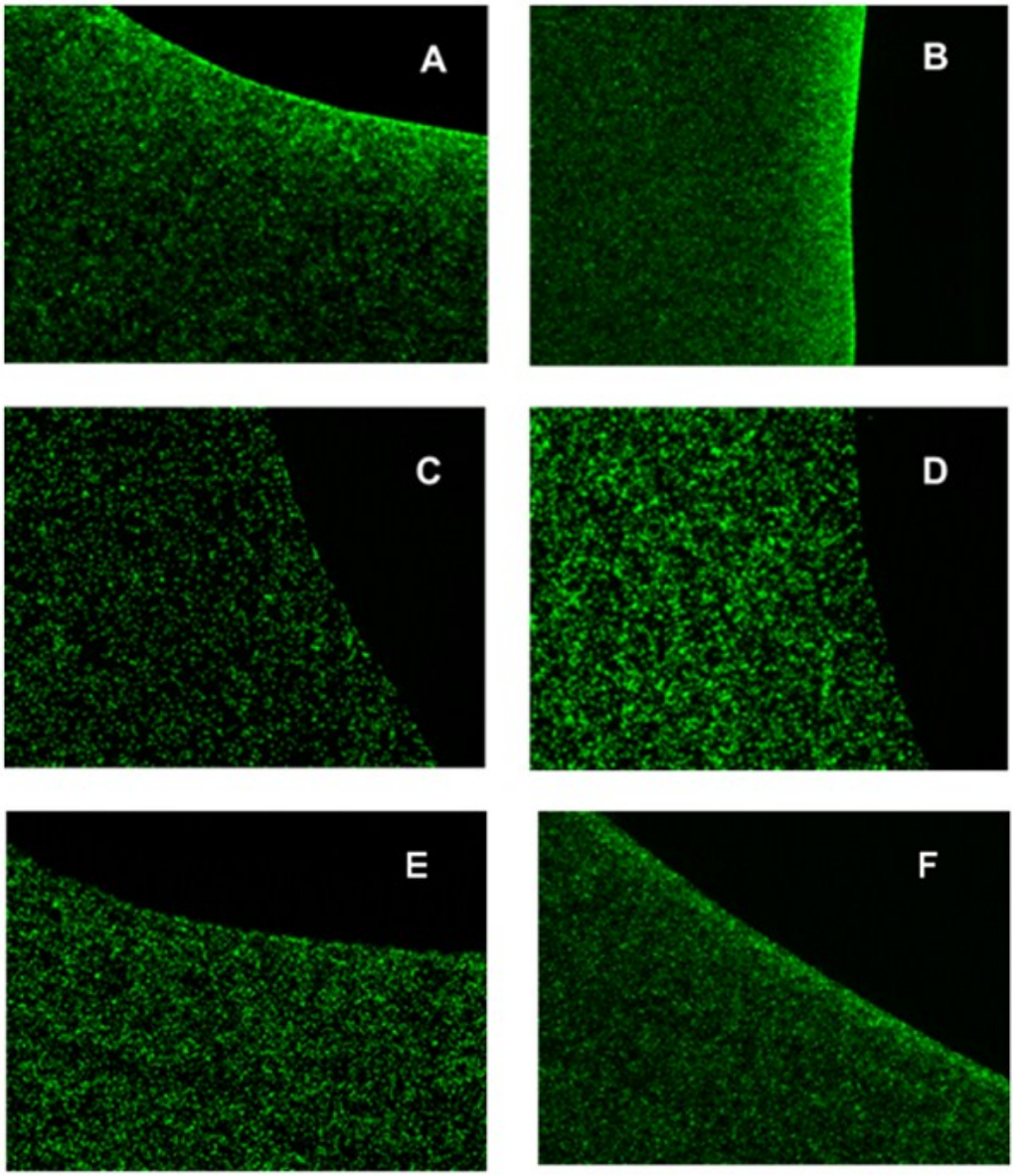

Figure 4.7. Response of *S. typhimurium* to *L*-serine and AI-2 in the μPlug assay. Cells were resuspended in chemotaxis buffer, added to the μPlug device, and incubated at room temperature for 30 min. (**A**) *S. typhimurium* strain 14028 exposed to 200 μM *L*-serine in the plug. (**B**) 14028 exposed 200 μM AI-2 in the plug. (**C**) 14028 Δ*tsr* exposed to 200 μM *L*-serine in the plug. (**D**) 14028 Δ*tsr* exposed to 200 μM AI-2 in the plug (**E**) *S. typhimurium* strain MET259 (*lsrB::mudJ*) exposed to 200 μM AI-2 in the plug. (**F**) *S. typhimurium* strain MET235 (*lsrC::mudJ*) exposed to 200 μM AI-2 in the plug. Fluorescence images were taken at t = 30 min.

4.3.3 LsrB-AI-2 complex binds the periplasmic domain of Tsr

Zhang *et al*. (184) used the known structures of the periplasmic domain of *E. coli* Tar and the maltose binding protein (MBP) along with results of a mutational analysis, to develop a computationally derived model for the docking of MBP with Tar. In the model, the two domains of MBP contact the two subunits of the periplasmic domain of Tar. Since the periplasmic binding domains of Tar and Tsr are similar (**Fig. 4.8), and** structures for the ligand (AI-2)-bound LsrB (185) and the periplasmic domain of Tsr (186) are also available, we developed a computer-generated model for the Tsr/LsrB interaction using the MBP/Tar simulation as a guide. We developed an energy-minimized docking structure for AI-2-bound LsrB and Tsr (**Fig. 4.9B and D**) that was based on the docking model for maltose-bound MBP and Tar (**Fig. 4.9A and C**) (184). AI-2 bound to LsrB was docked with Tsr (187) by bringing the two proteins as close to each other as possible using the SPOCK software package. Next, the molecular dynamics module of the AMBER software package (188) was used to allow the side chains to repack in order to minimize the energy of interaction between the two proteins, so that regions in both binding clefts of LsrB that that possibly interact with Tsr could be identified. The amino acid regions of LsrB that were identified as possibly interacting with Tsr were positions 56-65 in the β2 sheet, and positions 196-211 and 221-236 in the α helices 6 and 7, respectively (**Fig. 4.10**). Thr-61 and Asp-63 in LsrB were found to be the closest to Asp 143 and Lysine 145 of the T subunit of Tsr. Thus, LsrB/Tsr docking served as the starting point for targeting areas of the LsrB and Tsr proteins for

mutational analysis in order to identify regions involved in the interactions of these two proteins.

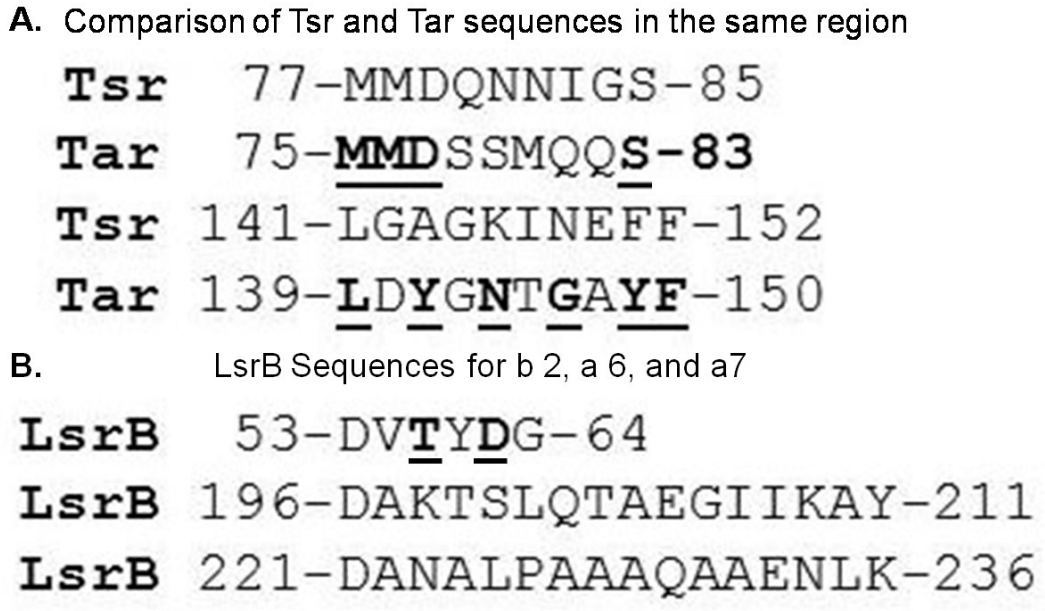

Fig. 4.8. Amino acid sequences in Tsr and LsrB that are candidates for Ala-scanning mutagenesis based on the computer-generated LsrB/Tsr docking model. (**A**) Tsr regions predicted to be in contact with LsrB; below the Tsr sequences, the equivalent sequences in *E. coli* Tar are shown. Bold-faced, underlined residues in the Tar sequence show positions at which residue substitutions gave specific defects in maltose chemotaxis. (**B**) LsrB regions to be in contact with Tsr; they correspond to β strand 2 and α helices 6 and 7.

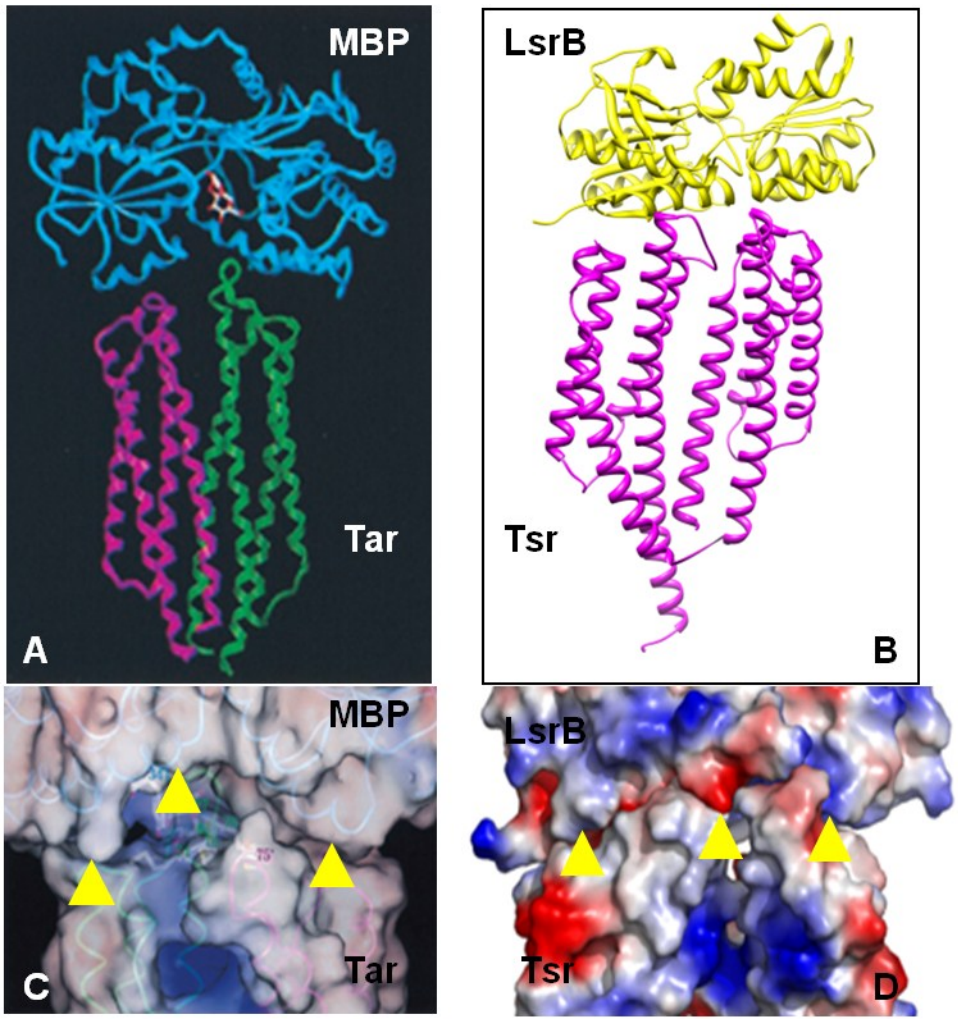

Fig. 4.9. Docking models for periplasmic binding proteins and chemoreceptors (MCPs). (**A**) The energy-minimized MBP/Tar docking model (184). MBP is shown in blue, and the two subunits of *E. coli* Tar are shown in magenta and green. (**B**) The energy-minimized LsrB/Tsr docking model. LsrB is shown in yellow, and the two subunits of *E. coli* Tsr are shown in magenta. (**C**) Close-up of the MBP/Tar interface in a space filling model. Positive surface charge is indicated in blue, negative surface charge is indicated in red. The yellow arrowheads point to the closest approach of MBP to Tar. (**D**) Close-up of the LsrB/Tsr interface in a space filling model. The yellow arrowheads point to the closest approach of LsrB to Tsr.

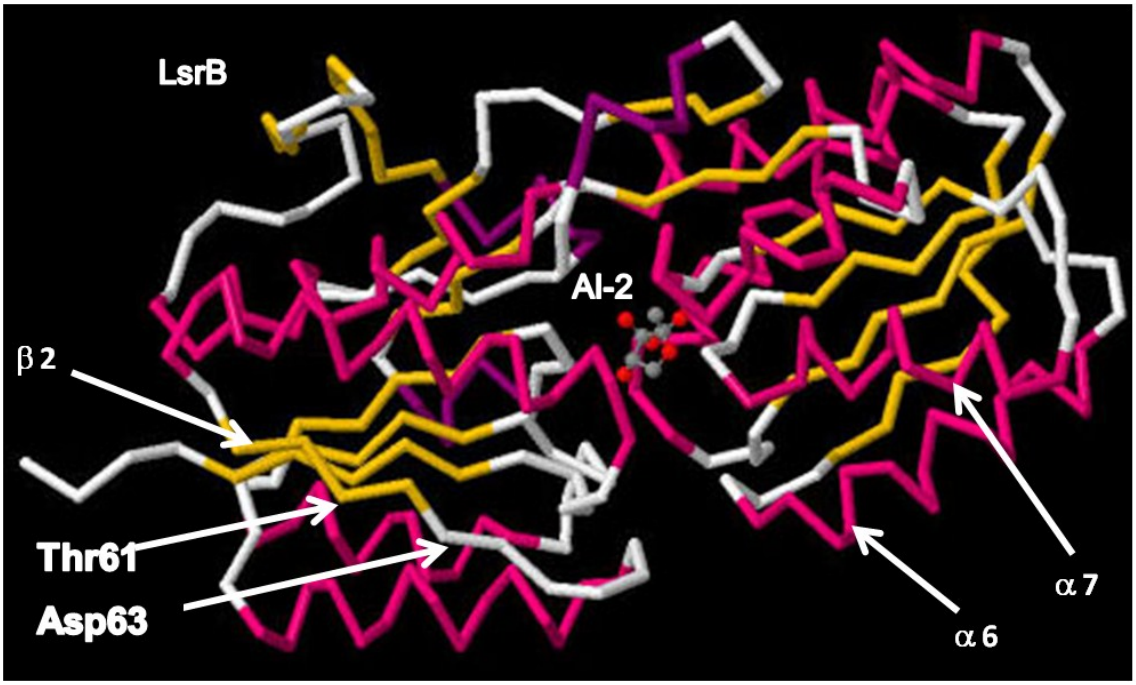

Fig. 4.10. 3-D geometry of LsrB in complex with AI-2 showing regions interacting with β2 and α6-7 regions interacting with periplasmic domain of Tsr (185).

4.3.4 Mutational analysis to identify regions of interactions between LsrB and Tsr

Based on the docking model, we performed site directed alanine scanning mutagenesis by replacing every amino acid in the region 56-65 of LsrB with alanine. We also replaced two amino acids that were predicted to be the closest amino acids interacting with Tsr - Thr-61 and Asp-63 - to isoleucine and valine, respectively. The amino acid substitutions that are most important for AI-2 sensing by Tsr were identified using capillary assays. At the highest concentration tested (1 mM), the net accumulation of CV1 Δ*lsrB* cells complemented with plasmid producing LsrB wt (i.e., the native LsrB protein) in the capillary varied between 70,000 and 86,000 (**Fig. 4.11A and B**). The chemotaxis response of the alanine substitutions to AI-2 was attenuated compared to the

unmodified LsrB protein. Among the ten alanine substitutions tested, T61A and D63A were the two substitutions that significantly reduced the response to 1 mM AI-2 by ~2.1 and 3.3 fold respectively (**Fig. 4.11A**). When threonine (polar) at position 61 was changed to isoleucine (nonpolar), the response to 1 mM AI-2 was ~2 fold less than the native LsrB protein (**Fig. 4.11B**). However, when the polar amino acid Asp (position 63) was changed to the non-polar valine, the response to 1 mM AI-2 was reduced further to ~4.7 fold (**Fig. 4.11B**). These results along with those obtained from alanine substitutions indicated that Thr-61 and Asp-63 are important in the LsrB/Tsr interaction, and validates the prediction of the docking model. We further confirmed this by making a double substitution of amino acids 61 and 63 (T61A D63A) (**Fig. 4.11A**) and T61I D63V (**Fig. 4.11A**), which removed AI-2 chemotaxis. The P65A (**Fig. 4.11A**) replacement abolished AI-2 chemotaxis as the accumulation inside the capillary upon exposure to 1 mM AI-2 was comparable to the control. Since proline is an important residue required for protein folding, it is possible that replacing proline altered the overall structure of LsrB and changed its interaction with AI-2 and Tsr.

Since LsrB is also involved in AI-2 uptake (189), we also performed the AI-2 uptake assay (27) to investigate if the amino acid substitutions in LsrB affected the transport of AI-2 into the cell. All the single amino acid substitutions between positions 56 and 64 did not affect AI-2 uptake as the intra-cellular accumulation of AI-2 was with the different substitutions was similar to that seen with the native LsrB protein. However, the P65A substitution demonstrated ~30 fold less AI-2 uptake than the unmodified LsrB

protein, which further confirmed that the proline substitution altered the overall structure of LsrB.

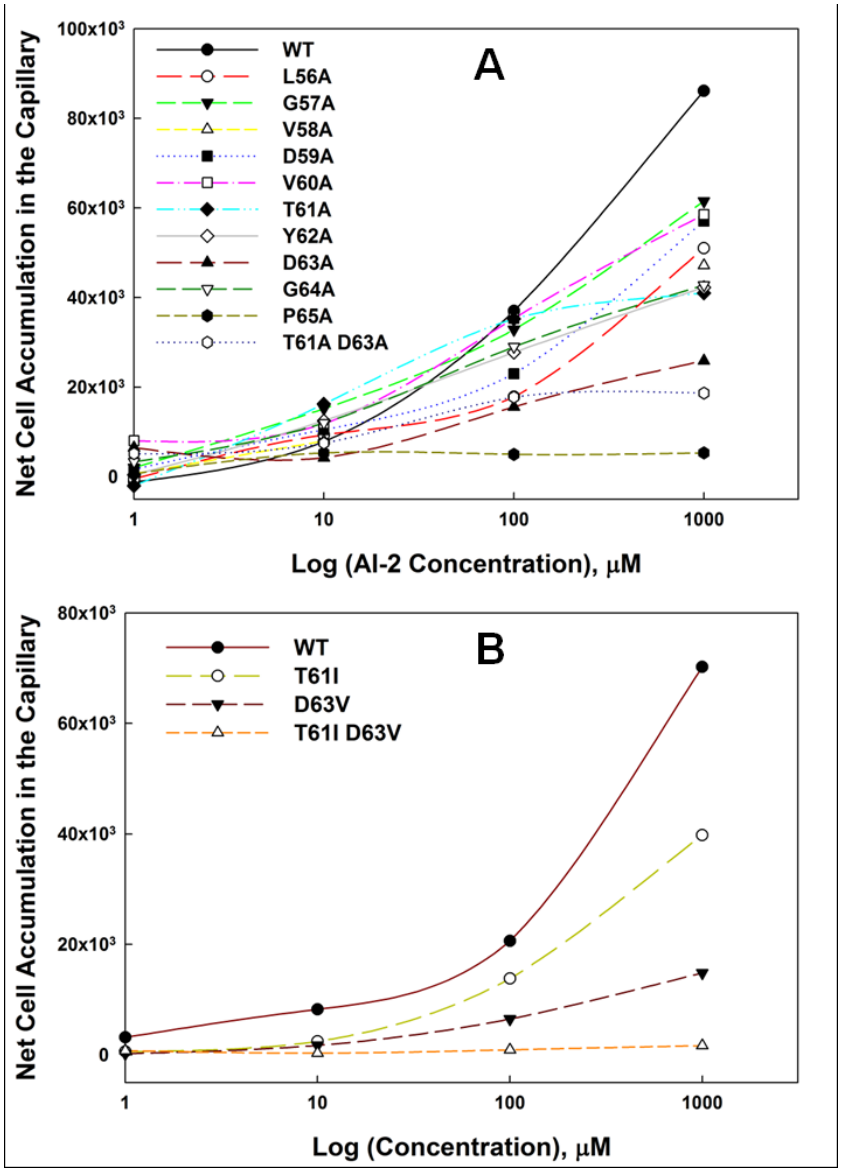

Fig. 4.11. Capillary assays with CV1 Δ*lsrB* complemented with *lsrB* mutated at codons for amino acid positions in the β2 sheet of LsrB. (**A**) comparison of cells accumulated in the capillary with LsrB wt producing CV1 Δ*lsrB* versus those producing LsrB with substitution in each amino acid between positions 56-65 with alanine. (**B**) Comparison of cells accumulated in the capillary with LsrB wt producing CV1 Δ*lsrB* versus those producing mutated LsrB, in which threonine (T) at position 61 is replaced by isoleucine (I) and/or aspartic acid (D) at position 63 is replaced by valine (V).

4.4 Discussion

In this chapter, we report that AI-2 is sensed as a chemoattractant by non-pathogenic *E. coli* and pathogenic *Salmonella typhimurium* through the Tsr chemoreceptor. Tsr analogues have been reported in many bacterial species (190), and it seems possible that all motile bacteria that produce both Tsr and LsrB exhibit chemotaxis to AI-2.

Tsr is the only one of the four canonical chemoreceptors of *E. coli* not known to interact with a substrate-binding protein. The reason why LsrB is essential for chemotaxis to AI-2 is not known. The role of LsrB in chemotaxis does not seem to be essential for transport of AI-2 into the cytoplasm, because strain MJ102, which carries the *lsrC*ΩKan^r mutation, is defective for AI-2 transport (191) but is still able to carry out AI-2 chemotaxis. By analogy with other binding-protein-dependent chemoreceptors systems, such as maltose-binding protein (MBP) and Tar (180), it may be that AI-2-bound LsrB assumes a conformation that enables it to interact with Tsr directly in the periplasm. Similar interactions have been postulated for the involvement of galactose-binding protein (192) and ribose-binding protein (193) with the Trg chemoreceptor in taxis to those two sugars, and for dipeptide-binding protein with Tap (194).

Although we do not know the level of LsrB present in the periplasm of cells grown under various conditions, it is likely to be lower than other binding proteins, which typically far outnumber their cognate membrane-bound partners in a transport system. The K_D for AI-2 binding to LsrB has been reported as ~160 μM (195), which is higher by a factor of a hundred than the K_D values of most sugar-binding proteins for their ligands. Thus, the typical binding-protein paradigm of high affinity for ligand but low

affinity for the chemoreceptor partner, as seen with maltose, MBP, and Tar (180), could be very different for AI-2, LsrB, and Tsr.

AI-2, unlike other known attractants for *E. coli*, does not serve as food for bacteria (177), but is, rather, an intra-specific and inter-specific signal of cell density. Therefore, chemotaxis to AI-2 may not have the rather narrow dose-response range that is characteristic of most indirectly binding chemoattractants (196). For nutrients, migration to concentrations higher than those needed for the maximum rate of uptake has no selective value. Given that AI-2 is produced by many different species of biofilm-forming bacteria (197), it may be that chemotaxis to AI-2 serves to recruit free-swimming, planktonic bacteria to biofilms (198). If so, there is no obvious reason why the response to AI-2 should saturate; the selective pressure may be to swim as close as possible to a source of AI-2. We are currently characterizing the molecular mechanism of AI-2 chemotaxis in order to understand how it has evolved to match to the ecological context in which AI-2 chemotaxis occurs.

4.5 Summary

Given that AI-2 has been reported as a universal quorum-sensing molecule and inter-species signal, chemotaxis to AI-2 by both pathogenic and non-pathogenic bacteria is likely to be important in microbial ecology and virulence. Indeed, several bacterial species that colonize the oral cavity or the human gastrointestinal (GI) tract are known to produce AI-2 or to possess the *luxS* gene needed for its production. AI-2 chemotaxis may ultimately serve as a mutually beneficial, general chemical homing device that

allows aggregations of bacteria to recruit new members and that enables free-swimming, planktonic bacteria to identify and join such aggregates.

4.6 Materials and methods

4.6.1 Bacterial strains, materials, and growth media

Strain CV1, which is equivalent to strain RP437 (199), was used as the wild-type *E. coli* strain for chemotaxis, and strain 14028 was used as the wild-type *S. enterica* serovar Typhimurium. All relevant strains and plasmids are listed in **Table 4.1**. Tryptone broth (TB; 10 g/L tryptone and 8 g/L NaCl) was used to grow *E. coli*, and lysogeny broth (LB; 10 g/L tryptone, 5 g/L yeast extract, and 10 g/L NaCl) was used to grow *S.* Typhimurium. Chemically synthesized DPD (3.9 mM), dissolved in water, was purchased from Omm Scientific (Dallas, TX). *L*-serine was obtained from Fisher Scientific (Fair Lawn, NJ).

4.6.2 Fabrication of the µPlug and µFlow microfluidic devices

Microfluidic devices were fabricated as previously described (175, 200) in the Materials Characterization Facility at Texas A&M University. Briefly, device designs were drawn in AutoCAD and used to create a high-resolution (>3000 dpi) photolithography mask with a laser printer (Advanced Reproductions, North Andover, MA). Standard photolithography techniques, using an SU-8 2050 photoresist (Microchem Corp, MA), generated imprints of the microfluidic devices on silicon.

Table 4.1. Bacterial strains and plasmids

Strain or Plasmid	Genotype	Resistance[a]	Source
Escherichia coli			
CV1	Chemotaxis wild type (same as RP437)	Str	(203)
TG1/pDS-Red Express	Wild type, dead cell control	Amp	Stratagene
CV5	CV1 Δ*tsr*	Str	This study[b]
CV12 *lsrC*ΩKan^r	CV1 Δ*tar-tap trg*::Tn*10*	Str Tet	This study[c]
MJ101	CV1 *lsrB*ΩKan^r	Str Kan	This study[d]
MJ102	CV1 *lsrC*ΩKan^r	Str Kan	This study[e]
BW25113 *lsrB*ΩKan^r	*lsrB*ΩKan^r	Kan	(204)
BW25113 *lsrC*ΩKan^r	*lsrC*ΩKan^r	Kan	(204)
Plasmids			
pCM18	GFP-expressing vector	Erm	(205)
pDS-RedExpress	RFP-expressing vector	Amp	Clonetech
pCA24N-*lsrB*	pCA24N $P_{T5\text{-}lac}$::*lsrB*; expresses *E. coli* LsrB from p*lacZYA*	Cm	(206)

[a] Str-streptomycin, Tet-tetracycline, Kan-kanamycin, Erm-erythromycin, Amp-ampicillin, Cm-chloramphenicol

[b] Made by introducing Δ*tsr9101* (207) into CV1 by phage P1 transduction (208) with selection for Thr$^+$ and screening for Tsr$^-$.

[c] Made in two steps: Δ*tar-tap5201* (209) was introduced into CV1 by phage P1 transduction with selection for Eda$^+$, followed by screening for Tar$^-$, then *trg*::Tn*10* was introduced by phage P1 transduction followed by selection for Tet^r on lysis broth (LB; (170)) agar plates contain 10 μg/mL tetracycline, followed by screening for Trg$^-$.

[d] Made by introducing *lsrB*ΩKan^r (204) into CV1 by phage P1 transduction with selection for Kan^r and confirmation of the *lsrB* gene disruption by PCR.

[e] Made by introducing *lsrC*ΩKan^r (204) into CV1 by phage P1 transduction with selection for Kan^r and confirmation of the *lsrC* gene disruption by PCR.

wafers. The silicon-wafer templates, called SU-8 masters, were used as negative molds to generate the chemotaxis devices in poly(dimethyl)siloxane (PDMS), using standard soft-lithography protocols (175). Chamber dimensions were measured using a profilometer. Devices were fabricated by bonding the patterned PDMS slab to clean glass slides, using oxygen-plasma bonding in a plasma etcher (100 mTorr, 100 W, 40 sec) to create optically transparent devices. Access ports were punched into the PDMS using a blunt 19-gauge needle.

The μPlug assay (175, 200) is an improved version of the well-established plug-in-pond assay (201). It consists of a 15 X 15 mm square chamber with a height of ~75 μm. Agarose mixed with chemoeffector is introduced through a 1.5 mm diameter hole in the middle of the chamber. Two additional holes are punched with a blunt 19-gauge needle along the diagonal to introduce cells into the chamber and to provide a vent, respectively.

The μFlow assay (175, 200) measures the chemotaxis response of bacteria, fluorescently labeled by GFP expression, when they encounter a stable concentration gradient of a chemoeffector established across the width of a microfluidic chamber. The μFlow chemotaxis device consists of two modules – a concentration-gradient generator and a chemotaxis-observation chamber. The gradient generator comprises a network of microfluidic channels that uses diffusive mixing from two or five inputs to generate nearly linear or highly non-linear concentration gradients, respectively, across the width of the observation chamber. The length of the network is 13,500 μm and 18,570 μm for the linear and non-linear gradient generators, respectively. The width of each inlet

entering the observation chamber is 500 μm. The observation module is a chamber (20 x 1050 x 11,500 μm) connected to the gradient-generator module. A secondary inlet (50 μm) is used to introduce bacteria into the observation module at the mid-point of the concentration gradient; these cells were pre-incubated with the mid-point concentration of chemoeffector. The bacteria and the concentration gradients are introduced into the device through silicon tubing.

4.6.3 Growth of bacteria for the μPlug and μFlow chemotaxis assays

Bacteria were prepared for chemotaxis assays as described by Mao *et al.* (202). Briefly, overnight cultures of GFP-expressing bacteria, grown overnight at 32^{o}C in TB containing 150 μg/mL erythromycin or at 37^{o}C in LB containing 150 μg/mL erythromycin (for *E. coli* and *S.* Typhimurium, respectively), were inoculated into 25 mL of the same medium lacking erythromycin to a turbidity of ~ 0.05 at 600 nm. Cultures were grown at 32^{o}C or 37^{o}C, as appropriate, to late-exponential phase (turbidity of 0.5 at 600 nm). A three mL aliquot of cells was centrifuged at 400 x *g* for 5 min at room temperature and very gently resuspended in 2 mL of chemotaxis buffer (CB; 1X phosphate-buffered saline, 0.1 mM EDTA, 0.01 mM *L*-methionine, and 10 mM *DL*-lactate). TG1 cells expressing RFP were killed by exposure to 1 mM kanamycin for 1 h (complete killing was verified by lack of growth on LB agar plates) and mixed with GFP-expressing motile cells at approximately equal densities. Both assays were performed within ~10 min after resuspension of the bacteria in CB.

4.6.3.1 μPlug assay

The agarose plug was made by melting 25 mg low-melting-temperature agarose in

900 μL of CB and 100 μL of 5% bromophenol blue solution (to provide optical contrast) at 70°C. The temperature of the agarose was reduced to 55°C, and chemoeffector was added to the final concentration desired and thoroughly mixed. An 8 μL aliquot of the agarose mixture was introduced into the μPlug device via the center hole, as shown in Supplemental Information **Figure SI 2**. The device was allowed to sit for 5 min to cool to room temperature. The mixture of GFP-expressing (live) and RFP-expressing (dead) cells was introduced gently via one of the corner holes until the chamber was full, taking care to avoid air bubbles. Green and red fluorescent images of the cells around the plug were taken immediately after the device was placed on the microscope stage and every 5 min thereafter for 30 min during incubation at room temperature (~23^{o}C). The uniform distribution of red cells was used to ensure that no bulk flow had occurred.

4.6.3.2 μFlow assay

The assay was performed as described previously (175, 200). A mixture of GFP-expressing and RFP-expressing cells was resuspended in CB containing the chemoeffector at the concentration expected at the mid-point of the observation chamber: 2 μM for the non-linear gradient and 100 μM for the linear gradient. All experiments were conducted at room temperature. The flow rate in the microfluidic device was controlled using a PicoPlus programmable pump (Harvard Apparatus, Holliston, MA). The assembled device was positioned on the stage of a Leica TCS SP5 resonant-scanner confocal microscope. Multiple 500 μL gas-tight glass syringes

(Hamilton, Reno, NV), containing either CB or CB with chemoeffector, were carefully connected to the inlets of the gradient-generator module to avoid introducing air bubbles into the device. The bacterial mixture was introduced into the chemotaxis chamber through the bacterial inlet port, using a 50 μL gas-tight glass syringe. The syringes connected to the gradient generator and the bacterial inlet were operated at the same flow rate, using different pumps. The total flow rate in the observation module (from the five gradient inlets and one bacterial inlet for the non-linear gradient, or the two gradient inlets and one bacterial inlet for the linear gradient) was maintained at 2100 nL/min. Green and red fluorescence images were acquired for 20 min. For each experiment, 100 images for each fluorophore were collected ~7 mm from the inlet at 2.5 sec intervals. The 2.5 sec imaging interval was chosen based on our observation that bacteria take an average of 2.5-3 sec to traverse a 100 μm imaging field-of-view at this flow rate (175). Therefore, bacteria were exposed to the gradient for an average of 18-21 sec prior to imaging.

4.6.4 Quantification of chemotaxis using image analysis

The migration and distribution of bacteria in each image was quantified using a Matlab (Mathworks, Natick, MA) image-analysis subroutine developed in house (175, 200). The analysis consisted of the following steps: (i) removal of background pixels in the image based on pixel size and intensities; (ii) determination of the center of the image (i.e., where bacteria enter the observation chamber), using the dead cells (red fluorescence) as a reference; (iii) location of green cells (i.e., live bacteria expressing

GFP) in the images relative to the center, determined by calculating the centroid; and (iv) quantification of the number of live cells in 16 μm-wide intervals. There are a total of 64 intervals across the width of the chemotaxis chamber. These steps were repeated for each image, and the total counts of cells in each image were summed for analysis. The quantified live and dead cell counts in each interval were scaled to facilitate plotting and comparison.

4.6.5 Chemotaxis migration coefficient (CMC)

The migration profile was used to calculate the CMC, which weights the migration of cells by the distance they move from the center of the observation chamber, as previously described (175, 202). For example, a cell that moved to the farthest high-concentration position at the right (interval 64) was given a weighting factor of +1, and a cell that moved to the farthest low-concentration position at the left (interval 1) was given a weighting factor of -1. Green cells in the middle of the chamber (intervals 31-34) were excluded from the analysis: they could be non-motile cells or cells that remained in the middle of the z-dimension and thus flowed through the chamber too rapidly to be able to respond to the gradients for a significant time.

4.6.6 Capillary assays

The capillary assay was performed as previously described (45) except that plastic gaskets of the proper diameter and thickness were used to create the chamber, or "pond.". About one sixth (60^{o}) of the circular gasket was removed to provide a portal for

entry of the capillary tubes. Capillaries contained either CB alone or CB with the indicated concentration of AI-2 or *L*-serine. The maximum concentration of AI-2 that could be used was 1 mM, because the concentration of the stock solution of AI-2 was only 3.9 mM. The assay was run for 45 min at 32^{o}C, and the number of cells entering the capillary was determined by plating dilutions of the capillary contents on LB agar containing 50 mg/mL streptomycin and counting colonies after 24 h incubation at 37^{o}C.

4.6.7 Computerized docking simulation

A computer-generated model was generated for the Tsr/LsrB interaction using the MBP/Tar simulation as a guide. The most recent high resolution crystal structures for *E. coli* Tsr (http://www.pdb.org/pdb/explore/explore.do?structureId=2D4U) and LsrB in complex with AI-2 (89) were docked manually by using the SPOCK software (187) to align amino acid residues in AI-2 bound LsrB that were in closest contact with Tsr. Steric overlap was held to a minimum during this initial phase of the docking. Specifically, we aligned LsrB and Tsr such that residues Thr-61 and Asp-63 of LsrB were brought as close as possible to residues Ala-145 and Lys-147 in subunit T' of Tsr. Visual inspection of the docking model revealed that the steric collisions still present could be eliminated by reorientation of the side chains. To allow the side chains to repack, we refined the model using the molecular dynamics facilities of the AMBER software (188). Molecular dynamics calculations were performed by moving Tsr about 1.4 Å away from LsrB to eliminate all overlap and by using AMBER to simulate the docking. All simulations were carried out by using a distance-dependent dielectric field

at an initial temperature of 300 K with a time step of 0.001 ps and by using the default force field prescribed by AMBER.

4.6.8 Site-directed mutagenesis of LsrB

Point mutations were introduced in β2 sheet and α6 and 7 helices of LsrB using QuikChange™ Site-Directed Mutagenesis Kit (Stratagene, La Jolla, CA). Primers were designed to replace each amino acid between positions 56-65 and positions 221-236 to alanine using principles outlined by P. Carter (210). Briefly, two synthetic oligonucleotide primers containing the desired mutation were designed. The oligonucleotide primers, each complementary to opposite strands of the pCA24N-*lsrB* vector, are extended during temperature cycling by using PfuTurbo DNA polymerase. Following temperature cycling, the product is treated with Dpn I. The Dpn I endonuclease (target sequence: 5′-Gm6ATC-3′) is specific for methylated and hemimethylated DNA and is used to digest the parental DNA template and to select for mutation-containing synthesized DNA. The *lsrB* fused into pCA24N was derived from *E. coli* and DNA isolated from almost all *E. coli* strains is dam methylated and therefore susceptible to Dpn I digestion.

CHAPTER V

A MICROFLUIDIC DEVICE FOR INVESTIGATING CONCENTRATION-DEPENDENT INTERACTION BETWEEN SIGNALS ON BACTERIAL BIOFILM FORMATION

5.1 Overview

Biofilms are highly organized communities formed by bacteria attached to surfaces. They are ubiquitous in nature and are found in a diverse range of environments such as medical implants, pipes, and heat exchangers. Biofilm formation often leads to the failure of materials and causes infections when occurring inside the human body. Biofilm infections are important clinically because of their high tolerance to antimicrobial compounds and persistence in spite of sustained host defenses. A key feature of biofilm development is that the community is organized in a specific spatio-temporal sequence, in which different bacterial species are recruited to the developing biofilm at different times and are found only in specific locations along the biofilm depth. The formation and organization of biofilms has been attributed, in part, to the soluble signals present in the biofilm microenvironment. The effects of signals such as AI-2 and indole on *Escherichia coli* biofilm formation have been well characterized. While indole inhibits *E. coli* biofilm formation, we have also shown before how two different derivatives of indole (7-hydroxyindole and isatin) have opposite effects on *E. coli* biofilm formation, in that 7-hydroxyindole decreases and isatin increases biofilm formation. Most of these biofilm studies were performed in regular flow cells using a

single concentration of the signal being investigated. In this Chapter, we report the development of a microfluidic model for simultaneously investigating bacterial biofilm formation and organization in response to different concentrations of soluble signals (7-hydroxyindole and isatin), either individually or in combination. A key feature of the proposed model is that the gradient concentration of QS molecules is generated in each chamber by diffusive mixing of signals in the single mixer connected to the microchambers. This model can be used for developing a fundamental understanding of events leading to bacterial attachment to surfaces that are important in infections and chemicals that influence the biofilm formation or inhibition.

5.2 Introduction

Bacteria form biofilms by adhering to almost every surface and developing complex communities called biofilms (1). Multicellular aggregates of cells in biofilms are encased in an extracellular polymeric substance matrix produced by the bacteria themselves (211, 212). Biofilms impact humans in many ways as they can form in natural, medical, and industrial settings. For example, formation of biofilms on medical devices, such as catheters or implants often result in difficult-to-treat chronic infections (213). Inside the human body, complex multispecies commensal biofilms are naturally found in the oral cavity intestinal tract (214, 215). Although a wide number of these commensal bacterial species exist and interact with the normal host in symbiosis and help in normal functions (e.g., food digestion, immune system development, protection from exogenous pathogens) (216), ecological shifts may occur within the microbial

community and result in diseases such as dental caries and periodontal disease in the oral cavity (217) or ulcerative colitis or bowel disorders in the intestine (61).

Bacterial cell-cell communication through chemical signals is one of the mechanisms that have been shown to play a role in the development and sustenance of biofilm communities (218, 219). Interfering with cell-cell communication has could be a promising alternative for disrupting biofilm formation (220). One such chemical signal that has been shown to be an important determinant of biofilm formation is the bacterial stationary phase signal indole (21). Indole is found at high concentrations (600 μM per ~10^9 cells) in *E. coli* is grown in rich medium (24) and is produced when tryptophan undergoes degradation by *tnaA* which encodes the tryptophanase enzyme. Work from our laboratory has shown that indole signaling is a crucial determinant of enterohaemorrhagic *E. coli* (EHEC) O157:H7 infections, as it repels the pathogen, decreases motility, decreases adherence to epithelial cells, downregulates the expression of genes related to virulence and infection, and decreases its biofilm formation (22). Also, we have shown that hydroxylation and oxidation products indoles are interspecies biofilm signals that affect EHEC, *E. coli* K-12, and *P. aeruginosa* PAO1 by controlling biofilm-related genes (22, 23). The hydroxyl- and oxo- byproducts of indole are present at high concentrations (24) as many of the bacterial oxygenases, such as toluene o-monooxygenase (TOM) produced by *Burkholderia cepacia* G4 (221), readily convert indole to oxidized compounds, such as 2-hydroxyindole, 3-hydroxyindole, 4-hydroxyindole, 7-hydroxyindole, isatin (indole-2,3,-dione), indigo, isoindigo, and indirubin (221). Although, indole and 7-hydroxyindole (7-HI) inhibits *E. coli* biofilm

formation (21, 23), isatin, formed by the oxidation of indole and its derivatives, has been shown to increase biofilm formation (23). Intriguingly indole and 7-HI both promote *P. aeruginosa* biofilm formation (23), suggesting that the same signal can be used by many species differently.

It should be noted that these studies, while scientifically rigorous and accurate, tested only a single concentration of the different signals due to the low throughput of the flow cell used in these studies. However, biofilm formation or dispersal is QS controlled and every stage of biofilm cycle (attachment, maturation, aggregation, and dispersal) is affected by the concentration of different biofilm-influencing signals around the cells (222-224). Hence, different concentrations need to be tested to develop a comprehensive understanding of the role of indole and indole-derivatives on biofilm formation or inhibition. Therefore, we developed a microfluidic biofilm model that enables high-throughput investigation of biofilm formation by integrating a diffusive mixing-based concentration generator with multiple flow cells in a single experiment. Using the microfluidic biofilm model, we simultaneously explored the effects of 7-HI and isatin at a range of concentrations, either individually or in combination, to understand their role in the dynamics of biofilm formation.

Biofilms are constantly or intermittently subjected to fluid shear stress in natural environments (225). Conventional studies for investigating biofilm formation under conditions of shear utilize macro-scale flow cells in which the biofilm is formed on a glass slide and fresh medium or a dilute cell suspension is continuously perfused through the system (226). While widely used, this system has the obvious disadvantages of

requiring large volumes (limiting when using signals that are not readily available), is not suited for high-throughput investigation, and does not facilitate spatial and temporal control of bacterial introduction and adhesion. These problems can be addressed in a microfluidic flow cell system. Our experimental design required us to simultaneously investigate the effect of a range of concentrations of a single signal or combinations of multiple signals on EHEC biofilm formation, which precluded the use of previously described microfluidic flow cells (30-33). For example, the micro flow cell design used by Lee *et al*. (32) to study *Staphylcoccus epidermidis* biofilms contains a single channel with multiple inlets, and cannot be used for studying the effect of different concentrations on biofilm organization as the gradient is created across a single channel; also, the inability of the design to separate the cell seeding port from the nutrient media inlet creates a possibility of biofouling of the plastic tubes supplying media and disrupting the flow dynamics. The design used by Cho *et al.* (33) to study the self-organization of *E. coli* colonies into biofilms, and Kim *et al.* (30) to study the effect of a gradient of antibiotics on *P. aeruginosa* biofilms have constraints similar to the device described by Lee *et al* (32). The design proposed by Benoit *et al.* (31) eliminates the use of tubes, and thereby, prevents biofouling and is amenable to high-throughput studies (simultaneous operation of 24 reactors). However, the non-customizable and bulky accessories such as air compressors and electropneumatic regulators that are required do not make this device a cost-effective option. Moreover, any manipulation of signal concentration needs to be performed manually. The microscale device proposed in this Chapter is customizable, contains eight separate microchambers for cultivating biofilms

exposed to eight different concentrations of signals through a single gradient mixer. The presence of pneumatic valves and a separate cell seeding port that is independent from gradient-mixing channels offers complete isolation of the biofilm microchamber from the gradient mixer and also the ability to operate the device under flow, batch or semi-batch conditions.

5.3 Results and discussion

5.3.1 Operation of the μBF device

The aim of this study was to develop a microfluidic flow cell (μBF) device for investigating the effect of different bacterial signaling molecules on biofilm formation. The μBF device consisted of a glass slide and two PDMS layers, a bottom layer with a diffusive gradient-mixer and eight microchambers, and a top layer which contains the pneumatic elements for controlling microvalves (**Fig. 5.1**). The eight microchambers were used for developing bacterial biofilms and exposing them to different concentrations of soluble signals generated on-chip in the gradient-mixer. Eight different concentrations of individual signals or combination of multiple signaling molecules can be generated in the serpentine network of channels in the diffusive mixer.

For seeding cells in the device, bacteria were introduced through the cell inlet in the top layer and the connected cell seeding port in the bottom layer into each microchamber. During this operation the main inlet valves were closed by applying compressed air and seeding valves were opened by applying vacuum (**Fig. 5.2A**). The

main inlet valves connecting the gradient-mixer and microchamber were closed to prevent cells seeded into the microchamber bacteria from entering the gradient mixer channels. After seeding cells into the microchamber, all three valves (main inlet, main outlet, and seeding valves) remained closed so that cells attached to the glass surface without flow (i.e., under batch conditions). After attachment of bacteria for 2 h, the inlet and outlet valves were opened by applying vacuum (**Fig 5.2B**) and unattached or loosely attached bacteria were removed by flowing culture media. Biofilms were allowed to form and develop by perfusing media containing different concentrations of signaling molecule(s) into the microchambers.

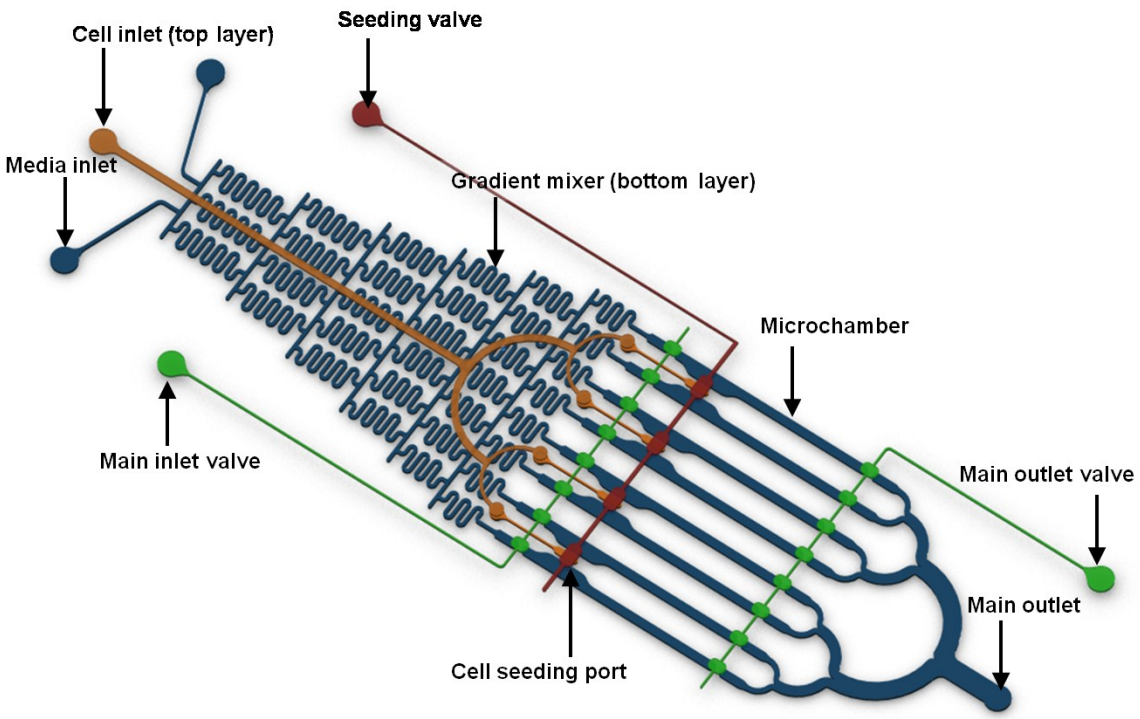

Fig. 5.1. Microfluidic model of flow cell for studying bacterial biofilm (µBF device).

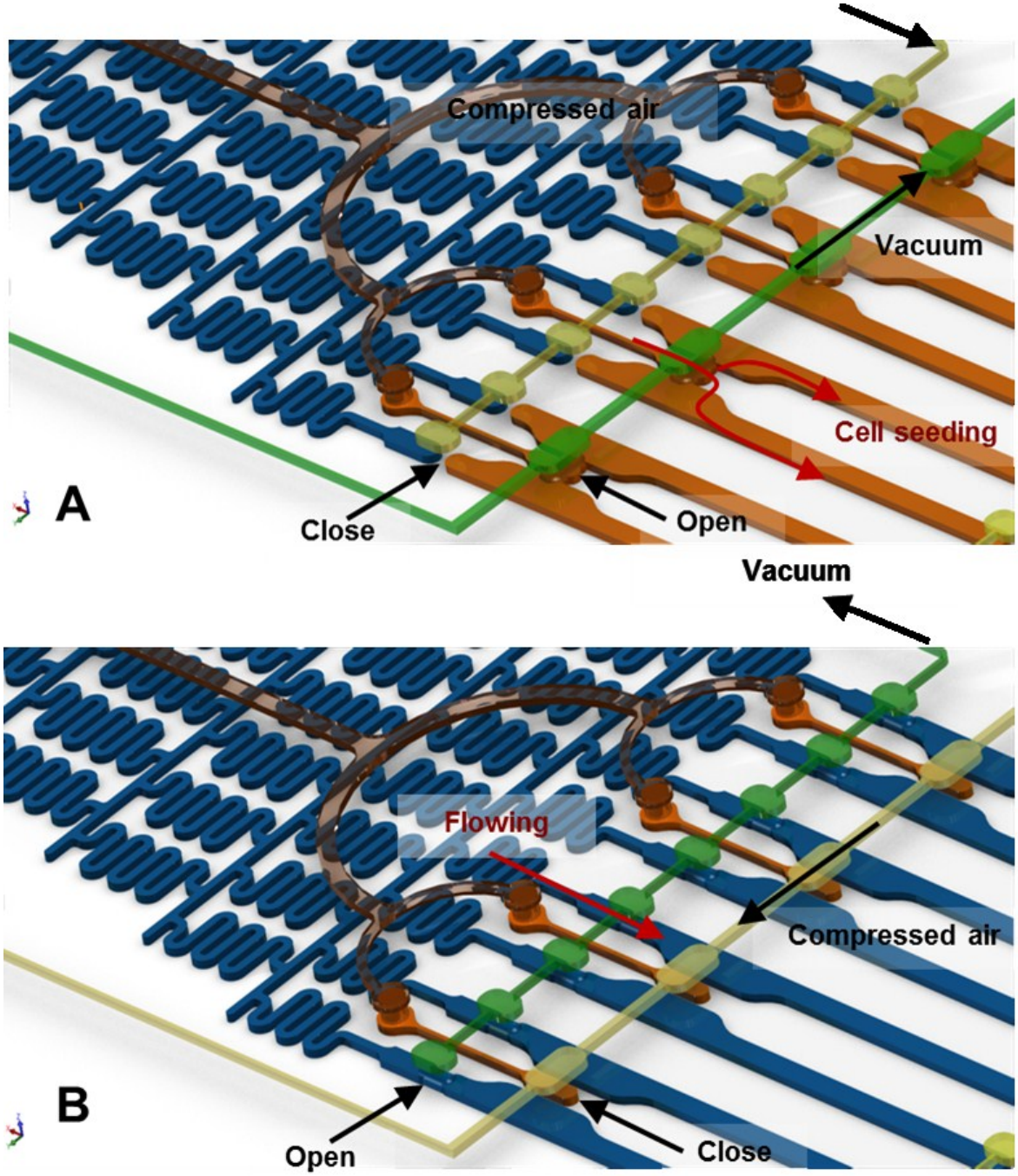

Fig. 5.2. Operation of valves. (**A**) During cell seeding into the microchambers, the seeding valve is opened and main inlet valve is closed to prevent back flow of cells into the gradient mixer (**B**) During biofilm development in the microchamber, the seeding valve is closed and main inlet valve is opened for the culture media to flow through the microchamber.

5.3.2 Effect of range of concentrations of 7-HI and isatin on EHEC biofilm

Our lab previously demonstrated that indole and 7-HI inhibit EHEC biofilm development, but isatin promotes biofilm formation (23). However, we investigated only a single concentration of each signaling molecule (e.g. 1000 μM for 7-HI and 250 μM for isatin) on EHEC biofilm formation using macroscale flow cells. Indole is shown to be an important signal in modulating *E. coli* biofilm formation (21). Indole can also be converted to hydroxyindoles and isatin by oxygenases in strains such as *Pseudomonas putida* PpG7(227), *Ralstonia picketti* PK01(228), *Pseudomonas mendocina* KR(229), *Burkholderia cepacia* G4 (221), and these derivatives could also be present in a wide concentration range in bacterial communities. Therefore, we used the μBF device to investigate the effect of a broad range of concentrations of 7-HI and isatin on EHEC biofilm in a single experiment.

We tested the effect of eight equally distributed concentrations of 7-HI ranging from 0 (microchamber 1) to 500 μM (microchamber 8) on EHEC biofilm in LB medium. EHEC formed robust biofilm in LB at 37^{o}C. After 8 hours, EHEC formed a biofilm with an average height of 4.2 ± 0.7 μm and biomass of 3.8 ± 0.4 $\mu m^3/\mu m^2$ in microchamber 1 (i.e., no 7-HI). Between, zero and 357 μM 7-HI, the biofilm height and biomass decreased linearly with increasing concentration of 7-HI (**Table 5.1**). The biofilm thickness and biomass formed in microchamber 6 containing 357 μM of 7-HI was ~35- and ~42-fold, respectively, less than that observed in microchamber 1. No significant biofilm was formed in microchambers 7 and 8 containing 7-HI concentrations above 357 μM (**Fig. 5.3A and Table 5.1**). Thus 7-HI concentrations above ~350 μM may be

completely inhibiting *E. coli* biofilm formation.

Unlike 7-HI, exposure to isatin increased the formation of EHEC biofilms (**Fig. 5.3B and Table 5.1)**. The increase in both biofilm thickness and biomass levels were linear in the 0-200 μM range, with microchamber 1 (no isatin) having a biofilm thickness of 5.6 ± 0.9 μm and biomass of 4.4 ± 0.4 $\mu m^3/\mu m^2$, and microchamber 8 (200 μM isatin) having a thickness of 13.3 ± 0.6 μm and biomass of 11.2 ± 0.4 $\mu m^3/\mu m^2$. These results are consistent with prior studies (23) and demonstrate the utility and validity of our microfluidic biofilm device for high-throughput biofilm studies. It should be noted that although the current prototype allows investigation of biofilm formation under eight conditions simultaneously, it can be scaled to 12 to 16 concentrations based on the size of the prototype that can fit a single 50 by 22 mm glass slide.

7-Hydroxyindole regulates the cysteine synthesis operon (*cysADEIJP*) (23), and overproducing CysB, which positively regulates the biosynthesis of cysteine in *E. coli* (230), decreases EHEC biofilm formation (23). 7-HI was less potent in reducing EHEC biofilm formation in the absence of cysteine (23). Hence, increasing 7-HI could be increasing the production of cysteine, thereby inhibiting biofilm formation. Similarly, isatin regulates AI-2 transporter genes (*lsrABCDFGKR*) thereby increasing AI-2 levels and activity in the cell (23). AI-2 also increased EHEC biofilm formation (23). Isatin also induces flagellar genes (*flgABCDEFGHIJK* and *fliAEFGILMNOPQ*) and increases swimming motility of EHEC (23). Hence, the increase in EHEC biofilm formation with increasing concentrations of isatin could be related to the increased motility of the cells and increased AI-2 activity.

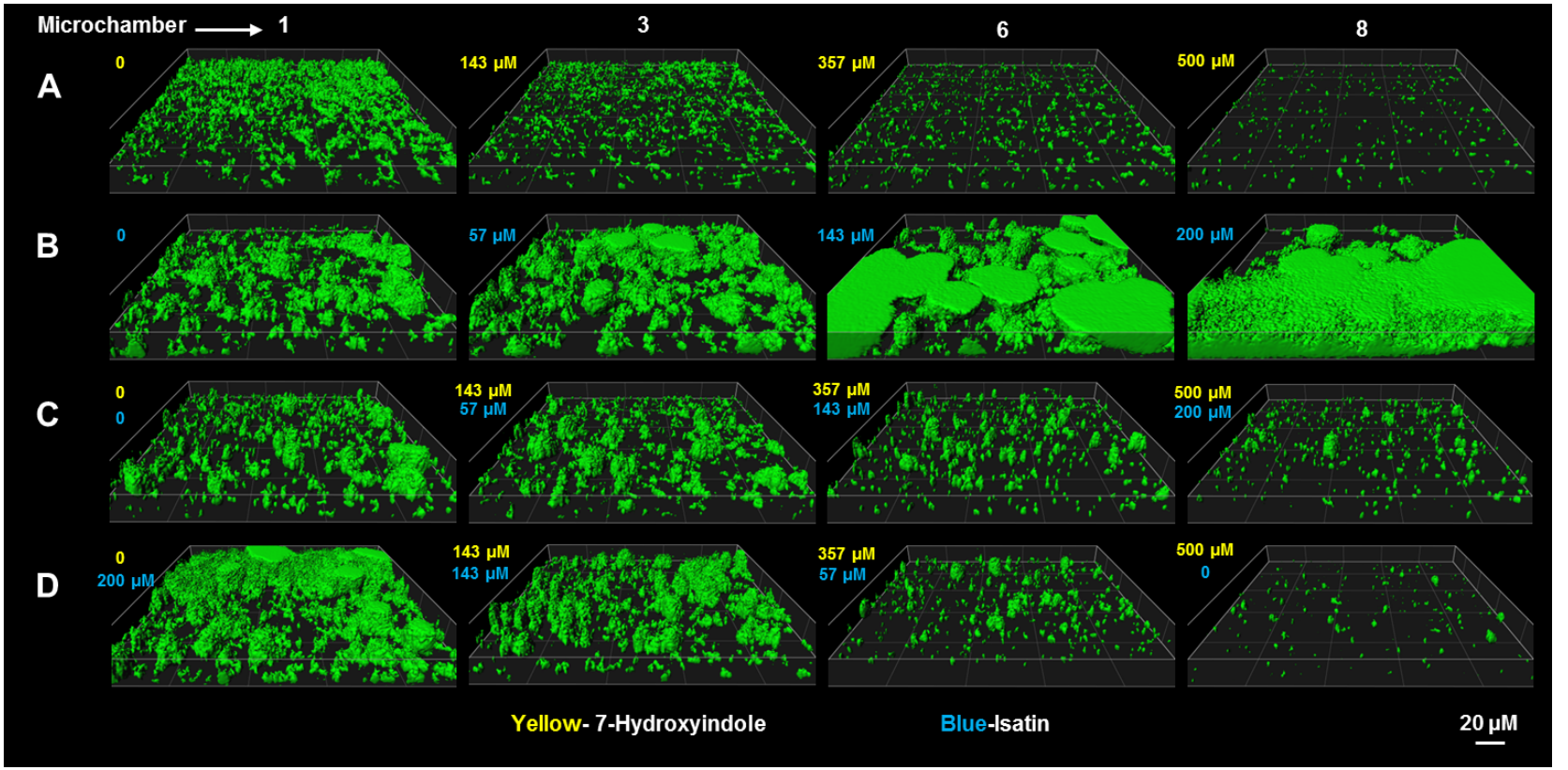

Fig. 5.3. Effect of 7-HI and isatin on EHEC biofilm formation. IMARIS pictures showing the biofilm architecture of EHEC formed in microchambers 1, 3, 6, and 8 after 8 h exposure to (A) 7-HI (0-500 µM) (B) Isatin (0-200 µM) (C) 7-HI (500 µM) and isatin (200 µM) introduced through same inlet and plain media through the other inlet (D) 7-HI (500 µM) and isatin (200 µM) introduced through separate inlets. The concentration of 7-HI is shown in yellow and that of isatin is in blue.

Table 5.1. COMSTAT analysis showing the variation in average EHEC biofilm height and biomass in LB at 37^{o}C upon 8 h exposure to (i) a 0-500 µM gradient of 7-HI, (ii) a 0-200 µM gradient of isatin.

Microchamber	7-HI (0-500 µM)			Isatin (0-200 µM)		
	Concentration (µM)	Average Biofilm Height (µm)	Biomass ($\mu m^3/\mu m^2$)	Concentration (µM)	Average Biofilm Height (µm)	Biomass ($\mu m^3/\mu m^2$)
1	**0**	4.2 ± 0.7	3.8 ± 0.4	**0**	5.6 ± 0.9	4.4 ± 0.4
2	**71**	3.7 ± 0.5	3.4 ± 0.4	**29**	6.9 ± 0.4	5.6 ± 0.4
3	**143**	3.1 ± 0.5	2.5 ± 0.3	**57**	7.4 ± 0.5	6.2 ± 0.3
4	**214**	1.9 ± 0.6	1.7 ± 0.2	**86**	10.2 ± 1.3	8.8 ± 0.2
5	**286**	0.6 ± 0.1	0.41 ± 0.03	**114**	12.1 ± 0.8	10.1 ± 0.7
6	**357**	0.12 ± 0.04	0.09 ± 0.03	**143**	11.9 ± 0.6	9.8 ± 0.7
7	**429**	0.07 ± 0.05	0.03 ± 0.02	**171**	12.6 ± 0.3	10.7 ± 0.3
8	**500**	0.03 ± 0.01	0.02 ± 0.01	**200**	13.3 ± 0.6	11.2 ± 0.4

5.3.3 Effect of combinations of 7-HI and isatin on EHEC biofilm formation

In addition to high-throughput investigations of biofilm formation, a second advantage of the microfluidic biofilm model is the ability to investigate the effect of different combinations of signals on biofilm formation in a high-throughput manner, which allows interrogation of the interaction between different signals on biofilm formation. This is ecologically and physiologically relevant as biofilms are rarely present as mono-cultures in natural environments or *in vivo* (61, 215, 216) and the different signals present may exert divergent effects on bacterial physiology. An example of this is evident from the results in **Fig. 5.3** as 7-HI and isatin can both be generated in a bacterial community from indole, and yet, they exert divergent effects on EHEC biofilm formation. Therefore, we used the microfluidic biofilm model to investigate the effect of simultaneous exposure (i.e., combination gradient) to 7-HI and isatin on EHEC biofilm formation.

Two types of combination gradients can be generated in diffusive mixers as signals can be introduced in two ways into the diffusive mixer. The first is a competing gradient, which is formed when 7-HI and isatin are both introduced through the same inlet and media without any signals is introduced through the other inlet. This allows investigation of the effect that each signal has on biofilm formation in the presence of increasing levels of the other signal, at different concentrations. The second, a cross-mixed gradient, is formed when signals are introduced through different inlets and the resultant gradient enables investigation of the effect of increasing levels of each signal in the presence of decreasing levels of the other signal on biofilm formation.

Using competing gradients, where the concentrations of 7-HI and isatin increased simultaneously across the eight chambers from 0-500 μM and 0-200 μM respectively, we found that when both the signals were present in concentrations similar in orders of magnitude, EHEC biofilm decreases (**Table 5.2, Fig. 5.3C**). This suggests that the effect of 7-HI on EHEC biofilm formation was more dominant than the effect of isatin. Using cross-mixed gradients, where the concentrations of 7-HI increased from 0-500 μM and isatin decreased from 200-0 μM across the eight chambers, we found that when the concentration of isatin was equal to or greater than that of 7-HI, EHEC biofilm increased (**Table 5.2**, panels 1 and 2 in **Fig 5.3D**) compared to untreated control (panel 1, **Fig 5.3C**). This indicated that isatin is more dominant when it is present at equal or higher concentration compared to 7-HI. But, when the 7-HI concentration in the cross-mixed gradient exceeded the isatin concentration (panel 3 and 4, **Fig 5.3D**), 7-HI was more dominant than isatin, and the biomass and height of the *E. coli* biofilm decreased (**Table 5.2, Fig. 5.3C and 5.3D**). Thus, if the isatin concentration exceeds that of 7-HI, *E. coli* biofilm increases and if the concentration of 7-HI exceeds that of isatin (in both competing and cross-mixed gradients), *E. coli* biofilm decreases.

Table 5.2. COMSTAT analysis showing the variation in average EHEC biofilm height and biomass in LB at 37^{o}C upon 8 h exposure to (i) competing gradients of 7-HI and isatin (i.e., 500 µM 7-HI and 200 µM isatin introduced with LB through the same media inlet with plain LB introduced through the other inlet) (ii) cross-mixed gradient of 7-HI and isatin (i.e., 500 µM 7-HI and 200 µM isatin introduced with LB through the different inlets). Data from microchamber 1 for competing gradients (No 7-HI and isatin treatment) was used as a control for comparing the effect of 7-HI and/or isatin on EHEC biofilm.

Microchamber	Competing gradients 7-HI (0-500 µM) + Isatin (0-200 µM)				Cross-mixed 7-HI (0-500 µM) + Isatin (200 µM-0)			
	7-HI (µM)	Isatin (µM)	Average Biofilm Height (µm)	Biomass ($\mu m^3/\mu m^2$)	7-HI (µM)	Isatin (µM)	Average Biofilm Height (µm)	Biomass ($\mu m^3/\mu m^2$)
1	**0**	**0**	4.8 ± 0.5	4.0 ± 0.4	**0**	**200**	8.6 ± 0.8	6.3 ± 0.4
2	**71**	**29**	4.5 ± 0.5	3.9 ± 0.4	**71**	**171**	6.3 ± 0.2	4.8 ± 0.4
3	**143**	**57**	4.3 ± 0.3	3.6 ± 0.3	**143**	**143**	5.6 ± 0.4	4.1 ± 0.3
4	**214**	**86**	3.7 ± 0.6	3.3 ± 0.2	**214**	**114**	3.8 ± 0.6	2.6 ± 0.5
5	**286**	**114**	3.3 ± 0.4	2.5 ± 0.4	**286**	**86**	3.1 ± 0.3	1.9 ± 0.4
6	**357**	**143**	2.7 ± 0.7	2.1 ± 0.6	**357**	**57**	2.2 ± 0.3	1.1 ± 0.4
7	**429**	**171**	2.1 ± 0.4	1.8 ± 0.2	**429**	**29**	1.3 ± 0.4	0.06 ± 0.03
8	**500**	**200**	1.2 ± 0.3	1.1 ± 0.3	**500**	**0**	0.07 ± 0.02	0.03 ± 0.01

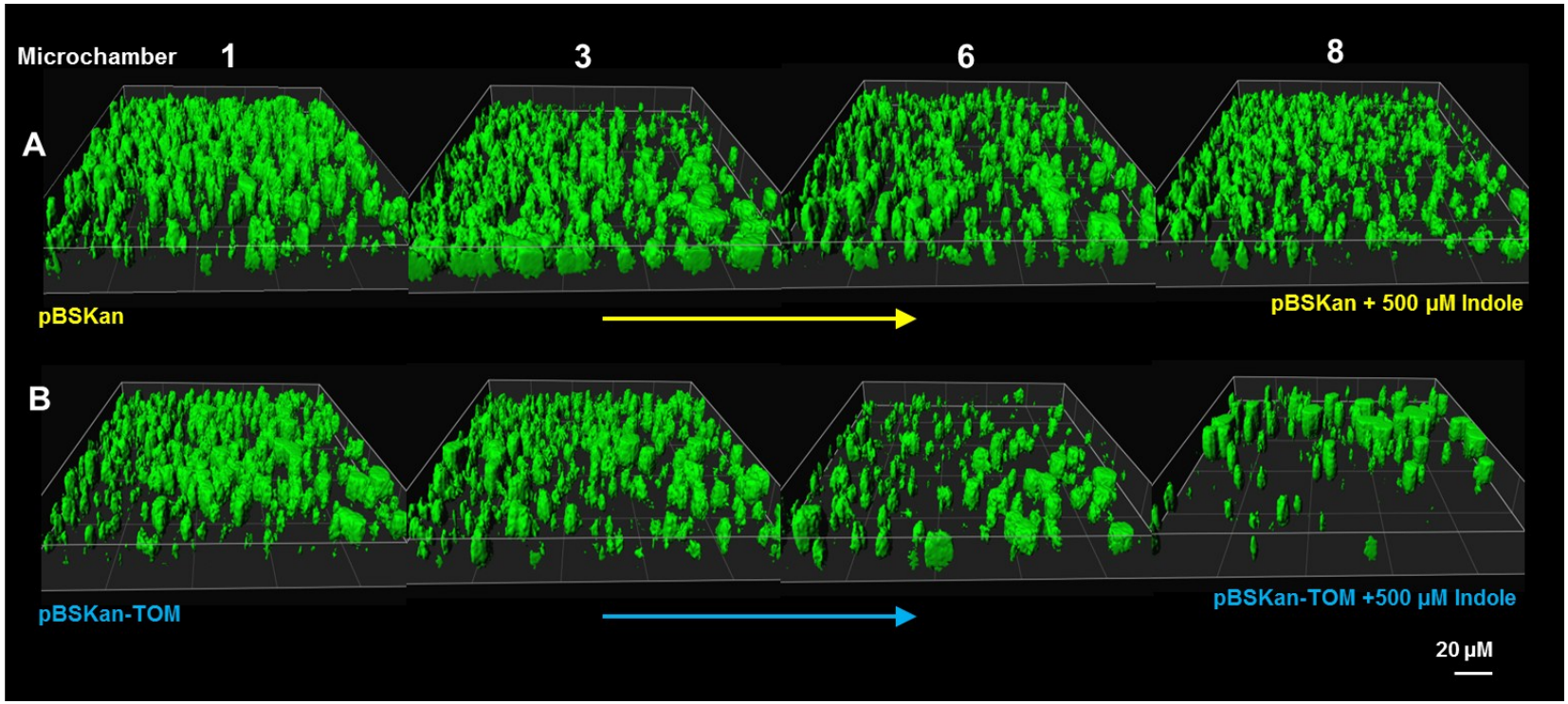

Fig. 5.4. Effect of indole derivatives on EHEC biofilm architecture. IMARIS representation showing the biofilm architecture of EHEC formed in microchambers 1, 3, 6, and 8 after 8 h exposure to (**A**) a gradient formed by mixing cell-free supernatant of *E. coli* BW25113 Δ*tnaA*/pBSKan grown in LB supplemented with kanamycin (50 µg/mL) without and with 500 µM indole, (**B**) gradient formed by mixing cell-free supernatant of *E. coli* BW25113 Δ*tnaA*/pBSKan-TOM grown in LB supplemented with kanamycin (50 µg/mL) without and with 500 µM indole.

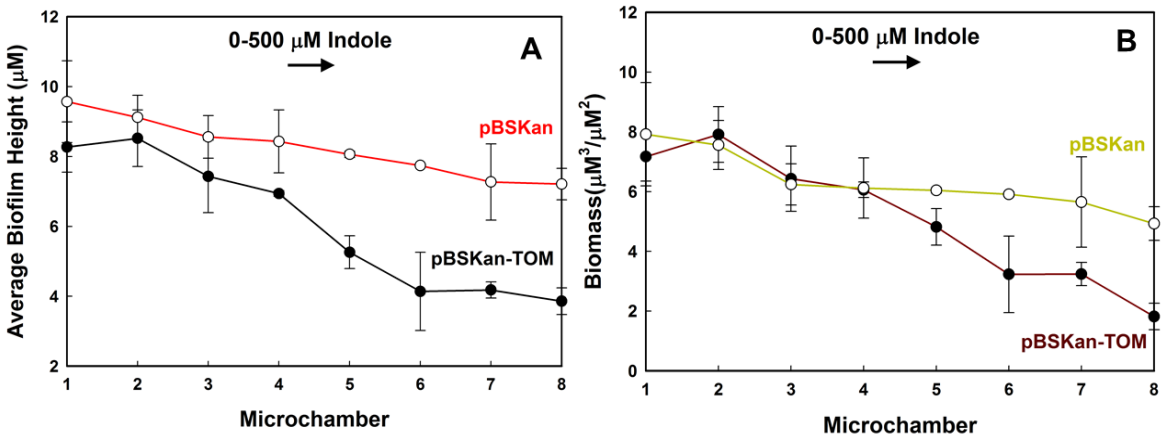

Fig. 5.5. Effect of indole derivatives on EHEC biofilm thickness and biomass. COMSTAT analysis results showing the variation in average (A) EHEC biofilm height and (B) biomass across the eight microchambers after 8 h exposure to gradient formed my mixing supernatant of *E. coli* BW25113 Δ*tnaA*/pBSKan grown in LB supplemented with kanamycin (50 μg/mL) without and with 500 μM indole, or gradient formed my mixing supernatant of *E. coli* BW25113 Δ*tnaA*/pBSKan-TOM grown in LB supplemented with kanamycin (50 μg/mL) without and with 500 μM indole.

5.3.4 Effect of indole derivatives on EHEC biofilm

The indole produced by bacteria such as *E. coli* can be further modified (e.g., through oxidation or hydroxylation) by other bacteria in the community such as *B. cepacia* which do not synthesize it (221), which, in turn, can lead to the presence of a diverse range of modified signals (i.e., indole-like signals) in the biofilm microenvironment However, as shown in our prior work (21, 23) and in **Fig 5.3B**, not all indole derivatives exert the same effect on biofilm formation. Thus, a non-indole producing bacterial species present in the biofilm can alter the effect of indole on biofilm formation through depletion of the parent signal and production of different derivatives that have divergent effects. More importantly, the range and identity of these derivatives can vary depending on the

bacterial species colonizing the biofilm community.

In this work, we studied the effect of a mixture of indole-derivatives (i.e., containing various hydroxylated and/or oxidation products of indole produced by *E. coli*) on EHEC biofilm formation. Spent medium extracted from toluene-*o*-monooxygenase (TOM) negative EHEC Δ*tnaA*/pBS(Kan) grown in the presence of 1 mM indole to a turbidity at 600 nm of ~1.0 decreased EHEC biofilm thickness and biomass by only 1.3 fold (**Figs 5.4 A-B**), indicating only a modest effect of indole on EHEC biofilm formation. On the other hand, spent medium containing different soluble derivatives of indole along with some unconverted indole, formed after culturing EHEC Δ*tnaA*/pBS(Kan)TOM with indole to a turbidity at 600 nm of ~1.0, significantly affected EHEC biofilm (**Fig. 5.4B**) by decreasing the thickness and biomass by ~2.3 fold (**Fig. 5.5A**) and ~3.4 fold (**Fig. 5.5B**) respectively. Rui *et al.* (221) found that in stationary phase cultures of TOM expressing *E. coli* grown overnight (13-14 h), all indole was converted into indigoid compounds such as isoindigo (86%), indirubin (7%), and isatin (6%) after oxidation. But, in cultures that are not in the stationary phase (such as what was used in this study), indole oxidation may yield a mixture of hydroxyindoles, isatin, and indigoid compounds, in which hydroxyindoles slowly dimerize to more indigoids (231). Since the spent medium used in our experiments were in mid-exponential phase (turbidity at 600 nm of ~1.0), they most likely contained hydroxyindoles, isatin, and indigoids (isoindigo, indirubin etc.), in addition to unconverted indole. Without knowing the composition of the spent medium, it is not clear whether the decrease in EHEC biofilms is because of the hydroxyindoles or the indigoids present in the spent medium. The exact composition

of the spent media needs to be determined by thin layer chromatography (221).

5.4 Summary

In summary, we have developed a simple, user-friendly microfluidic flow cell device that precisely measures the effect of a wide range of concentrations of single soluble signals or combinations of two or more signals on bacterial biofilm formation. Since antibiotic treatments are not effective in complete removal of bacterial biofilms formed by pathogens (57), alternative strategies are needed to treat bacterial biofilms. This device enables screening of compounds and their concentrations that effectively inhibit biofilm formation of pathogenic bacteria. Also, this device can be used to perform competition based studies to study the overall effect of two or more compounds on biofilm formation and check which compound is most important in controlling biofilm.

5.5 Materials and methods

5.5.1 Bacterial strains, epithelial cells, materials and growth media

E. coli O157:H7 (CDC EDL933; referred to as EHEC) was obtained from American Type Culture Collection (ATCC 43895, Manassas, VA, USA). The EHEC isogenic mutant deficient in indole (Δ*tnaA*) , and containing plasmids pBS(Kan)TOM (232) and pBS(Kan)(232) were constructed in the lab. Plasmids pCM18 (205) was used to constitutively express the green fluorescent protein (GFP) in EHEC. Erythromycin (150 μg mL^{-1}) was used for maintaining the pCM18 and kanamycin (50 μg mL^{-1}) was used

for maintaining pBS(Kan)TOM or pBS(Kan) in EHEC. Isatin, indole, and 7-HI were obtained in powdered form from Thermo Fisher Scientific (New Jersey, USA). EHEC strains were cultured in either Luria Bertani broth (LB; 10 g L^{-1} tryptone, 10 g L^{-1} NaCl, 5 g L^{-1} yeast extract) or in M9 minimal medium(233) supplemented with 0.2% glucose for biofilm experiments.

5.5.2 Microdevice design and fabrication

The PDMS-based μBF device (**Fig. 5.1**) was fabricated in the Materials Characterization Facility at Texas A&M University using soft lithographic techniques as described previously (234). The μBF device consists of a glass cover slip and two PDMS layers, a bottom layer with a diffusive-mixer and eight microchambers, and a top layer which contains the pneumatic elements for opening and closing microvalves that separate the diffusive mixer and bacteria seeding ports from the microchambers, as well as the inlet and outlets of the microchambers. The top layer also contains a bacterial seeding port for introducing bacteria into the microchambers. The diffusive gradient-mixer in the bottom layer was used to generate different concentrations of 7-HI or isatin and to perfuse growth media into the microchambers. The dimension of the diffusive mixer was 200 μm (width) x 200 μm (height) and the biofilm microchambers were 8000 μm (length) x 600 μm (width) x 200 μm (height). All pneumatic channels were 200 μm thick. The two PDMS layers were fabricated separately and assembled by sequential oxygen plasma treatment and bonding (100 mTorr, 100 W, 40 s) in a plasma etcher. The top pneumatic layer membrane was first aligned and bonded to the bottom diffusive-

mixer/microchamber layer, followed by bonding of the combined PDMS layer to a cover glass (22 x 50 mm). Tygon tubing (0.01" ID x 0.03" OD, Saint Gobain performance plastics, OH, USA) was used for all fluidic connections. Two PicoPlus 11 syringe pumps (Harvard Apparatus, MA, USA) were used to separately control fluid flow rates in the two layers. A temperature controlled metal slide holder was used to maintain the temperature of the device at 37^{o}C. Moist air flowed continuously over the device in order to maintain humidity and avoid bubble formation inside the microchambers. The opening and closing of valves were pneumatically controlled by introducing vacuum or compressed air.

5.5.3 Biofilm development in microfluidic devices

An overnight culture of EHEC grown in LB at 37^{o}C was washed and resuspended in M9-glucose media at turbidity at 600 nm of ~1.0. The bacterial suspension was introduced into the eight biofilm microchambers through the cell inlet (**Fig 5.1**). During this process, the main inlet valves (**Fig. 5.2A**) remained closed to prevent cells from entering and attaching to the gradient mixing channels (which would disrupt mixing in the channels). The main outlet valves and seeding valves were then closed and culture was maintained without flow for 2 h to promote attachment of bacteria to the glass surface. We found that the cells suspended in M9-glucose media attached better to glass compared to LB media. After 2 h, the main inlet and outlet valves were opened (**Fig. 5.2B**), and unattached cells were removed by perfusing nutrient rich LB media for robust biofilm growth at a flow rate of 8 μL/min. The attached bacteria were allowed to form

biofilm at 37^{o}C by flowing LB and LB supplemented with a specific concentration of a specific signal (i.e., 7-HI or isatin) through the two inlets of the diffusive mixer into the microchambers at 8 µL/min for 8 h. For individual treatments, 7-HI concentrations across the eight microchambers were 0, 71, 143, 214, 286, 357, 429, and 500 µM respectively and isatin concentrations were 0, 29, 57, 86, 114, 143, 171, and 200 µM respectively. 7-HI and isatin were cytotoxic beyond 1 mM and 250 µM. Hence concentrations used were below this range.

5.5.4 Confocal microscopy

Images were taken on a TCS SP5 scanning confocal laser microscope (Leica Microsystems, Wetzlar, Germany) using a 40X/0.85 NA dry objective. Z-stack images were taken at a zoom level of 2 such that the image covered 90% of width of the microchamber. Two individual positions per microchamber covering a total of 70% of the microchamber length were chosen for imaging. 3-D reconstruction of the biofilm architecture was performed using IMARIS 3D and 4D Real-Time Interactive Data Visualization software (Bitplane Inc., CT, USA). Biomass and average biofilm height were obtained using the COMSTAT image-processing software.

5.5.5. Generation of spent medium containing soluble derivatives of indole oxidation and hydroxylation by TOM

EHEC Δ*tnaA*/pBS(Kan)TOM producing wild-type toluene *o*-monooxygenase (TOM) of *Burkholderia cepacia* G4 and EHEC Δ*tnaA*/ pBS(Kan) that does not produce

TOM were grown overnight separately at 37^{o}C in LB supplemented with kanamycin (50 μg mL^{-1}). Overnight cultures of both strains were diluted in flasks containing 100 mL LB or 100 mL LB with 1 mM indole to a turbidity at 600 nm of 0.05 and grown until turbidity at 600 nm of ~1. Since the Δ*tnaA* strain of EHEC does not produce any indole, TOM converts most of the externally added indole into hydroxylated products such as 2-HI, 3-HI, or 7-HI, or oxidation products such as isatin, indigo, isoindigo, and indirubin (221). The cultures were then centrifuged at 10,000x*g* for 10 minutes to remove cell material and insoluble byproducts of indole metabolism to obtain a cell-free spent medium containing a mixture of different soluble indole byproducts. Cell-free supernatants from strains lacking the TOM enzyme or without any external indole addition were also similarly obtained.

CHAPTER VI

SYNTHETIC QUORUM SENSING CIRCUIT TO CONTROL CONSORTIAL BIOFILM FORMATION AND DISPERSAL IN A MICROFLUIDIC DEVICE

6.1 Overview

Bacteria grow primarily as biofilms, and to utilize them for chemical transformations in biorefineries, they periodically need to be replaced. Previously, we engineered global regulator Hha and cyclic diguanylate-binding BdcA to create proteins that enable biofilm dispersal. Here, we devise a biofilm circuit that utilizes these two dispersal proteins along with a population-driven quorum sensing switch. With this synthetic circuit, in a novel microfluidic channel, we (i) formed an initial colonizer biofilm, (ii) introduced a second cell type (dispersers) into this existing biofilm, (iii) formed a robust dual-species biofilm, (iv) displaced the initial colonizer cells in the biofilm with an extra-cellular signal from the disperser cells, and (v) removed the disperser biofilm with a chemically-induced switch. Therefore, for the first time, cells have been engineered that are able to displace an existing biofilm and then be removed on command allowing one to control consortial biofilm formation for various applications.

---

* Submitted in part as "Synthetic quorum sensing circuit to control consortial biofilm formation and dispersal in a microfluidic device" by Seok Hoon Hong*, Manjunath Hegde*, Jeongyun Kim*, Arul Jayaraman, and Thomas K. Wood, Nature Methods (In revision). * These authors contributed equally to this work.

6.2 Introduction

Biofilms are groups of cells at an interface cemented together by polysaccharides, protein, DNA, and lipids (60). Biofilms are related to most bacterial chronic inflammatory and infectious diseases (235) as well as involved in biocorrosion (236) and biofouling (237) in diverse areas. They also may be used for beneficial applications such as bioremediation and hold much potential for chemical transformations in biorefineries (238). For these applications, compared to monocultures, mixed populations have the advantages of being able to perform more complex transformations (e.g., those requiring multiple steps), and they are more resistant to environmental stress (239). For these reasons, consortia have been heralded as the new frontier in synthetic biology (239). However, to date, it has not been possible to control consortial biofilm formation.

Based on an understanding of signals and regulatory networks during biofilm development(240), biofilms have been engineered by manipulating extracellular/intercellular signals and regulators (238). The first engineered biofilm was a consortium where *Bacillus subtilis* was engineered to secrete the peptide antimicrobials indolicidin and bactenecin to inhibit the growth of sulfate-reducing bacteria and thereby decrease corrosion (241). Also, the first synthetic signaling circuit to control biofilm formation was developed for *Escherichia coli* and *Pseudomonas fluorescens* by manipulating the extracellular concentration of the signal indole produced by *E. coli*(21); indole is a biofilm inhibitor for *E. coli*. In addition, using directed evolution, SdiA was reconfigured to decrease biofilm formation by increasing indole(242), and the global regulator H-NS was evolved to decrease biofilm formation via prophage excision and

cell death(243).

To remove existing biofilms, T7 bacteriophage was engineered to produce dispersin B of *Actinobacillus actinomycetemcomitans* to disrupt the glycosidic linkages of polymeric β-1,6-*N*-acetyl-*D*-glucosamine found in the biofilm matrix during bacteriophage infection (244). In addition, global transcriptional regulator Hha was engineered using protein engineering to enhance biofilm dispersal primarily by inducing protease HslV (245), and BdcA, which increases biofilm dispersal by decreasing the concentration of the second messenger cyclic diguanylate (c-di-GMP) by binding it, was engineered for nearly complete dispersal of biofilms(246). Therefore, new genetic modules are available for manipulating biofilms(238).

Synthetic biology is an emerging field to develop biological systems that perform novel functions by assembling genetic modules(247). The genetic modules include switches, cascades, pulse generators, time-delayed circuits, oscillators, spatial patterning, and logic formulas, and they can be utilized to control transcription, translation, and post-translational operations in order to tune gene expression, protein production, metabolism, and cell-cell communication(248). Among these genetic modules, bacterial quorum sensing (QS) systems are becoming important components of a wide variety of engineered biological devices(249), since autoinducers are useful as input signals because most are small, diffuse freely in aqueous media, and are easily imported by cells(250). Because the engineered cells synthesize their own QS signals, they are able to monitor their cell density and modulate their activities(251) accordingly without supervision. Hence, QS based circuits have a wide range of potential engineering

applications such as production of biochemicals, tissue engineering, and mixed-species fermentations as well as developing biosensors and controlling biofouling (250). For example, LuxI from *Vibrio fischeri*, which produces *N*-(3-*oxo*-hexanoyl)-*L*-homoserine lactone (3*o*C6HSL) and AiiA from *Bacillus thuringiensis*, which degrades 3*o*C6HSL, were utilized to generate synchronized oscillations(252). Also, the LuxI/LuxR QS system was coupled to the production of a toxin protein CcdB to induce cell death at high cell densities(253).

The two best-characterized QS systems of *Pseudomonas aeruginosa* are the LasI/LasR and RhlI/RhlR systems, which regulate biofilm formation, virulence, swarming motility, and antibiotic efflux pumps(254). LasI produces autoinducer molecule, *N*-(3-*oxo*-dodecanoyl)-*L*-homoserine lactone (3*o*C12HSL), which is sensed by LasR(255). Likewise, RhlI produces *N*-butyryl-*L*-homoserine lactone (C4HSL) that is sensed by RhlR(255). The LasI/LasR and RhlI/RhlR QS systems have been used to engineer bidirectional communication(256), and the LasI/LasR QS system was used to both construct a predator-prey ecosystem(257) and create a synthetic ecosystem in *E. coli*(258). Furthermore, the RhlI/RhlR QS system was utilized to demonstrate roles for self-organization and aggregation in a synthetic biofilm consortium(259). Hence, synthetic QS circuit systems have potential in that population-driven QS switches may be utilized to develop synthetic genetic networks for a variety of applications.

Since biofilm formation and dispersal are ultimately genetic processes, they may be manipulated like other genetic systems(238) using the tools of synthetic biology(248) and directed evolution. In this work, our goal was to control biofilm displacement via a

population-driven QS switch coupled to engineered biofilm dispersal proteins. Controlling biofilm dispersal creates a synthetic biological platform for sophisticated patterning of biofilms for engineering applications. The LasI/LasR QS module of *P. aeruginosa* was combined with engineered Hha (245) and BdcA (246) biofilm dispersal proteins, and the system was utilized to selectively remove one type of cell from an existing biofilm, and then remove the second biofilm to create a surface ready for additional biofilms.

6.3 Results

6.3.1 Microfluidic biofilm engineering (μBE) circuit

The μBE signaling circuit was constructed in *E. coli* using two engineered biofilm-dispersing proteins, Hha13D6(245) and BdcAE50Q(246), along with the *P. aeruginosa* LasI/LasR QS system (**Fig. 6.1a**). *E. coli hha* (260) was used as the host since deletion of *hha* increases biofilm formation(261) and provides a background in which there is no wild-type Hha. Lactococcal promoter CP25(262) was used as the strong constitutive promoter for two of the three proteins on each plasmid. To obtains high concentrations of intercellular signal 3*o*C12HSL and regulator LasR, a synthetic ribosomal binding site (RBS II) (262) was first utilized. However, high expression of *lasI* or *lasR* was deleterious; thus, we used the native RBS of these genes. All the cloned genes for the two cell types were placed on a single plasmid (pCA24N derivative, **Fig. 6.2**) to avoid plasmid instability and so that a single antibiotic could be used to maintain the key

plasmid during growth of the consortia.

In the μBE circuit, disperser cells (*lasI*$^+$, *hha13D6*$^+$, *gfp*$^+$ via *E. coli hha/*pHha13D6-*gfp-lasI*) produce constitutively green fluorescent protein (GFP) and the quorum-sensing signal 3*o*C12HSL and have *hha13D6* induced upon addition of isopropyl-β-D-thiogalactopyranoside (IPTG) (**Fig. 6.1a**). The initial colonizer cells (*lasR*$^+$, *bdcAE50Q*$^+$, *rfp*$^+$ via *E. coli hha/*pBdcAE50Q-*rfp-lasR*) produce constitutively red fluorescent protein (RFP) and regulator LasR, the receptor of 3*o*C12HSL. The initial colonizer cells also have *bdcAE50Q* under the control of the *lasI* promoter which is activated via the 3*o*C12HSL + LasR complex (263) (**Fig. 6.1a**). Thus, disperser cells produce the signaling molecule 3*o*C12HSL, and the initial colonizer biofilm-forming cells sense it and disperse when the disperser cells reach a quorum.

Since we desire the disperser cells to supplant the initial colonizer cells, we checked the specific growth rates of the two strains to see if they are comparable; the disperser cells grew 14% slower than initial colonizer cells in rich medium (LB glucose, $\mu_{disperser} = 1.13 \pm 0.08\ h^{-1}$ and $\mu_{initial\ colonizer} = 1.31 \pm 0.05\ h^{-1}$). The slower growth of the disperser cells is most likely due to leaky expression of toxin *hha13D6* from the *T5-lac* promoter (264). Corroborating this difference in cell growth, disperser cells formed biofilms more slowly compared to initial colonizer cells: the biomass of initial colonizer cells after 9 h was $5.7 \pm 0.1\ \mu m^3/\mu m^2$ (**Fig. 6.3a**) while the biomass of the disperser cells after 9 h was $4.1 \pm 0.1\ \mu m^3/\mu m^2$ (**Fig. 6.3b**).

Fig. 6.1. µBE metabolic circuit and microfluidic device. (a) The two *E. coli* cell types communicate by using the LasI/LasR QS module. In the disperser cell, the LasI protein is constitutively produced and synthesizes 3*o*C12HSL. 3*o*C12HSL freely diffuses into the initial colonizer cell and makes a complex with LasR, and the 3*o*C12HSL + LasR complex induces biofilm dispersal protein BdcAE50Q by activating the *lasI* promoter. The biofilm dispersal protein Hha13D6 in the disperser cell is induced upon adding IPTG. Plasmid maps for the synthetic µBE circuit are shown in **Fig. 2. (b)** The novel microfluidic device is shown with its two PDMS layers, a bottom layer with a diffusive-mixer and eight microchambers, and a top layer containing a second diffusive mixer and the pneumatic elements to control microvalves. The diffusive mixer in the bottom layer was used to generate different concentrations of dispersal signals (e.g., IPTG for removing disperser cells and 3*o*C12HSL for dispersing initial colonizer cells) and to perfuse growth media into the biofilm microchambers. The mixer in the top layer was used to introduce bacteria into the microchambers at different cell densities.

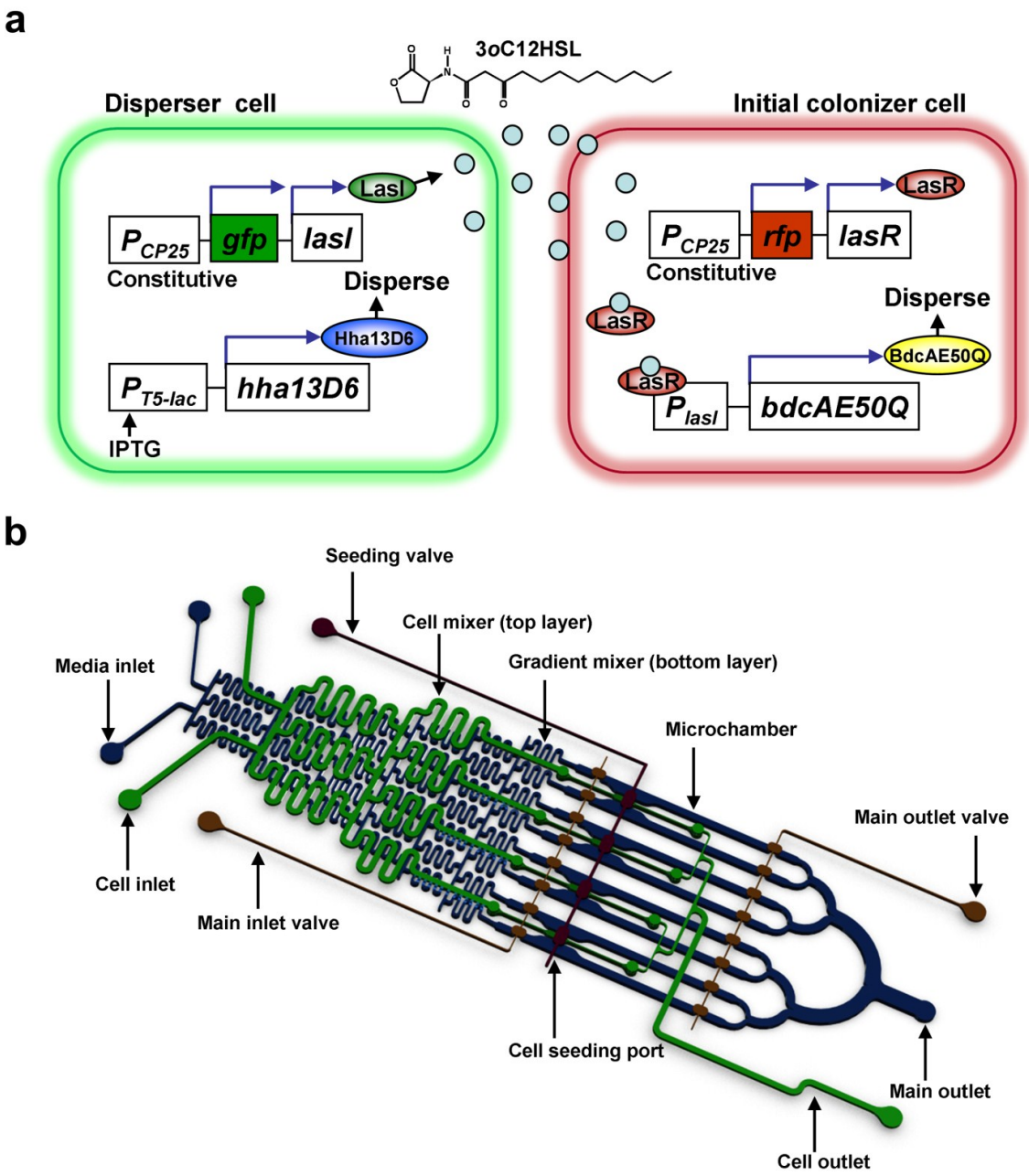
a
3oC12HSL
Disperser cell
Initial colonizer cell
LasI
P CP25
gfp
lasI
Constitutive
Disperse
Hha13D6
P T5-lac
hha13D6
IPTG
LasR
P CP25
rfp
lasR
Constitutive
Disperse
LasR
BdcAE50Q
LasR
P lasI
bdcAE50Q
b
Seeding valve
Cell mixer (top layer)
Media inlet
Gradient mixer (bottom layer)
Microchamber
Main outlet valve
Cell inlet
Main inlet valve
Cell seeding port
Main outlet
Cell outlet

6.3.2 Disperser cells produce 3*o*C12HSL

To confirm the disperser μBE circuit synthesizes 3*o*C12HSL, we measured the 3*o*C12HSL concentration of the disperser cells (*E. coli hha/*pHha13D6-*gfp-lasI*) in the biofilm using a *lacZ* reporter (*lasB-lacZ* translational fusion) that is activated by 3*o*C12HSL (265). In flow-cells, disperser cells in biofilms produced 13-fold higher concentrations of 3*o*C12HSL compared to the planktonic cells in the effluent (6.7 ± 3 μM vs. 0.5 ± 0.2 μM) and produced 48-fold higher concentrations of 3*o*C12HSL compared to planktonic cells in shake flasks (0.1 ± 0.1 μM). The negative control (no *lasI*) had no detectable 3*o*C12HSL. These results confirm that autoinducer concentrations in biofilms are higher than in planktonic cultures (266) and compare well to levels of 3*o*C12HSL produced in *P. aeruginosa* biofilms (1 (267) to 600 μM (266)). Since maximum activity of the *lasI* promoter is obtained with 0.1 μM of 3*o*C12HSL with LasR (263), 3*o*C12HSL production in the disperser biofilms should induce the *lasI* promoter in the initial colonizer cells to express *bdcAE50Q* to disperse the initial colonizer biofilms. Moreover, since 3*o*C12HSL diffusion is significantly slower compared to C4HSL diffusion (268), local concentrations of 3*o*C12HSL in biofilms may be much higher than the 3*o*C12HSL concentration measured here.

6.3.3 3*o*C12HSL disperses the initial colonizer biofilm

To demonstrate that 3*o*C12HSL disperses biofilms produced by the initial colonizer cells (*E. coli hha/*pBdcAE50Q-*rfp-lasR*) by binding LasR and inducing *bdcAE50Q*, exogenous 3*o*C12HSL at different concentrations was added to biofilms formed by the

initial colonizer cells in microfluidic channels. As expected, the initial colonizer biofilms were dispersed upon adding 3*o*C12HSL in a dose-dependent manner (**Fig. 6.3c**); nearly complete biofilm dispersal was obtained at 500 μM of 3*o*C12HSL (**Fig. 6.4a**). In contrast, there was no dispersal in the absence of 3*o*C12HSL (**Fig. 6.4b**), and the initial colonizer cells formed thick biofilms (10.8 ± 0.6 $\mu m^3/\mu m^2$) (**Fig. 6.3c**). Hence, initial colonizer cells recognize 3*o*C12HSL and this signal may be used to disperse initial colonizer biofilms.

6.3.4 IPTG removes the disperser biofilm

To demonstrate that IPTG disperses biofilms produced by disperser cells by inducing *hha13D6*, exogenous IPTG at different concentrations was added to biofilms formed by disperser cells in microfluidic channels. As expected, disperser biofilms were dispersed upon adding IPTG in a dose-dependent manner (**Fig. 6.3d**) with nearly complete biofilm dispersal at 2 mM IPTG (**Fig. 6.4c**); hence, we used 2 mM IPTG in subsequent experiments. In contrast, there was no dispersal in the absence of *hha13D6* (**Fig. 6.4d**). Thus, the disperser cell produces 3*o*C12HSL at concentrations adequate to disperse the initial colonizer biofilm and has active *hha13D6* to disperse its own biofilm upon IPTG addition. Taken together, both disperser and initial colonizer cells were constructed to allow us to manipulate biofilm dispersal using a population-driven switch.

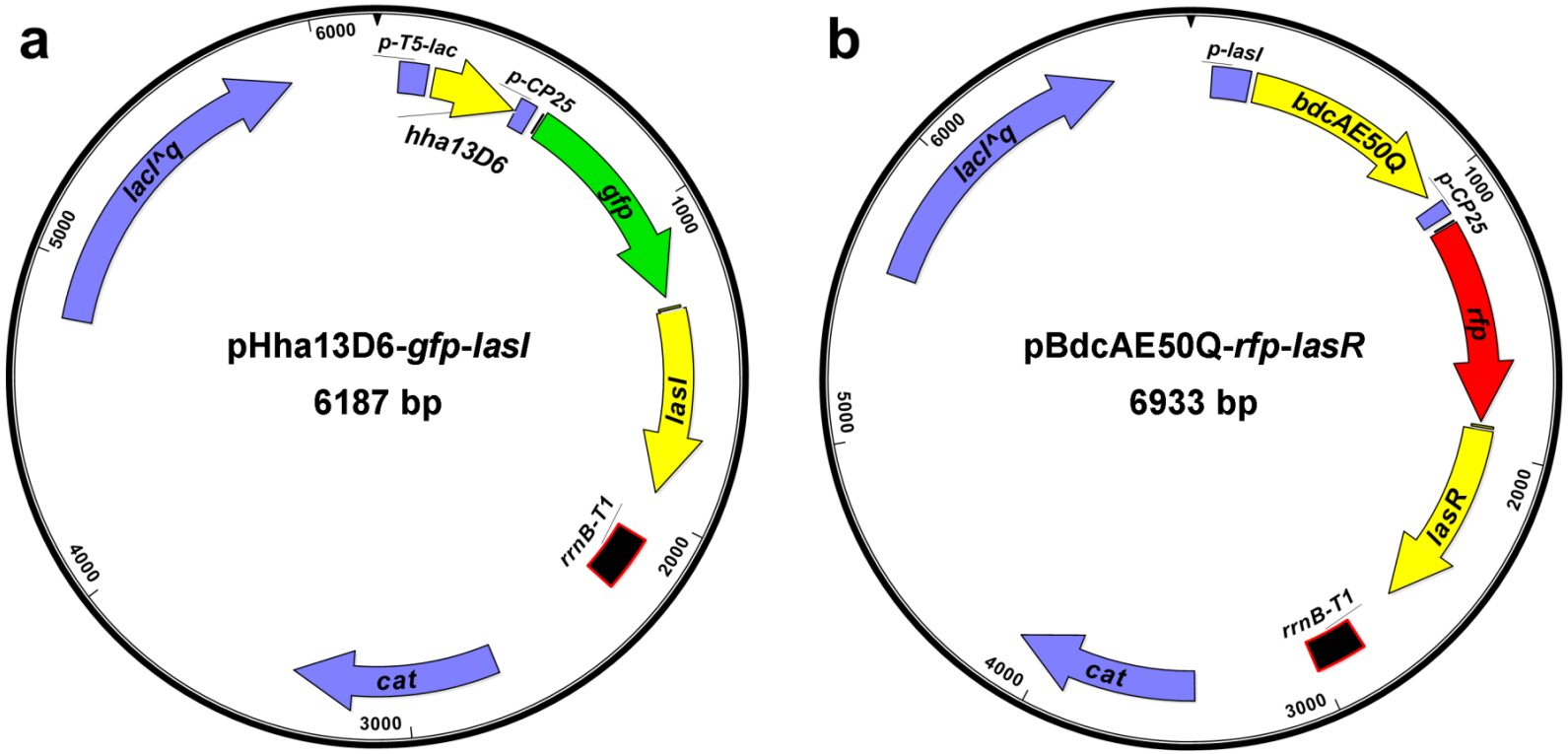

Fig. 6.2. Plasmid maps of the disperser plasmid and the initial colonizer plasmid that are used to create the µBE circuit. (a) pHha13D6-*gfp-lasI* with *hha13D6* under control of the *T5-lac* promoter and *gfp* and *lasI* under control of the constitutive CP25 promoter. (b) pBdcAE50Q-*rfp-lasR* with *bdcAE50Q* under control of the *lasI* promoter and *rfp* and *lasR* under control of the constitutive CP25 promoter. *cat* encodes chloramphenicol acetyltransferase, *lacI^q* encodes a repressor mutant of the *lac* operator, and *rrnB-T1* indicates the *rrnB* T1 transcription termination sequence.

Fig. 6.3. Biomass of initial colonizer and disperser biofilms. (**a**) Biomass of initial colonizer biofilms (BdcAE50Q^{+}, LasR^{+}) with 500 μM of 3*o*C12HSL for 10 h. (**b)** Biomass of disperser biofilms (Hha13D6^{+}, LasI^{+}) with 2 mM of IPTG for 10 h. (**c**) Biomass after 19 for the initial colonizer biofilms with different concentrations of 3*o*C12HSL (0, 71, 143, 214, 286, 357, 429, and 500 μM for 10 h). (**d**) Biomass after 19 h for the disperser biofilms with different concentrations of IPTG (0, 0.3, 0.6, 0.9, 1.1, 1.4, 1.7, and 2.0 μM for 10 h). Robust biofilms at 9 h were formed by seeding the initial colonizer or the disperser cells into microchambers for (**a**), (**b**), (**c**), and (**d**). (**e**) Biomass of the initial colonizer (BdcAE50Q^{+}, LasR^{+}) and disperser (Hha13D6^{+}, LasI^{+}) biofilms. After 44 h, 2 mM of IPTG was added to remove the disperser biofilm for an additional 18 h. (**f**) Biomass of the initial colonizer (BdcAE50Q^{+}, LasR^{+}) and the no LasI disperser control (Hha13D6^{+}, LasI^{-}) biofilms. After 40 h, 2 mM of IPTG was introduced to disperse the no LasI disperser control biofilm for an additional 20 h. The initial colonizer biofilms were formed by seeding for 9 h, then disperser cells were seeded for 5 h to form both initial colonizer and disperser biofilms for (**e**) and (**f**).

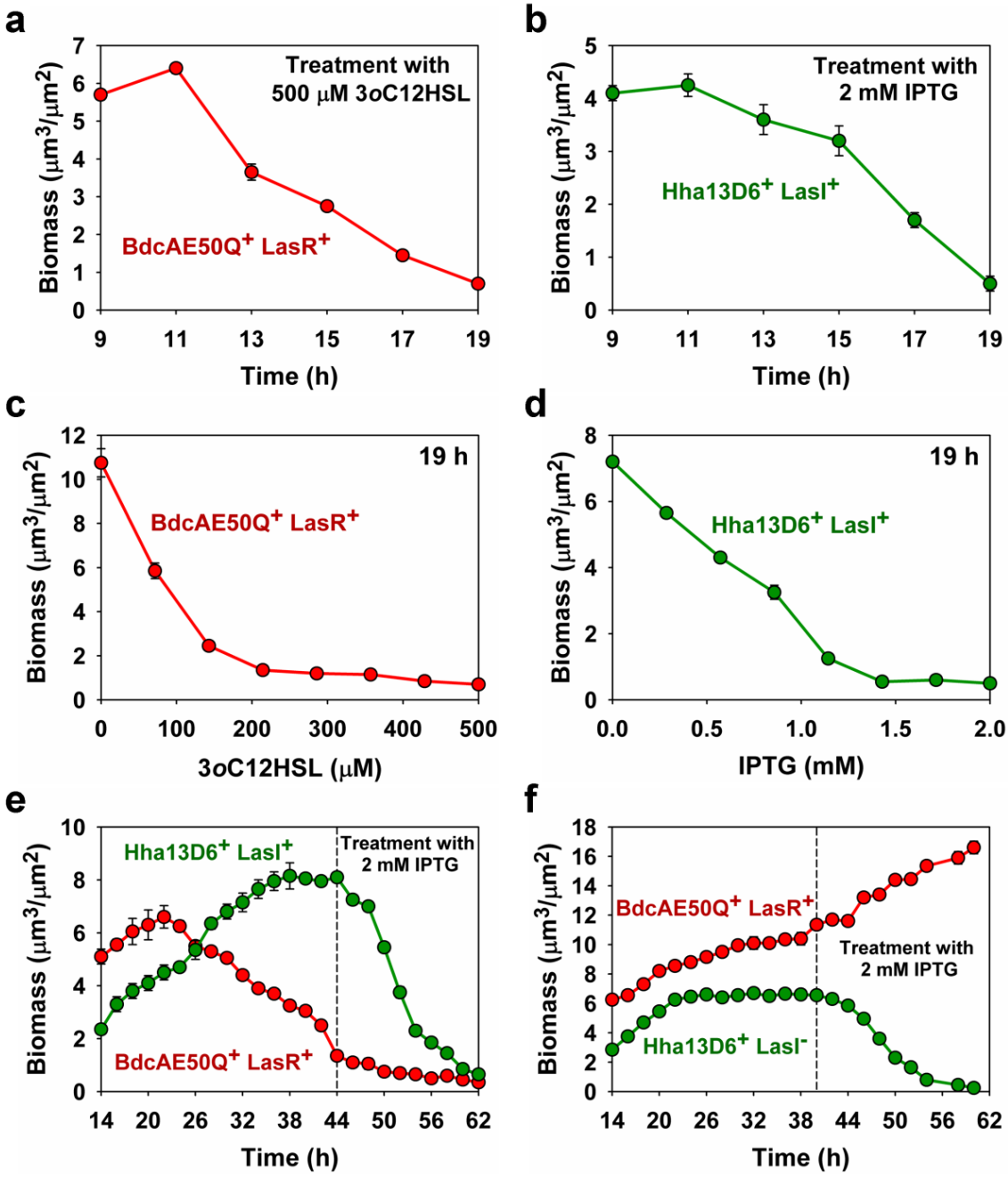
a
Biomass (μm³/μm²)
Time (h)
Treatment with
500 μM 3oC12HSL
BdcAE50Q+ LasR+
b
Biomass (μm³/μm²)
Time (h)
Treatment with
2 mM IPTG
Hha13D6+ LasI+
c
Biomass (μm³/μm²)
3oC12HSL (μM)
19 h
BdcAE50Q+ LasR+
d
Biomass (μm³/μm²)
IPTG (mM)
19 h
Hha13D6+ LasI+
e
Biomass (μm³/μm²)
Time (h)
Hha13D6+ LasI+
Treatment with
2 mM IPTG
BdcAE50Q+ LasR+
f
Biomass (μm³/μm²)
Time (h)
BdcAE50Q+ LasR+
Treatment with
2 mM IPTG
Hha13D6+ LasI-

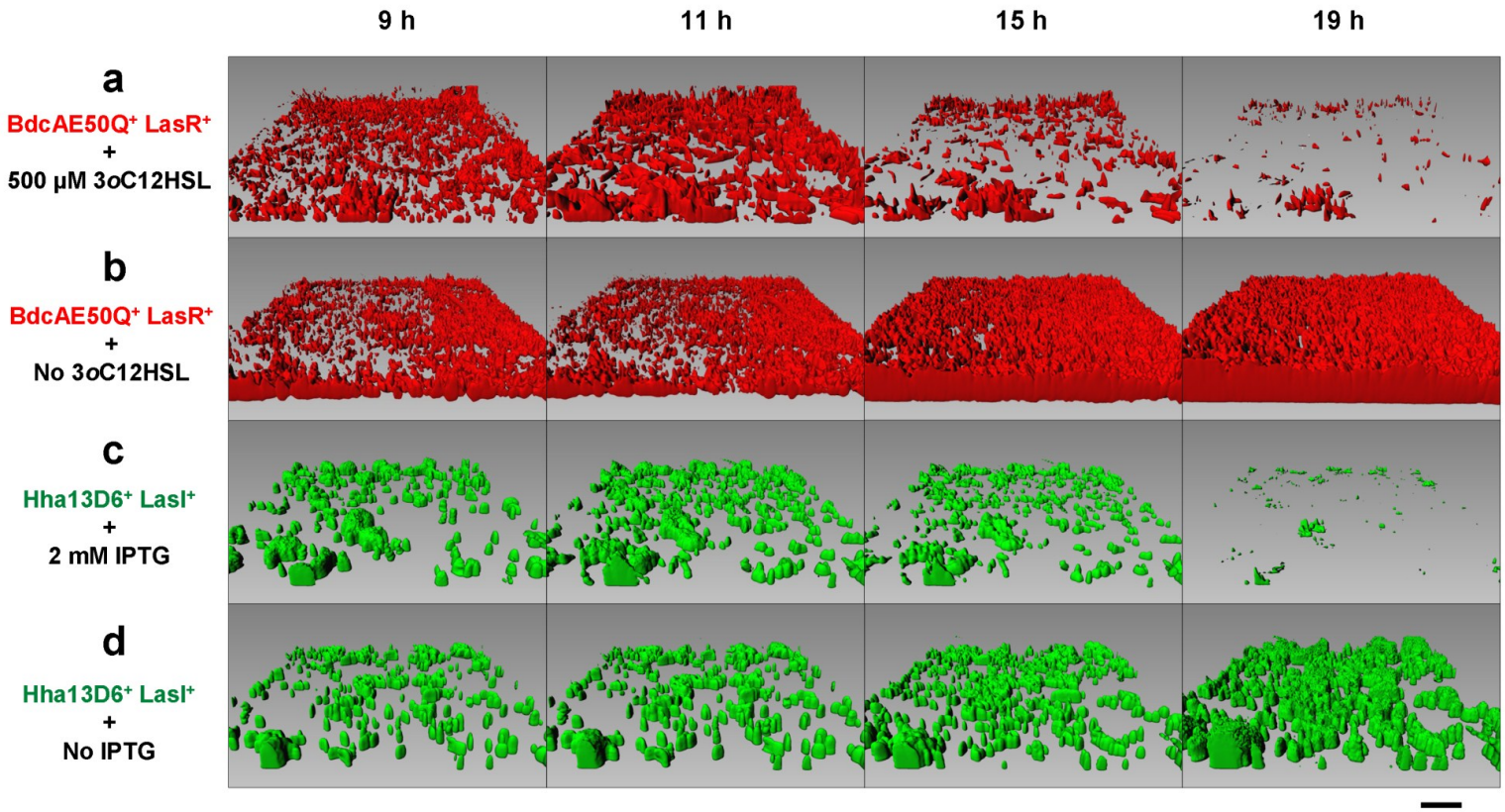

Fig. 6.4. Dispersal of mono-species biofilms. Initial colonizer biofilms (BdcAE50Q^{+}, LasR^{+}) were formed by seeding for 9 h, then 3*o*C12HSL (500 µM) was added for 10 h to induce biofilm dispersal (**a**) or not added (**b**). Disperser biofilms (Hha13D6^{+}, LasI^{+}) were formed by seeding disperser cells for 9 h, and then 2 mM of IPTG was added for 10 h to induce biofilm dispersal (**c**) or not added (**d**). Scale bar indicates 20 µm.

6.3.5 Engineered BdcA and Hha are necessary for biofilm dispersal

To confirm that the biofilm dispersal upon addition of 3*o*C12HSL and IPTG is the result of production of the engineered biofilm dispersal proteins, we performed dispersal experiments of initial colonizer cells that lack *bdcAE50Q* and disperser cells that lack *hha13D6*. As expected, initial colonizer biofilms formed without *bdcAE50Q* (via *E. coli hha/*pRFP-*lasR*) did not disperse in the presence of 3*o*C12HSL (**Fig. 6.5a**)**,** while initial colonizer biofilms formed with *bdcAE50Q* dispersed with 3*o*C12HSL (**Fig. 6.4a**). Similarly, disperser biofilms formed without *hha13D6* (via *E. coli hha/*pGFP-*lasI*) did not disperse upon addition of IPTG (**Fig. 6.5b**), while disperser biofilms formed with *hha13D6* dispersed with IPTG (**Fig. 6.4c**). Taken together, BdcAE50Q and Hha13D6 are necessary to disperse the initial colonizer and disperser biofilms, respectively.

6.3.6 Disperser cells displace initial colonizer biofilms

Having verified the disperser and initial colonizer cell elements of the μBE signaling circuit, we combined both cell types to form a consortial biofilm and investigated whether the disperser cells could displace the initial colonizer cells. First, robust biofilms of initial colonizer cells were formed for 9 h, and then disperser cells were added to the initial colonizer biofilms for 5 h to form the biofilm consortium (**Fig. 6.6a**). Since disperser cells synthesize 3*o*C12HSL constitutively, 3*o*C12HSL should bind to LasR when the concentration of 3*o*C12HSL is increased as the disperser biofilms mature. Then, the 3*o*C12HSL + LasR complex should induce dispersal of initial colonizer biofilms by switching on *bdcAE50Q* under control of the *lasI* promoter. As expected, the

initial colonizer biofilms were displaced from the surface as the disperser cells grew (**Fig. 6.6a)**. After 44 h, 80% of the maximum initial colonizer biofilm formed was removed (**Fig. 6.3e, Fig. 6.6a**). The displacement of the initial colonizer cells by the disperser cells was accomplished by the production of 3*o*C12HSL from the disperser biofilms not by shear force since the disperser biofilms that lack LasI did not reduce initial colonizer biofilms; i.e., both no *lasI* disperser and initial colonizer biofilms grew when 3*o*C12HSL was not produced (**Fig. 6.6b**), and the biofilm became essentially that of the faster-growing initial colonizer cells after 40 h (**Fig. 6.3f, Fig. 6.6b**). Hence, the disperser cells completely displaced the initial colonizer biofilm via the population-driven synthetic μBE systems.

The second key element of our design was the removal of the disperser biofilm; we found we could remove the disperser biofilm by inducing Hha13D6 with IPTG (**Fig. 6.6a**). After 62 h (18 h with 2 mM IPTG), 92% of the maximum disperser biofilm was removed (**Fig. 6.3e**).

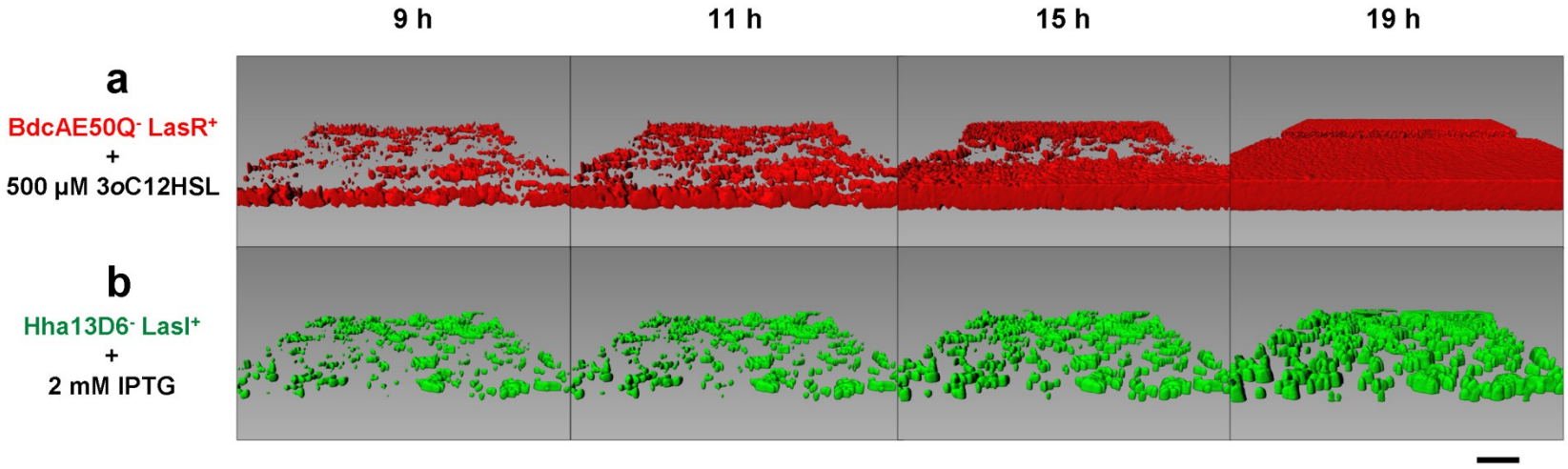

Fig. 6.5. Biofilms formed by cells that lack their respective biofilm dispersal proteins in the presence of 3*o*C12HSL or IPTG. (**a**) Initial colonizer biofilms that lack BdcA (BdcAE50Q$^-$, LasR$^+$ via *E. coli hha/*pRFP-*lasR*) with 500 µM of 3*o*C12HSL for 10 h. (**b**) Disperser biofilms that lack Hha (Hha13D6$^-$, LasI$^+$ via *E. coli hha/*pGFP-*lasI*) with 2 mM of IPTG for 10 h. Robust biofilms at 9 h were formed by seeding initial colonizer or disperser cells into microchambers. Scale bar indicates 20 µm.

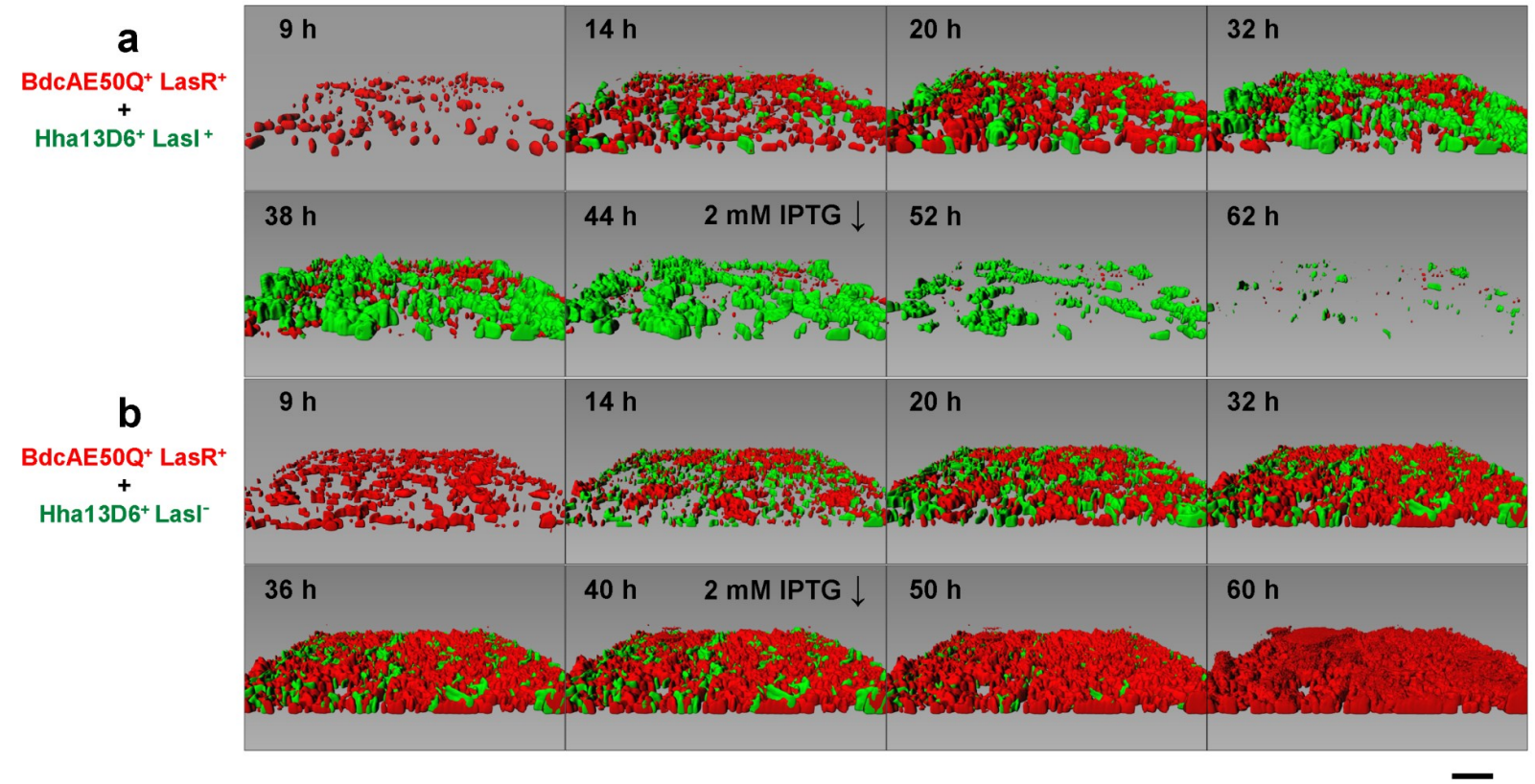

Fig. 6.6. Dispersal of dual-species biofilms. (**a**) An initial colonizer biofilm (BdcAE50Q$^+$, LasR$^+$) was formed by seeding for 9 h (red), and then disperser cells (green) were seeded for 5 h to form both initial colonizer and disperser biofilms. After 44 h, 2 mM of IPTG was added for an additional 18 h to remove the disperser biofilm. (**b**) Initial colonizer biofilms (BdcAE50Q$^+$, LasR$^+$) were formed by seeding for 9 h, then control disperser which lack LasI were seeded for 5 h to form both initial colonizer and control disperser biofilms. After 40 h, 2 mM of IPTG was introduced for an additional 20 h to try to disperse the no *lasI* disperser biofilms. Scale bar indicates 20 μm.

6.4 Discussion

We developed a synthetic μBE system by combining a QS signaling module with two engineered biofilm dispersal proteins. With this synthetic circuit, in a microfluidic channel, we (i) formed an initial colonizer biofilm with cells tagged red, (ii) introduced a second cell type (dispersers, tagged green) into this existing biofilm, (iii) created a means of communication between the two cell types, (iv) formed a robust biofilm with the disperser cells in an existing initial colonizer biofilm, (v) displaced the initial colonizer cells in the biofilm with a QS signal from the disperser cells, and (vi) removed the disperser cells with a chemically-induced switch. Our work demonstrates that biofilms can be formed, that new cells may be engineered to integrate and then replace the initial colonizer biofilm and that both cell types may be removed which is a promising strategy for applications requiring different kinds of engineered cells such as creating a biorefinery.

Although some of the biofilm may be dispersed naturally upon changes in environmental conditions (e.g., nutrition level and oxygen depletion)(269), it is a significant challenge to remove biofilms (270, 271) since cells in biofilms are cemented in place by the secreted polymer matrix consisting of polysaccharide, protein, DNA, and lipids (60). The matrix holds bacterial cells together and forms a protective barrier conferring resistance to killing by nonspecific and specific host defenses during infection and conferring tolerance to various antimicrobial agents such as disinfectants and antibiotics (60). Thus, the defensive nature of the biofilm colony makes most biofilms difficult or impossible to eradicate (269); hence, our demonstration that both the initial

colonizer and disperser biofilms may be nearly completely removed is highly significant.

To preferentially remove one type of cell in a biofilm, in our system it requires that the second cell elicit robust growth such that it can attach to an existing biofilm and propagate, that it flourishes, that it communicates to another cell as the QS signals generated within the biofilm must be perceived at a relatively high local concentration compared to planktonic cultures (266), and that it displaces the existing biofilm without itself being displaced but instead it forms a strong biofilm. Here, we produced the QS signal in the biofilm itself to remove the initial colonizer cells. As the signal accumulated, the engineered BdcA in the initial colonizer cells reduces c-di-GMP levels which results in a cascade of events, such as an increase in motility and reduction in adhesion production, that allows the initial colonizer cells to disperse (246).

As the initial colonizer cells disperse, the disperser cells must form a robust biofilm. After the disperser biofilm is formed, the engineered Hha protein must be able to cause dispersal since it induces cell lysis which leads to dispersal (245). Therefore, our synthetic μBE system provides a useful platform for the removal of existing deleterious biofilms via generating signaling molecules *in situ*. In addition, since the disperser cells grow more slowly than the initial colonizer ones, the disperser cells cannot displace the initial colonizer biofilm based on a difference in growth rates. This demonstrates clearly that QS circuit was required to complete this feat of progressive biofilm development/dispersal. Since, several biofilm dispersal signals have been identified including the auto-inducing peptide of the *agr* QS system of *Staphylococcus aureus* (272), changes in carbon sources (273), reduction in the concentration of c-di-GMP(246)

(as utilized here with BdcA), surfactant (274), *cis*-2-decenoic acid (275), as well as *D*-amino acids (276), we envision that other biofilm dispersal mechanisms may also be utilized to control biofilms.

The μBE device described here offers several advantages over the commercially available BioFlux device developed by Benoit *et al.* (31) and other microfluidic devices used for biofilm study (277). With our device, we can (i) precisely control the development of biofilm by intermittent flow of nutrients, (ii) completely isolate the biofilm from the media inlet and gradient generating channels using the pneumatic valves, and (iii) sequentially introduce different kinds of cell into the biofilm chamber. Of course, the ability to study a range of concentrations simultaneously with the eight channels (e.g., **Fig. 6.3cd**) was instrumental in analyzing the effect of various concentrations of 3*o*C12HSL and IPTG.

Bacterial QS systems have the attractive design features that they utilize diffusible signals(250). Here we show, for the first time, that a QS system may be utilized with biofilm dispersal proteins to control consortial biofilm formation; i.e., that an existing biofilm may be formed and then replaced by another biofilm which then may be removed. These types of synthetic QS circuits may be used to pattern biofilms by facilitating the re-use of platforms and to create sophisticated reactor systems that will be used to form bio-refineries. Furthermore, these systems may be adopted in industrial and clinical processing as an alternative strategy to overcome the current limitations of biofilm control.

6.5 Materials and methods

6.5.1 Bacterial strains and growth conditions

The bacterial strains and plasmids used in this study are listed in **Table 6.1** and were cultured at 37^{o}C. LB (278) with 0.2% glucose (LB-glucose) was used in all of the non-microfluidic experiments, and both M9(278) supplemented with 0.2% glucose (M9-glucose) and LB glucose were used in the microfluidic device. Kanamycin (50μg/mL) was used for overnight cultures, chloramphenicol (100 μg/mL) was used for maintaining the pCA24N-based plasmids, and erythromycin (300 μg/mL) was used for maintaining the pCM18-based plasmids.

6.5.2 Plasmid construction

All primers used for cloning are listed in **Table 6.2**. Plasmid pHha13D6-*gfp*-*lasI* (**Fig. 6.2a**) encodes *hha13D6* (245) under the control of the IPTG-inducible *T5*-*lac* promoter, as well as *gfp* and *lasI* under the control of constitutive CP25 promoter. To form this plasmid, *gfp* was amplified by three rounds of PCR: the first PCR with primers gfp-F3 and gfp-R and template pCM18 (262) was to amplify *gfp* with the same RBS of *rfp*, and the second PCR with primers gfp-F2 and gfp-R using the first PCR product as a template and the third PCR with primers gfp-F1 and gfp-R using the second PCR product as a template were performed to include the constitutive CP25 promoter of pCM18. pHha13D6-*gfp* was constructed by cloning the third PCR product into pCA24N-*hha13D6* (245) using the NotI and BlpI restriction sites after *hha13D6*.

Table 6.1. Strains and plasmids used in this study. Km^R, Cm^R, Em^R, and Ap^R are kanamycin, chloramphenicol, erythromycin, and ampicillin resistant, respectively.

Strains and plasmids	Genotype/relevant characteristics	Source
Strains		
E. coli hha	BW25113 Δ*hha* Ω Km^R	(260)
E. coli MG4/pKDT17	Ap^R, P_{lasB}::*lasB*$^+$-*lacZ*$^+$ translational fusion, P_{lac}::*lasR*$^+$	(265)
P. aeruginosa PAO1	Wild-type	T. McDermott
Plasmids		
pCA24N-*hha13D6*	Cm^R; *lacI*^{q}, pCA24N $P_{T5\text{-}lac}$::*hha13D6*$^+$	(245)
pHha13D6-*gfp*	Cm^R; *lacI*^{q}, pCA24N $P_{T5\text{-}lac}$::*hha13D6*$^+$ P_{CP25}::*gfp*$^+$	This study
pHha13D6-*gfp*-*lasI*	Cm^R; *lacI*^{q}, pCA24N $P_{T5\text{-}lac}$::*hha13D6*$^+$ P_{CP25}::*gfp*$^+$-*lasI*$^+$	This study
pCA24N-*bdcAE50Q*	Cm^R; *lacI*^{q}, pCA24N $P_{T5\text{-}lac}$::*bdcAE50Q*$^+$	(246)
pBdcAE50Q	Cm^R; *lacI*^{q}, pCA24N P_{lasI}::*bdcAE50Q*$^+$	This study
pBdcAE50Q-*rfp*-*lasR*	Cm^R; *lacI*^{q}, pCA24N P_{lasI}::*bdcAE50Q*$^+$ P_{CP25}::*rfp*$^+$-*lasR*$^+$	This study
pCM18	Em^R, P_{CP25}::*gfp*$^+$	(262)
pGFP-*lasI*	Em^R, P_{CP25}::*gfp*$^+$-*lasI*$^+$	This study
pCM18-X	Em^R, *gfp*-disrupted	This study
pRFP-*lasR*	Em^R, P_{CP25}::*rfp*$^+$-*lasR*$^+$	This study
pDsRed-Express	Ap^R, P_{lac}::*rfp*$^+$	Clontech
pDsRed-*lasR*	Ap^R, P_{lac}::*rfp*$^+$-*lasR*$^+$	This study
pDsRed-BlpIX-*lasR*	Ap^R, P_{lac}::*rfp*$^+$-*lasR*$^+$ (BlpI site disrupted)	This study

Table 6.2. Primers used for constructing plasmids for the μBE circuit. Underlined italic text indicates the restriction enzyme sites: AvaI in plasI-F, BlpI in lasI-F, lasI-R, rfp-lasR-F1, rfp-lasR-F3, and rfp-lasR-R, BseRI in plasI-R, and NotI in gfp-F1. Italicized bold text indicates the site-directed mutation for disruption of the BlpI restriction site (5'-GCTGAGC to 5'-TCTGAGC) in BlpI-X-F and BlpI-X-R. Underlined bold text indicates the site-directed mutation site for the codon corresponding to truncation at GFP Y66 (5'-TAT to 5'-TA**A** for Y66X) in gfpX-F and gfpX-R.

Primer Name	Primer Sequence (listed 5' to 3')
Construction of the plasmid for the disperser circuit (pHha13D6-*gfp-lasI*)	
gfp-F1	GGACTC*GCGGCCGC*TAAGGGCTTTGGCAGTTTATTCTTGACATGTAGTGAGGGGGCTGGT
gfp-F2	ACATGTAGTGAGGGGGCTGGTATAATAAAATAGTACTGTTCGGGTGAGCGGATAACAATT
gfp-F3	TTCGGGTGAGCGGATAACAATTTCACACAGGAAACAGCTATGCGTAAAGGAGAAGAACTT
lasI-F	CCTGCA*GCTGAGC*TTCTTCAGCTTCCTATTTGGAGGAAGTG
lasI-R	GCTCGACG*GCTCAGC*AGGTCCCCGTCATGAAACCGCCAGTCGC
Construction of the plasmid for the initial colonizer circuit (pBdcAE50Q-*rfp-lasR*)	
plasI-F	CGACGCCG*CTCGAG*GGGCTGTGTTCTCTCGTGTG
plasI-R	GCCGTGC*ATAGTTAATTTCTCCTC*TTTAATGGAAGCTGAAGAATTTATGC
BlpI-X-F	GTGCTCGCGGCGAACTCGGCGC***TCTGAGC***CTCAGCGTGGAAGCGG
BlpI-X-R	CCGCTTCCACGCTGAG***GCTCAGA***GCGCCGAGTTCGCCGCGAGCAC
BlpI-X-seq-F	GAACGCCTTCATCGTCGGCAACTACC
rfp-lasR-F1	GGACTC*GCTGAGC*GCTTTGGCAGTTTATTCTTGACATGTAGTGAGGGGGCTGGTATAATA
rfp-lasR-F2	GTGAGGGGGCTGGTATAATAAAATAGTACTGTTCGGGTGAGCGGATAACAATTTCACAC
rfp-lasR-F3	CCGGACTC*GCTGAGC*ATAACAATTTCACACAGGAAACAGCTATGACCATGATTACGC
rfp-lasR-R	GCTCGACG*GCTCAGC*AGGTCCCGCTCAGAGAGTAATAAGACCC
gfpX-F	CAACACTTGTCACTACTTTCGGT**TAA**GGTGTTCAATGCTTTGCGAGATAC
gfpX-R	GTATCTCGCAAAGCATTGAACACC**TTA**ACCGAAAGTAGTGACAAGTGTTG

The final construct pHha13D6-*gfp*-*lasI* was formed by cloning *lasI* with its native RBS from the *P. aeruginosa* PAO1 chromosome by using the lasI-F and lasI-R primers; the PCR product was cloned into pHha13D6-*gfp* using the BlpI restriction site. As a control plasmid for producing GFP and LasI but not producing Hha13D6, pGFP-*lasI* was constructed by inserting *lasI* into pCM18 using lasI-F and las-R primers.

Plasmid pBdcAE50Q-*rfp*-*lasR* (**Fig. 6.2b**) encodes *bdcAE50Q* (246) under the control of the *lasI* promoter, as well as *rfp* and *lasR* under the control of the constitutive CP25 promoter. pBdcAE50Q was constructed by replacing the *T5*-*lac* promoter in pCA24N-*bdcAE50Q* (246) with the *lasI* promoter from *P. aeruginosa* using the plasI-F and plasI-R primers; the PCR fragment was cloned into the Ava1 and BseRI restriction sites. Plasmid pDsRed-*lasR* was constructed by inserting *lasR* and its native RBS into the NotI site downstream of the *rfp* sequence in pDsRed-Express (Clontech, CA, USA) using the lasR-F and lasR-R primers. Since a BlpI restriction site lies within *lasR* but was required for the next cloning steps, the BlpI site in pDsRed-*lasR* was disrupted by site-directed mutagenesis (245) (5'-GCTGAGC to 5'-TCTGAGC) using the BlpIX-F and BlpIX-R primers (this mutation did not change the aa sequence), to form pDsRed-BlpIX-*lasR*. *rfp* and *lasR* were amplified from pDsRed-BlpIX-*lasR* by two rounds of PCR to include the constitutive CP25 promoter of pCM18: the first PCR was performed using the rfp-lasR-F2 and rfp-lasR-R primers and the second PCR was performed using the rfp-lasR-F1 and rfp-lasR-R primers with the first PCR product. The final construct pBdcAE50Q-*rfp*-*lasR* was formed by inserting the *rfp* and *lasR* PCR products into the BlpI site downstream of *bdcAE50Q* in pBdcAE50Q. As a control plasmid for producing

RFP and LasR but not producing BdcAE50Q, pRFP-*lasR* was constructed by inserting *rfp* and *lasR* using the rfp-lasR-F3 and rfp-lasR-R primers into pCM18-X in which *gfp* was disrupted by introducing a truncation at Y66 of GFP using the gfpX-F and gfpX-R primers in pCM18. All plasmids were confirmed by PCR and DNA sequencing.

6.5.3 Microfluidic device fabrication

The poly(dimethyl)siloxane (PDMS)-based μBE device (**Fig. 6.1b**) was fabricated in the Materials Characterization Facility at Texas A&M University using conventional soft lithographic techniques as described previously (234). The μBE device consists of a glass slide and two layers, a bottom layer with a diffusive-mixer and eight microchambers, and a top layer which contains the pneumatic elements for controlling microvalves and a second diffusive mixer. The diffusive mixer in the bottom layer was used to generate different concentrations of dispersal signals (e.g., IPTG for removing disperser cells) and to perfuse growth media into the biofilm microchambers. The mixer in the top layer was used to introduce bacteria into the microchambers at different cell densities (**Fig. 6.1b**). The dimensions of the diffusive mixers in both the top and bottom layers were 100 μm (width) × 150 μm (height) and 200 μm (width) × 200 μm (height) respectively, and the biofilm microchambers were 600 μm (width) × 150 μm (height). All pneumatic channels were 200 μm thick. The two layers were fabricated separately and assembled by sequential oxygen plasma treatment and bonding (100 mTorr, 100 W, 40 s) in a reactive ion etcher. The top pneumatic layer was first aligned and bonded to the bottom diffusive-mixer/microchamber membrane layer followed by bonding of the

combined PDMS layer to a cover glass (22 x 50 mm). Tygon tubing (0.01" ID × 0.03" OD, Saint Gobain performance plastics, OH, USA) was used for all fluidic connections. Two PicoPlus 11 syringe pumps (Harvard Apparatus, MA, USA) were used for each experiment to separately control fluid flow rates in the two layers. A temperature controlled micro-incubator was used to maintain the temperature of the device at 37^{o}C. Moist air flowed continuously over the device in order to maintain humidity and avoid bubble formation inside the microchambers. The opening and closing of valves were pneumatically controlled by introducing vacuum or compressed air through the solenoid valves. The operation of solenoid valves and syringe pumps were remotely controlled through programs developed in-house for the LabVIEW platform (National Instruments, TX, USA).

6.5.4 Microfluidic biofilm experiments

For mono-species biofilm dispersal experiments, overnight cultures were washed and resuspended in M9 medium supplemented with glucose (0.2%) at a turbidity at 600 nm of ~1.0. The bacterial suspension was introduced into the eight biofilm microchambers through the top layer in the PDMS device (**Fig. 6.1b**). During this process, the main inlet valves (**Fig. 6.1b**) remained closed to prevent cells from entering and forming biofilm in the gradient mixing channels and to ensure proper mixing of dispersal signals before they enter the microchambers. The main outlet valves and seeding valves were then closed, and the culture was maintained without flow for 2 h to enable attachment of bacteria to the glass surface (seeding). After 2 h, main inlet and outlet valves were

opened, unattached cells were removed, and the attached bacteria were allowed to grow by flowing LB-glucose at 2 μL/min. After 3 h, the medium was switched from LB-glucose to M9-glucose for 3 h because we found that a sudden depletion of nutrients promoted rapid development of biofilms. The biofilm was then developed for another 3 h by introducing LB-glucose into the chambers in a semi-batch mode (55 min static and 5 min flow). Thus, within 9 h after seeding, a robust and mature biofilm was formed. To disperse the biofilm, LB-glucose and LB-glucose containing a single concentration of the dispersal signal (IPTG for disperser cells and 3*o*C12HSL for initial colonizer cells) was introduced through the two media inlets and allowed to mix in the serpentine gradient generating channels to form eight concentrations of the dispersal signal in LB-glucose medium. Each stream leaving the diffusive mixer was used to perfuse a specific biofilm microchamber for 10 h.

For dual-species biofilm dispersal experiments, initial colonizer cell biofilm was developed uniformly across all eight microchambers for 9 h as for mono-species biofilms. During this 9 h period, unattached initial colonizer cells were continuously removed from the cell mixer and connecter tubing through the cell outlet by flowing M9 medium at 8 μL/min. After formation of the initial colonizer biofilm, disperser cells (turbidity at 600 nm of 2.0 in M9-glucose) were continuously perfused into the microchamber for 5 h to allow disperser cells to colonize the initial colonizer biofilm as well as the glass surface in vacant regions. After 5 h, LB-glucose was introduced into the microchamber in semi-batch mode (55 min static and 5 min flow) for 28-30 h. The static condition ensured biofilm development and build-up of 3*o*C12HSL needed for induction

of the BdcAE50Q dispersal protein in initial colonizer cells. To remove the disperser cell biofilm, LB-glucose containing 2 mM IPTG was introduced in semi-batch mode for 18 to 20 h.

6.5.5 Confocal microscopy

Images were taken every 1 to 2 h using a 40X/0.85 NA dry objective with a TCS SP5 scanning confocal laser microscope (Leica Microsystems, Wetzlar, Germany)(21). Z-stack images were taken at a zoom level of 2 such that the image covered 90% of width of the microchamber. Two individual positions per microchamber covering a total of 70% of the channel length were chosen for imaging. Using the confocal z-stack images, 3-D reconstruction of the biofilm architecture was performed using IMARIS 3D and 4D Real-Time Interactive Data Visualization software (Bitplane Inc., CT, USA). Biomass and average biofilm height were obtained using COMSTAT image-processing software(279).

6.5.6 Flow-cell biofilm experiments and biofilm volume analysis

Overnight cultures were diluted to a turbidity at 600 nm of 0.05 in LB-glucose and pumped through the flow-cell (BST model FC81, Biosurface Technologies, MT, USA) at 10 mL/h for 2 h, then LB-glucose was pumped for 48 h to form biofilms. The biofilms on the glass slides were visualized after robust biofilms were formed (48 h) using a confocal microscope. COMSTAT was used to analyze the biofilms formed at 13 positions. Biofilm volume was calculated by multiplying biofilm biomass and the

surface area (1400 mm^2) of the flow-cell.

6.5.7 3*o*C12HSL assay in biofilms

The flow-cell was disassembled, and biofilms samples were collected by wiping the coverslip, glass slides, and four sides of the flow-cell with paper towels (Kimwipes, 1.5 cm × 1.5 cm). This was repeated three times to ensure all biofilm cells were collected. The biofilm cells were resuspended in 5 mL of dH_2O, mixed, and centrifuged. The biofilm cells were resuspended in 3 mL of dH_2O and sonicated twice using a 60 Sonic Dismembrator (Fisher Scientific, PA, USA) at level 10 for 15 sec. 3*o*C12HSL was extracted as described previously(280) with slight modifications. The samples were extracted three times with a half volume of dichloromethane. The aqueous residue was removed after freezing the samples for 3 h at -20ºC. The solvent was evaporated via rotary evaporation, and the residue was resuspended in 200 µL of ethyl acetate. *E. coli* MG4/pKDT17 was used to assay the 3*o*C12HSL levels(265). This reporter strain contains a copy of the *lasR* gene as well as a *lasB*::*lacZ* fusion. β-galactosidase activity was measured as described previously(281). Synthetic 3*o*C12HSL (Sigma-Aldrich, MO, USA) was used as the standard (**Fig. 6.7**), and planktonic cultures of *E. coli hha*/pHha13D6-*gfp,* which does not produce 3*o*C12HSL, was used as a negative control. As additional controls, effluent from the flow-cell and planktonic cultures were used to compare with 3*o*C12HSL concentrations from the biofilm.

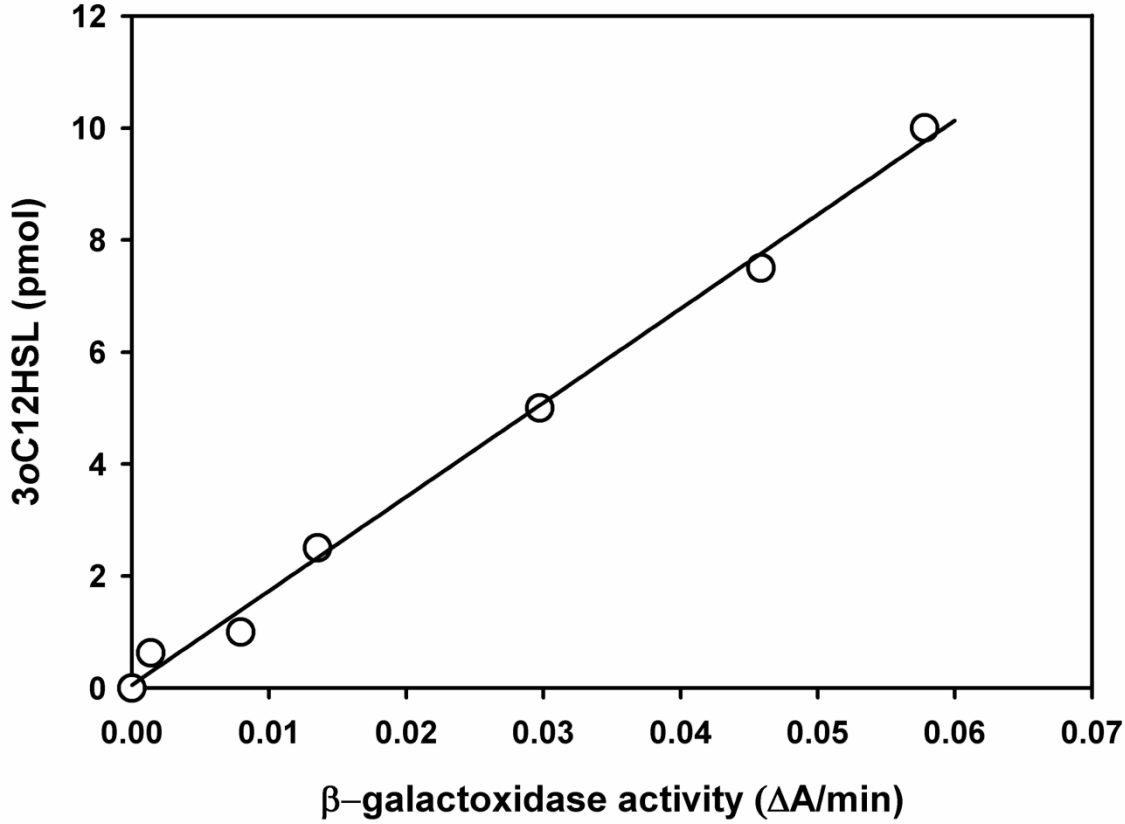

Figure 6.7. Standard curve for determining 3*o*C12HSL concentrations. β-galactosidase activity was measured using reporter *E. coli* MG4/pKDT17 upon adding different amounts of 3*o*C12HSL.

CHAPTER VII

CONCLUSIONS AND RECOMMENDATIONS

7.1 Conclusions

We showed that norepinephrine (NE) is an important host signal produced during stress that increases *P. aeruginosa* growth, motility, attachment, and virulence, all of which are integral to infection (Chapter III). Based on this, we hypothesize the *P. aeruginosa* causes gut-derived sepsis during chronic stress, by utilizing the NE released in the gut to produce more motile, more adherent, and potentially more virulent cells. Our data also showed that the actions of NE are mediated primarily through the LasR, and not the RhlR QS system.

We also investigated the molecular mechanism involved in the chemo-sensing of the bacterial cell-cell communication molecule autoinducer-2 by *E. coli* and *S. typhimurium* (Chapter IV). We performed different chemotaxis assays (capillary, microPlug and microFlow assays) to demonstrate that AI-2 is a potent attractant for *E. coli* and *S. typhimurium* and that the Tsr chemoreceptor and LsrB are necessary for sensing AI-2, although uptake of AI-2 into the cytoplasm is not required. We concluded that LsrB, when bound to AI-2, interacts directly with the periplasmic domain of Tsr primarily at the Thr-61 and Asp-63 residues of LsrB, making LsrB the first known periplasmic-protein partner for Tsr. Thus, we propose that chemotaxis toward a bacterial communication signal like AI-2 may be an important virulence factor within the

gastrointestinal (GI) tract that could help free-swimming, planktonic bacteria colonize developing biofilms.

We developed a simple user-friendly microfluidic flow cell device (μBF device, Chapter V) that is customizable and contains eight separate microchambers for cultivating biofilms exposed to eight different concentrations of signals through a single gradient mixer. The presence of pneumatic valves and a separate cell seeding port that is independent from gradient-mixing channels offered complete isolation of the biofilm microchamber from the gradient mixer, and also performed well under flow, batch or semi-batch conditions. The μBF device we fabricated can precisely measure the effect of a wide range of concentrations of single or combinations of two or more soluble signals on bacterial biofilm formation and development. The device enabled screening of compounds and their concentrations that effectively inhibit biofilm formation of pathogenic bacteria. Also, we showed that the μBF device can be used to perform competition based studies to study the overall effect of two or more compounds on biofilm formation (e.g., 7-HI vs. isatin) and check which compound is most important in controlling biofilm.

We also upgraded the μBF device by adding a second top layer that contains a gradient mixer and a few other features and named it the microfluidic biofilm engineering (μBE) device. We used this μBE device to manipulate *E. coli* biofilm formation using tools of synthetic biology and protein engineering. We constructed a synthetic biofilm circuit that utilizes the Hha and BdcA dispersal proteins of *E. coli* along with a quorum sensing (QS) switch that works based on the accumulation of the

signal *N*-(3-*oxo*-dodecanoyl)-*L*-homoserine lactone (3-*o*-C12HSL) and implemented it in the μBE device. We showed that a QS system may be utilized with biofilm dispersal proteins to control consortial biofilm formation by removing an existing biofilm and then removing the biofilm that displaced the first one. These types of synthetic QS circuits may be used to pattern biofilms by facilitating the re-use of platforms and to create sophisticated reactor systems that will be used to form bio-refineries.

7.2 Recommendations

The μBF device has significant potential for studying the role of inter- and intra-kingdom signaling on bacterial biofilm formation and colonization and for quantitatively investigating bacterial chemotaxis, especially repellent taxis. The μBF prototype can be modified for investigating the role of signal-mediated bacterial chemotaxis in colonization and biofilm formation in the GI tract. For example, we can use the device to test the hypothesis that recognition of AI-2 and the resultant migration (i.e., chemotaxis) toward it contribute to recruitment of planktonic bacteria to bacterial communities. The effective concentration of AI-2 from a biofilm that planktonic bacteria encounter is not accurately known; therefore, we will create AI-2 concentration gradients arising from a biofilm with a microfluidic concentration generator and investigate if motile *E. coli* is recruited from the planktonic phase to colonize a surface. The modified μBF device will consist of three layers (**Fig. 7.1A**). The bottom layer (biofilm module) will be similar to the top layer of the μBF device with eight biofilm chambers where AI-2 can be introduced or

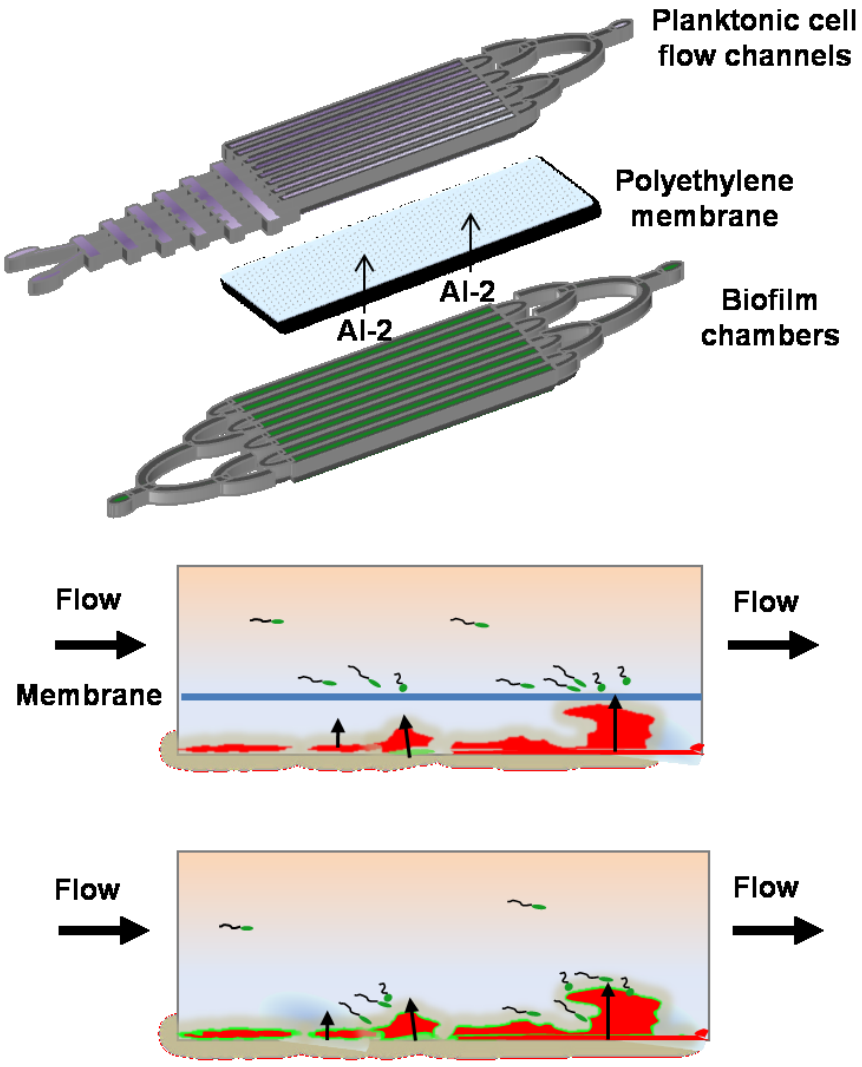

Fig 7.1. Using the µBF device to monitor the biofilm formation and recruitment of planktonic bacteria to an existing biofilm. (**A**) The dual-microchamber construction used to examine attraction of planktonic cells to biofilm, in which the upper chambers can be used to flow motile bacteria, and the lower chambers can be used to flow AI-2 or to form a biofilm. A permeable membrane will separate the two chambers. Diffusion of AI-2 through the membrane is indicated by arrows. (**B**) Response of planktonic cell expressing GFP to AI-2 producing biofilms, whose cells express RFP; the arrows indicate relative strengths of AI-2 generation. Cells should accumulate at the membrane above AI-2 generating biofilm clusters. The cells are shown adhering to the membrane. (C) The same experiment in B except that cells will be allowed direct access to the developing biofilm; in this case, the planktonic cells are actually forming and joining the biofilms.

where bacteria can be cultured and biofilm communities developed. The top layer will also have an additional module containing eight chemotaxis microchambers identical to the biofilm chambers in the bottom layer. The two layers will be separated by a porous PDMS or agarose membrane. The device will be aligned such that each chemotaxis chamber is directly underneath a single biofilm chamber. When a stream containing a specific concentration of AI-2 flows through the bottom layer (**Fig. 7.1B**) or AI-2 producing biofilms are present in the bottom biofilm chambers, AI-2 will diffuse through the porous membrane so that cells in the top layer are exposed to it. If an attractant signal is produced, bacteria should accumulate on or near the membrane.

We discovered through our *in vitro* studies that human stress hormone NE is an inter-kingdom signal that increases pathogenesis of *P. aeruginosa* (Chapter III). Building on these results, we need to investigate if NE produced *in vivo* in the gut during chronic stress actually contributes to *P. aeruginosa* gut-derived sepsis by increasing its colonization and virulence. We can develop a *P. aeruginosa* sepsis model in rats to determine the regions in the gut the pathogen colonizes when the animal is stressed (e.g., burn injury) and extract tissue samples to measure the concentration of NE in those regions. If this is not a feasible option, microfluidic devices can be designed to mimic the actual *in vivo* environment (282). The modified μBF (Fig. 7.1A) with dual-microchamber construction can be used to examine attraction of planktonic cells *P. aeruginosa* cells to NE and intestinal epithelial cells, in which the upper chambers can be used to flow bacteria, and the lower chambers can be used to cultivate mucus producing intestinal epithelial cell line in the presence of different concentrations of NE.

Different concentrations of NE can diffuse through the permeable membrane that separates the two chambers and generate gradients of different strength, thereby generating an environment similar to that seen in vivo where the concentrations of signals are not uniform (283).

In Chapter IV, we performed different chemotaxis assays (capillary, microPlug and microFlow assays) to investigate the molecular mechanism involved in the chemo-sensing of the bacterial cell-cell communication molecule AI-2 by *E. coli* and *S. typhimurium* and demonstrated that AI-2 is a potent attractant for *E. coli* and *S. typhimurium* and that the Tsr chemoreceptor and LsrB are necessary for sensing AI-2, although uptake of AI-2 into the cytoplasm is not required. Similarly, we can perform chemotaxis assays on chemoreceptor knockout mutants available in our lab to investigate how pathogens such as EHEC and *S. typhimurium* sense inter-kingdom signals such as human hormones such as NE, dopamine, and serotonin, and intra-kingdom signals such as indole, hydroxyindoles, isatin, and homoserine lactones (**Fig 7.2**).

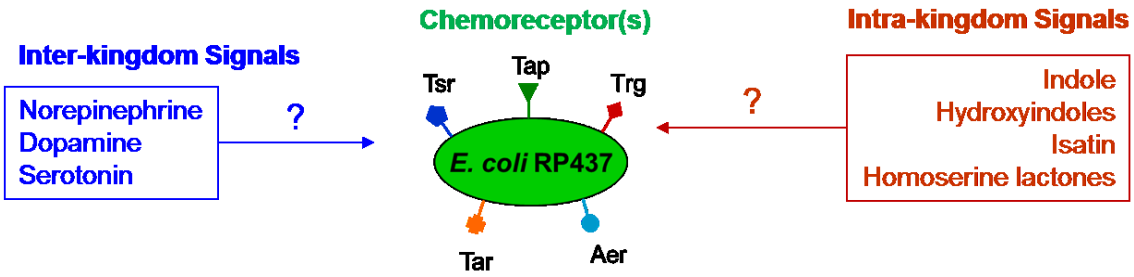

Fig 7.2. Recognition of inter- and intra-kingdom signals by *E. coli* chemoreceptors

REFERENCES

1. Costerton JW, Lewandowski Z, Caldwell DE, Korber DR, & Lappin-Scott HM (1995) Microbial biofilms. *Ann Rev Microbiol* 49(1):711-745.

2. Lederberg J (2000) Infectious history. *Science* 288(5464):287-293.

3. Ley RE, Peterson DA, & Gordon JI (2006) Ecological and evolutionary forces shaping microbial diversity in the human intestine. *Cell* 124(4):837-848.

4. Kau AL, Ahern PP, Griffin NW, Goodman AL, & Gordon JI (2011) Human nutrition, the gut microbiome and the immune system. *Nature* 474(7351):327-336.

5. Hooper LV & Gordon JI (2001) Commensal host-bacterial relationships in the gut. *Science* 292(5519):1115-1118.

6. Gilmore MS & Ferretti JJ (2003) The thin line between gut commensal and pathogen. *Science* 299(5615):1999-2002.

7. Lamps LW (2003) Pathology of food-borne infectious diseases of the gastrointestinal tract: an update. *Adv Anatom Pathol* 10(6):319-327.

8. WHO (2007) Food safety and foodborne illness. (http://www.who.int/mediacentre/factsheets/fs237/en/index.html).

9. Samadpour M, Barbour MW, Nguyen T, Cao TM, Buck F*, et al.* (2006) Incidence of enterohemorrhagic *Escherichia coli*, *Escherichia coli* O157, *Salmonella*, and *Listeria monocytogenes* in retail fresh ground beef, sprouts, and mushrooms. *J Food Prot* 69:441-443.

10. Alverdy J, Holbrook C, Rocha F, Seiden L, Wu RL*, et al.* (2000) Gut-derived sepsis occurs when the right pathogen with the right virulence genes meets the right host: evidence for in vivo virulence expression in *Pseudomonas aeruginosa*. *Ann Surg* 232(4):480-489.

11. Kaper JB, Nataro JP, & Mobley HLT (2004) Pathogenic *Escherichia coli*. *Nat Rev Micro* 2(2):123-140.

12. FDA (2010) Foodborne illness costs nation $152 billion annually. (http://www.producesafetyproject.org/media?id=0009).

13. CDC (2011) CDC Estimates of Foodborne Illness in the United States. (http://www.cdc.gov/foodborneburden/2011-foodborne-estimates.html).

14. Pennington H (2010) *Escherichia coli* O157. *Lancet* 376(9750):1428-1435.

15. Goldwater PN (2007) Treatment and prevention of enterohemorrhagic *Escherichia coli* infection and hemolytic uremic syndrome. *Exp Rev Anti-infect Ther* 5(4):653-663.

16. Shimizu K, Ogura H, Goto M, Asahara T, Nomoto K*, et al.* (2006) Altered gut flora and environment in patients with severe SIRS. *J Trauma* 60(1):126-133.

17. Alverdy JC & Chang EB (2008) The re-emerging role of the intestinal microflora in critical illness and inflammation: why the gut hypothesis of sepsis syndrome will not go away. *J Leukoc Biol* 83(3):461-466.

18. Schook LB, Carrick L, Jr., & Berk RS (1976) Murine gastrointestinal tract as a portal of entry in experimental *Pseudomonas aeruginosa* infections. *Infect Immun* 14(2):564-570.

19. Federle MJ & Bassler BL (2003) Interspecies communication in bacteria. *J Clin Invest* 112(9):1291-1299.

20. Fuqua C & Greenberg EP (2002) Listening in on bacteria: acyl-homoserine lactone signalling. *Nat Rev Mol Cell Biol* 3(9):685-695.

21. Lee J, Jayaraman A, & Wood TK (2007) Indole is an inter-species biofilm signal mediated by SdiA. *BMC Microbiol* 7:42.

22. Bansal T, Englert D, Lee J, Hegde M, Wood TK*, et al.* (2007) Differential effects of epinephrine, norepinephrine, and indole on *Escherichia coli* O157:H7 chemotaxis, colonization, and gene expression. *Infect Immun* 75(9):4597-4607.

23. Lee J, Bansal T, Jayaraman A, Bentley WE, & Wood TK (2007) Enterohemorrhagic *Escherichia coli* biofilms are inhibited by 7-hydroxyindole and stimulated by isatin. *Appl Environ Biotechnol* 73(13):4100-4109.

24. Domka J, Lee J, & Wood TK (2006) YliH (BssR) and YceP (BssS) regulate *Escherichia coli* K-12 biofilm formation by influencing cell signaling. *Appl Environ Microbiol* 72(4):2449-2459.

25. Hughes DT & Sperandio V (2008) Inter-kingdom signalling: communication between bacteria and their hosts. *Nat Rev Micro* 6(2):111-120.

26. Otto M (2009) Bacterial sensing of antimicrobial peptides. *Contrib Microbiol* 16:136-149.

27. Bansal T, Jesudhasan P, Pillai S, Wood TK, & Jayaraman A (2008) Temporal regulation of enterohemorrhagic *Escherichia coli* virulence mediated by autoinducer-2. *Appl Microbiol Biotechnol* 78(5):811-819.

28. Hazelbauer GL, Falke JJ, & Parkinson JS (2008) Bacterial chemoreceptors: high-performance signaling in networked arrays. *Trends Biochem Sci* 33(1):9-19.

29. Englert DL, Jayaraman A, & Manson MD (2009) Microfluidic techniques for the analysis of bacterial chemotaxis. *Met Molecular Biol* 571:1-23.

30. Kim KP, Kim Y-G, Choi C-H, Kim H-E, Lee S-H*, et al.* (2010) In situ monitoring of antibiotic susceptibility of bacterial biofilms in a microfluidic device. *Lab Chip* 10(23):3296-3299.

31. Benoit MR, Conant CG, Ionescu-Zanetti C, Schwartz M, & Matin A (2010) New device for high-throughput viability screening of flow biofilms. *Appl Environ Microbiol* 76(13):4136-4142.

32. Lee J-H, Kaplan J, & Lee W (2008) Microfluidic devices for studying growth and detachment of *Staphylococcus epidermidis* biofilms. *Biomed Microdev* 10(4):489-498.

33. Cho H, Jönsson H, Campbell K, Melke P, Williams JW*, et al.* (2007) Self-organization in high-density bacterial colonies: efficient crowd control. *PLoS Biol* 5(11):e302.

34. Ley RE, Hamady M, Lozupone C, Turnbaugh PJ, Ramey RR*, et al.* (2008) Evolution of mammals and their gut microbes. *Science* 320(5883):1647-1651.

35. Whitman WB, Coleman DC, & Wiebe WJ (1998) Prokaryotes: the unseen majority. *Proc Nat Acad Sci USA* 95(12):6578-6583.

36. Possemiers S, Bolca S, Verstraete W, & Heyerick A (2011) The intestinal microbiome: a separate organ inside the body with the metabolic potential to influence the bioactivity of botanicals. *Fitoterapia* 82(1):53-66.

37. Mazmanian SK, Liu CH, Tzianabos AO, & Kasper DL (2005) An immunomodulatory molecule of symbiotic bacteria directs maturation of the host immune system. *Cell* 122(1):107-118.

38. Sekirov I, Russell SL, Antunes LCM, & Finlay BB (2010) Gut microbiota in health and disease. *Physiol Rev* 90(3):859-904.

39. Girard MP, Steele D, Chaignat C-L, & Kieny MP (2006) A review of vaccine research and development: human enteric infections. *Vaccine* 24(15):2732-2750.

40. Terry K, Williams SM, Connolly L, & Ottemann KM (2005) Chemotaxis plays multiple roles during *Helicobacter pylori* animal infection. *Infect Immun* 73(2):803-811.

41. Anderson GG, Palermo JJ, Schilling JD, Roth R, Heuser J*, et al.* (2003) Intracellular bacterial biofilm-like pods in urinary tract infections. *Science* 301(5629):105-107.

42. Lutgendorff F, Akkermans LM, & Soderholm JD (2008) The role of microbiota and probiotics in stress-induced gastro-intestinal damage. *Curr Mol Med* 8(4):282-298.

43. Nataro JP & Kaper JB (1998) Diarrheagenic *Escherichia coli*. *Clin Microbiol Rev* 11(1):142-201.

44. Vladimirov N & Sourjik V (2009) Chemotaxis: how bacteria use memory. *Biol Chem* 390(11):1097-1104.

45. Adler J (1973) A method for measuring chemotaxis and use of the method to determine optimum conditions for chemotaxis by *Escherichia coli*. *J Gen Microbiol* 74(1):77-91.

46. Adler J (1966) Chemotaxis in bacteria. *Science* 153(737):708-716.

47. Adler J (1975) Chemotaxis in bacteria. *Ann Rev Biochem* 44(1):341-356.

48. Tso W-W & Adler J (1974) Negative chemotaxis in *Escherichia coli*. *J Bacteriol* 118(2):560-576.

49. Berg HC & Brown DA (1972) Chemotaxis in *Escherichia coli* analysed by three-dimensional tracking. *Nature* 239(5374):500-504.

50. Parkinson JS (2004) Signal amplification in bacterial chemotaxis through receptor teamwork. *ASM News* 70:575-582.

51. Kearns DB (2010) A field guide to bacterial swarming motility. *Nat Rev Micro* 8(9):634-644.

52. Englert DL, Manson MD, & Jayaraman A (2010) Investigation of bacterial chemotaxis in flow-based microfluidic devices. *Nat Prot* 5(5):864-872.

53. Englert DL, Manson MD, & Jayaraman A (2010) A microfluidic device for quantifying bacterial chemotaxis in stable concentration gradients. *J Vis Exp* (38).

54. Beebe DJ, Mensing GA, & Walker GM (2002) Physics and applications of microfluidics in biology. *Ann Rev Biomed Eng* 4(1):261-286.

55. Mao H, Cremer PS, & Manson MD (2003) A sensitive, versatile microfluidic assay for bacterial chemotaxis. *Proc Nat Acad Sci USA* 100(9):5449-5454.

56. Englert DL, Manson MD, & Jayaraman A (2009) Flow-based microfluidic device for quantifying bacterial chemotaxis in stable, competing gradients. *Appl Environ Microbiol* 75(13):4557-4564.

57. Costerton JW, Stewart PS, & Greenberg EP (1999) Bacterial biofilms: a common cause of persistent infections. *Science* 284(5418):1318-1322.

58. Klemm P, Hancock V, Kvist M, & Schembri MA (2007) Candidate targets for new antivirulence drugs: selected cases of bacterial adhesion and biofilm formation. *Future Microbiol* 2(6):643-653.

59. Sutherland IW (2001) The biofilm matrix - an immobilized but dynamic microbial environment. *Trends Microbiol* 9:222-227.

60. Flemming H-C & Wingender J (2010) The biofilm matrix. *Nat Rev Micro* 8(9):623-633.

61. Macfarlane S & Dillon JF (2007) Microbial biofilms in the human gastrointestinal tract. *J Appl Microbiol* 102(5):1187-1196.

62. González Barrios AF, Zuo R, Hashimoto Y, Yang L, Bentley WE*, et al.* (2006) Autoinducer 2 controls biofilm formation in *Escherichia coli* through a novel motility quorum-sensing regulator (MqsR, B3022). *J Bacteriol* 188(1):305-316.

63. Méndez-Ortiz MM, Hyodo M, Hayakawa Y, & Membrillo-Hernández J (2006) Genome-wide transcriptional profile of *Escherichia coli* in response to high levels of the second messenger 3′,5′-cyclic diguanylic acid. *J Biol Chem* 281(12):8090-8099.

64. de Nys R, Wright AD, König GM, & Sticher O (1993) New halogenated furanones from the marine alga *Delisea pulchra* (cf. fimbriata). *Tetrahedron* 49(48):11213-11220.

65. Manefield M, de Nys R, Naresh K, Roger R, Givskov M*, et al.* (1999) Evidence that halogenated furanones from *Delisea pulchra* inhibit acylated homoserine lactone (AHL)-mediated gene expression by displacing the AHL signal from its receptor protein. *Microbiology* 145(2):283-291.

66. Ren D, Bedzyk LA, Ye RW, Thomas SM, & Wood TK (2004) Differential gene expression shows natural brominated furanones interfere with the autoinducer-2 bacterial signaling system of *Escherichia coli*. *Biotechnol Bioeng* 88(5):630-642.

67. Lee J, Bansal T, Jayaraman A, Bentley WE, & Wood TK (2007) Enterohemorrhagic *Escherichia coli* biofilms are inhibited by 7-Hydroxyindole and stimulated by isatin. *Appl. Environ. Microbiol.* 73:4100-4109.

68. Filiatrault MJ, Picardo KF, Ngai H, Passador L, & Iglewski BH (2006) Identification of *Pseudomonas aeruginosa* genes involved in virulence and anaerobic growth. *Infect Immun* 74(7):4237-4245.

69. Lewenza S, Falsafi RK, Winsor G, Gooderham WJ, McPhee JB*, et al.* (2005) Construction of a mini-Tn*5*-*luxCDABE* mutant library in *Pseudomonas aeruginosa* PAO1: a tool for identifying differentially regulated genes. *Gen Res* 15(4):583-589.

70. Stover CK, Pham XQ, Erwin AL, Mizoguchi SD, Warrener P*, et al.* (2000) Complete genome sequence of *Pseudomonas aeruginosa* PA01, an opportunistic pathogen. *Nature* 406(6799):959-964.

71. He J, Baldini RL, Déziel E, Saucier M, Zhang Q*, et al.* (2004) The broad host range pathogen *Pseudomonas aeruginosa* strain PA14 carries two pathogenicity islands harboring plant and animal virulence genes. *Proc Natl Acad Sci USA* 101(8):2530-2535.

72. Rahme LG, Ausubel FM, Cao H, Drenkard E, Goumnerov BC*, et al.* (2000) Plants and animals share functionally common bacterial virulence factors. *Proc Natl Acad Sci U S A* 97(16):8815-8821.

73. Smith RS & Iglewski BH (2003) *Pseudomonas aeruginosa* quorum-sensing systems and virulence. *Curr Opin Microbiol* 6(1):56-60.

74. Diggle SP, Matthijs S, Wright VJ, Fletcher MP, Chhabra SR*, et al.* (2007) The *Pseudomonas aeruginosa* 4-quinolone signal molecules HHQ and PQS play multifunctional roles in quorum sensing and iron entrapment. *Chem Biol* 14(1):87-96.

75. Wade DS, Calfee MW, Rocha ER, Ling EA, Engstrom E*, et al.* (2005) Regulation of *Pseudomonas* Quinolone signal synthesis in *Pseudomonas aeruginosa*. *J Bacteriol* 187(13):4372-4380.

76. Gallagher LA & Manoil C (2001) *Pseudomonas aeruginosa* PAO1 kills *Caenorhabditis elegans* by cyanide poisoning. *J Bacteriol* 183(21):6207-6214.

77. Holder IA, Neely AN, & Frank DW (2001) Type III secretion/intoxication system important in virulence of *Pseudomonas aeruginosa* infections in burns. *Burns* 27(2):129-130.

78. Lamont IL, Beare PA, Ochsner U, Vasil AI, & Vasil ML (2002) Siderophore-mediated signaling regulates virulence factor production in *Pseudomonas aeruginosa*. *Proc Natl Acad Sci USA* 99(10):7072-7077.

79. Lugtenberg BJ, Dekkers L, & Bloemberg GV (2001) Molecular determinants of rhizosphere colonization by *Pseudomonas*. *Annu Rev Phytopathol* 39:461-490.

80. Smith RS & Iglewski BH (2003) *P. aeruginosa* quorum-sensing systems and virulence. *Curr. Opin. Microbiol.* 6(1):56-60.

81. Pukatzki S, Kessin RH, & Mekalanos JJ (2002) The human pathogen *Pseudomonas aeruginosa* utilizes conserved virulence pathways to infect the social amoeba *Dictyostelium discoideum*. *Proc Natl Acad Sci USA* 99(5):3159-3164.

82. Hassett DJ, Charniga L, Bean K, Ohman DE, & Cohen MS (1992) Response of *Pseudomonas aeruginosa* to pyocyanin: mechanisms of resistance, antioxidant defenses, and demonstration of a manganese-cofactored superoxide dismutase. *Infect Immun* 60(2):328-336.

83. Bejarano PA, Langeveld JP, Hudson BG, & Noelken ME (1989) Degradation of basement membranes by *Pseudomonas aeruginosa* elastase. *Infect Immun* 57(12):3783-3787.

84. Zulianello L, Canard C, Köhler T, Caille D, Lacroix JS*, et al.* (2006) Rhamnolipids are virulence factors that promote early infiltration of primary

human airway epithelia by *Pseudomonas aeruginosa*. *Infect Immun* 74(6):3134-3147.

85. Winsor GL, Lo R, Ho Sui SJ, Ung KSE, Huang S*, et al.* (2005) *Pseudomonas aeruginosa* genome database and pseudoCAP: facilitating community-based, continually updated, genome annotation. *Nucleic Acids Res* 33(Database issue):D338-343.

86. Mok KC, Wingreen NS, & Bassler BL (2003) *Vibrio harveyi* quorum sensing: a coincidence detector for two autoinducers controls gene expression. *EMBO J* 22(4):870-881.

87. Schauder S, Shokat K, Surette MG, & Bassler BL (2001) The LuxS family of bacterial autoinducers: biosynthesis of a novel quorum-sensing signal molecule. *Mol Microbiol* 41(2):463-476.

88. Chen X, Schauder S, Potier N, Van Dorsselaer A, Pelczer I*, et al.* (2002) Structural identification of a bacterial quorum-sensing signal containing boron. *Nature* 415(6871):545-549.

89. Miller ST, Xavier KB, Campagna SR, Taga ME, Semmelhack MF*, et al.* (2004) *Salmonella typhimurium* recognizes a chemically distinct form of the bacterial quorum-sensing signal AI-2. *Mol Cell* 15(5):677-687.

90. Taga ME & Bassler BL (2003) Chemical communication among bacteria. *Proc Natl Acad Sci USA* 100:14549-14554.

91. Herzberg M, Kaye IK, Peti W, & Wood TK (2006) YdgG (TqsA) controls biofilm formation in *Escherichia coli* K-12 through autoinducer 2 transport. *J Bacteriol* 188(2):587-598.

92. Hegde M, Englert DL, Schrock S, Cohn WB, Vogt C*, et al.* (2011) Chemotaxis to the quorum-sensing signal AI-2 requires the Tsr chemoreceptor and the periplasmic LsrB AI-2-binding protein. *J Bacteriol* 193(3):768-773.

93. Crawford IP & Yanofsky C (1958) On the separation of the tryptophan rynthetase of *Escherichia Coli* into two protein components. *Proc Natl Acad Sci USA* 44(12):1161-1170.

94. Dalsgaard I, Hoi L, Siebeling RJ, & Dalsgaard A (1999) Indole-positive *Vibrio vulnificus* isolated from disease outbreaks on a Danish eel farm. *Dis Aquat Org* 35(3):187-194.

95. Stull TL, Hyun L, Sharetzsky C, Wooten J, McCauley JP, Jr.*, et al.* (1995) Production and oxidation of indole by *Haemophilus influenzae*. *J Biol Chem* 270(1):5-8.

96. Clemons KV & Gadberry JL (1982) Increased indole detection for *Pasteurella multocida*. *J Clin Microbiol* 15(4):731-732.

97. Liu Y, Mee BJ, & Mulgrave L (1997) Identification of clinical isolates of indole-positive *Klebsiella* spp., including *Klebsiella planticola*, and a genetic and molecular analysis of their beta-lactamases. *J Clin Microbiol* 35(9):2365-2369.

98. DeMoss RD & Moser K (1969) Tryptophanase in diverse bacterial species. *J Bacteriol* 98(1):167-171.

99. Jenkins SG, Birk RJ, & Zabransky RJ (1982) Differences in susceptibilities of species of the *Bacteroides fragilis* group to several beta-lactam antibiotics: indole production as an indicator of resistance. *Antimicrob Agents Chemother* 22(4):628-634.

100. Wang D, Ding X, & Rather PN (2001) Indole can act as an extracellular signal in *Escherichia coli*. *J Bacteriol* 183:4210-4216.

101. Domka J, Lee J, & Wood TK (2006) YliH (BssR) and YceP (BssS) regulate *Escherichia coli* K-12 biofilm formation by influencing cell signaling. *Appl. Environ. Microbiol.* 72:2449-2459.

102. Lee J, Zhang XS, Hegde M, Bentley WE, Jayaraman A*, et al.* (2008) Indole cell signaling occurs primarily at low temperatures in *Escherichia coli*. *ISME J* 2(10):1007-1023.

103. Hirakawa H, Inazumi Y, Masaki T, Hirata T, & Yamaguchi A (2005) Indole induces the expression of multidrug exporter genes in *Escherichia coli*. *Mol Microbiol* 55:1113-1126.

104. Nikaido B, Yamaguchi A, & Nishino K (2008) AcrAB multidrug efflux pump regulation in *Salmonella enterica* serovar typhimurium by RamA in response to environmental signals. *J Biol Chem*. 283(35):24245-24253

105. Aneman A, Eisenhofer G, Olbe L, Dalenback J, Nitescu P*, et al.* (1996) Sympathetic discharge to mesenteric organs and the liver: evidence for substantial mesenteric organ norepinephrine spillover. *J Clin Invest* 97(7):1640-1646.

106. Lyte M (2004) Microbial endocrinology and infectious disease in the 21st century. *Trends Microbiol* 12(1):14-20.

107. Hahn PY, Wang P, Tait SM, Ba ZF, Reich SS*, et al.* (1995) Sustained elevation in circulating catecholamine levels during polymicrobial sepsis. *Shock* 4(4):269-273.

108. Freestone PP, Sandrini SM, Haigh RD, & Lyte M (2008) Microbial endocrinology: how stress influences susceptibility to infection. *Trends Microbiol* 16(2):55-64.

109. Freestone PP, Haigh RD, Williams PH, & Lyte M (1999) Stimulation of bacterial growth by heat-stable, norepinephrine-induced autoinducers. *FEMS Microbiol Lett* 172(1):53-60.

110. Chen C, Brown DR, Xie Y, Green BT, & Lyte M (2003) Catecholamines modulate *Escherichia coli* O157:H7 adherence to murine cecal mucosa. *Shock* 20(2):183-188.

111. Green BT, Lyte M, Chen C, Xie Y, Casey MA*, et al.* (2004) Adrenergic modulation of *Escherichia coli* O157:H7 adherence to the colonic mucosa. *Am J Physiol Gastrointest Liver Physiol* 287(6):G1238-1246.

112. Cogan TA, Thomas AO, Rees LE, Taylor AH, Jepson MA*, et al.* (2007) Norepinephrine increases the pathogenic potential of *Campylobacter jejuni*. *Gut* 56(8):1060-1065.

113. Lyte M, Erickson AK, Arulanandam BP, Frank CD, Crawford MA*, et al.* (1997) Norepinephrine-induced expression of the K99 pilus adhesin of enterotoxigenic *Escherichia coli*. *Biochem Biophys Res Commun* 232(3):682-686.

114. Dowd SE (2007) *Escherichia coli* O157:H7 gene expression in the presence of catecholamine norepinephrine. *FEMS Microbiol Lett* 273(2):214-223.

115. Becker H & Gärtner C (2000) Polymer microfabrication methods for microfluidic analytical applications. *Electrophoresis* 21(1):12-26.

116. Whitesides GM, Ostuni E, Takayama S, Jiang X, & Ingber DE (2001) Soft lithography in biology and biochemistry. *Ann Rev Biomed Eng* 3(1):335-373.

117. Saleh-Lakha S & Trevors JT (2010) Perspective: microfluidic applications in microbiology. *J Microbiol Met* 82(1):108-111.

118. Richter L, Stepper C, Mak A, Reinthaler A, Heer R*, et al.* (2007) Development of a microfluidic biochip for online monitoring of fungal biofilm dynamics. *Lab Chip* 7(12):1723-1731.

119. Prakash A, Amrein M, & Kaler K (2008) Characteristics and impact of *Taq* enzyme adsorption on surfaces in microfluidic devices. *Microfluid Nanofluid* 4(4):295-305.

120. Chen Z, Mauk MG, Wang J, Abrams WR, Corstjens PLAM*, et al.* (2007) A microfluidic system for saliva-based detection of infectious diseases. *Ann N Y Acad Sci* 1098:429-436.

121. Ikeda M, Yamaguchi N, Tani K, & Nasu M (2006) Rapid and simple detection of food poisoning bacteria by bead assay with a microfluidic chip-based system. *J Microbiol Met* 67(2):241-247.

122. Lee Y-F, Lien K-Y, Lei H-Y, & Lee G-B (2009) An integrated microfluidic system for rapid diagnosis of dengue virus infection. *Biosen Bioelect* 25(4):745-752.

123. Ottesen EA, Hong JW, Quake SR, & Leadbetter JR (2006) Microfluidic digital PCR enables multigene analysis of individual environmental bacteria. *Science* 314(5804):1464-1467.

124. Zhang C, Xu J, Ma W, & Zheng W (2006) PCR microfluidic devices for DNA amplification. *Biotechnol Adv* 24(3):243-284.

125. Rasko DA, Moreira CG, Li DR, Reading NC, Ritchie JM*, et al.* (2008) Targeting QseC signaling and virulence for antibiotic development. *Science* 321(5892):1078-1080.

126. Aneman A, Eisenhofer G, Fandriks L, & Friberg P (1995) Hepatomesenteric release and removal of norepinephrine in swine. *Am J Physiol Regul Integr Comp Physiol* 268(4):924-930.

127. Garzon A, Li J, Flores A, Casadesus J, & Stewart V (1992) Molybdenum cofactor (chlorate-resistant) mutants of *Klebsiella pneumoniae* M5al can use hypoxanthine as the sole nitrogen source. *J Bacteriol* 174(19):6298-6302.

128. Attila C, Ueda A, Cirillo SLG, Cirillo JD, Chen W*, et al.* (2008) *Pseudomonas aeruginosa* PAO1 virulence factors and poplar tree response in the rhizosphere. *Microbial Biotechnol* 1(1):17-29.

129. Arora SK, Neely AN, Blair B, Lory S, & Ramphal R (2005) Role of motility and flagellin glycosylation in the pathogenesis of *Pseudomonas aeruginosa* burn wound infections. *Infect Immun* 73(7):4395-4398.

130. Caiazza NC, Shanks RMQ, & O'Toole GA (2005) Rhamnolipids modulate swarming motility patterns of *Pseudomonas aeruginosa*. *J Bacteriol* 187(21):7351-7361.

131. Deziel E, Lepine F, Milot S, & Villemur R (2003) *rhlA* is required for the production of a novel biosurfactant promoting swarming motility in

Pseudomonas aeruginosa: 3-(3-hydroxyalkanoyloxy)alkanoic acids (HAAs), the precursors of rhamnolipids. *Microbiology* 149(Pt 8):2005-2013.

132. Pesci EC, Pearson JP, Seed PC, & Iglewski BH (1997) Regulation of *las* and *rhl* quorum sensing in *Pseudomonas aeruginosa*. *J Bacteriol* 179(10):3127-3132.

133. Alverdy J, Holbrook C, Rocha F, Seiden L, Wu RL*, et al.* (2000) Gut-derived sepsis occurs when the right pathogen with the right virulence genes meets the right host: evidence for in vivo virulence expression in *Pseudomonas aeruginosa*. *Ann Surg* 232:480-489.

134. Yang S, Koo DJ, Zhou M, Chaudry IH, & Wang P (2000) Gut-derived norepinephrine plays a critical role in producing hepatocellular dysfunction during early sepsis. *Am J Physiol Gastrointest Liver Physiol* 279(6):G1274-1281.

135. Ahlman H, Bhargava HN, Dahlstrom A, Larsson I, Newson B*, et al.* (1981) On the presence of serotonin in the gut lumen and possible release mechanisms. *Acta Physiol Scand* 112:263-269.

136. Zhou M, Hank Simms H, & Wang P (2004) Increased gut-derived norepinephrine release in sepsis: up-regulation of intestinal tyrosine hydroxylase. *Biochim Biophys Acta* 1689:212-218.

137. Kopin IJ, Zukowska-Grojec Z, Bayorh MA, & Goldstein DS (1984) Estimation of intrasynaptic norepinephrine concentrations at vascular neuroeffector junctions in vivo. *Naunyn Schmiedebergs Arch Pharmacol* 325:298-305.

138. Leinhardt DJ, Arnold J, Shipley KA, Mughal MM, Little RA*, et al.* (1993) Plasma NE concentrations do not accurately reflect sympathetic nervous system activity in human sepsis. *Am J Physiol Endocrinol Metab* 265(2):E284-288.

139. Eldrup E & Richter EA (2000) DOPA, dopamine, and DOPAC concentrations in the rat gastrointestinal tract decrease during fasting. *Am J Physiol Endocrinol Metab* 279(4):E815-822.

140. Ernst RK, Guina T, & Miller SI (1999) How intracellular bacteria survive: surface modifications that promote resistance to host innate immune responses. *J Infect Dis* 179:S2326-2330.

141. Lyte M & Bailey MT (1997) Neuroendocrine-bacterial interactions in a neurotoxin-induced model of trauma. *J Surg Res* 70(2):195-201.

142. Vlisidou I, Lyte M, van Diemen PM, Hawes P, Monaghan P*, et al.* (2004) The neuroendocrine stress hormone norepinephrine augments *Escherichia coli* O157:H7-induced enteritis and adherence in a bovine ligated ileal loop model of infection. *Infect. Immun.* 72(9):5446-5451.

143. Lyte M & Ernst S (1992) Catecholamine induced growth of gram negative bacteria. *Life Sci* 50(3):203-212.

144. Freestone PPE, Lyte M, Neal CP, Maggs AF, Haigh RD*, et al.* (2000) The mammalian neuroendocrine hormone norepinephrine supplies iron for bacterial growth in the presence of transferrin or lactoferrin. *J Bacteriol* 182(21):6091-6098.

145. Cox CD (1986) Role of pyocyanin in the acquisition of iron from transferrin. *Infect Immun* 52(1):263-270.

146. Lamont IL, Beare PA, Ochsner U, Vasil AI, & Vasil ML (2002) Siderophore-mediated signaling regulates virulence factor production in *Pseudomonas aeruginosa*. *Proceedings of the National Academy of Sciences* 99(10):7072-7077.

147. Vasil ML & Ochsner UA (1999) The response of *Pseudomonas aeruginosa* to iron: genetics, biochemistry and virulence. *Mol Microbiol* 34(3):399-413.

148. Long J, Zaborina O, Holbrook C, Zaborin A, & Alverdy J (2008) Depletion of intestinal phosphate after operative injury activates the virulence of *P aeruginosa* causing lethal gut-derived sepsis. *Surgery* 144(2):189-197.

149. Usher LR, Lawson RA, Geary I, Taylor CJ, Bingle CD*, et al.* (2002) Induction of neutrophil apoptosis by the *Pseudomonas aeruginosa* exotoxin pyocyanin: a potential mechanism of persistent infection. *J Immunol* 168(4):1861-1868.

150. Van Delden C & Iglewski BH (1998) Cell-to-cell signaling and *Pseudomonas aeruginosa* infections. *Emerg Infect Dis* 4(4):551-560.

151. Diggle SP, Cornelis P, Williams P, & Camara M (2006) 4-quinolone signalling in *Pseudomonas aeruginosa*: old molecules, new perspectives. *Int J Med Microbiol* 296(2-3):83-91.

152. Hooi DSW, Bycroft BW, Chhabra SR, Williams P, & Pritchard DI (2004) Differential immune modulatory activity of *Pseudomonas aeruginosa* quorum-sensing signal molecules. *Infect Immun* 72(11):6463-6470.

153. Filloux A (2004) The underlying mechanisms of type II protein secretion. *Biochimica Biophysica Acta* 1694(1-3):163-179.

154. Reimmann C, Beyeler M, Latifi A, Winteler H, Foglino M*, et al.* (1997) The global activator GacA of *Pseudomonas aeruginosa* PAO positively controls the production of the autoinducer N-butyryl-homoserine lactone and the formation of the virulence factors pyocyanin, cyanide, and lipase. *Mol Microbiol* 24:309-319.

155. Kendall MM, Rasko DA, & Sperandio V (2007) Global effects of the cell-to-cell signaling molecules autoinducer-2, autoinducer-3, and epinephrine in a *luxS* mutant of enterohemorrhagic *Escherichia coli*. *Infect Immun* 75(10):4875-4884.

156. Overhage J, Bains M, Brazas MD, & Hancock RE (2008) Swarming of *Pseudomonas aeruginosa* is a complex adaptation leading to increased production of virulence factors and antibiotic resistance. *J Bacteriol* 190(8):2671-2679.

157. Liberati NT, Urbach JM, Miyata S, Lee DG, Drenkard E*, et al.* (2006) An ordered, nonredundant library of *Pseudomonas aeruginosa* strain PA14 transposon insertion mutants. *Proc Natl Acad USA* 103(8):2833-2838.

158. Ren D, Bedzyk LA, Thomas SM, Ye RW, & Wood TK (2004) Gene expression in *Escherichia coli* biofilms. *Appl Microbiol Biotechnol* 64(4):515-524.

159. Gonzalez Barrios AF, Zuo R, Hashimoto Y, Yang L, Bentley WE*, et al.* (2006) Autoinducer 2 controls biofilm formation in *Escherichia coli* through a novel motility quorum-sensing regulator (MqsR, B3022). *J Bacteriol* 188(1):305-316.

160. Ren D, Bedzyk LA, Ye RW, Thomas SM, & Wood TK (2004) Differential gene expression shows natural brominated furanones interfere with the autoinducer-2 bacterial signaling system of *Escherichia coli*. *Biotechnol Bioeng* 88(5):630-642.

161. Edgar R, Domrachev M, & Lash AE (2002) Gene expression omnibus: NCBI gene expression and hybridization array data repository. *Nucleic Acids Res* 30:207-210.

162. Ueda A & Wood TK (2008) Potassium and sodium transporters of *Pseudomonas aeruginosa* regulate virulence to barley. *Appl Microbiol Biotechnol* 79(5):843-858.

163. Ohman DE, Cryz SJ, & Iglewski BH (1980) Isolation and characterization of *Pseudomonas aeruginosa* PAO mutant that produces altered elastase. *J Bacteriol* 142(3):836-842.

164. Attila C, Ueda A, & Wood TK (2008) PA2663 (PpyR) increases biofilm formation in *Pseudomonas aeruginosa* PAO1 through the *psl* operon and stimulates virulence and quorum-sensing phenotypes. *Appl Microbiol Biotechnol* 78(2):293-307.

165. Gallagher LA, McKnight SL, Kuznetsova MS, Pesci EC, & Manoil C (2002) Functions required for extracellular quinolone signaling by *Pseudomonas aeruginosa*. *J Bacteriol* 184(23):6472-6480.

166. Stintzi A, Evans K, Meyer JM, & Poole K (1998) Quorum-sensing and siderophore biosynthesis in *Pseudomonas aeruginosa*: *lasR*/*lasI* mutants exhibit reduced pyoverdine biosynthesis. *FEMS Microbiol Lett* 166(2):341-345.

167. Bearson BL & Bearson SM (2008) The role of the QseC quorum-sensing sensor kinase in colonization and norepinephrine-enhanced motility of *Salmonella enterica* serovar Typhimurium. *Microb Pathog* 44(4):271-278.

168. Fleiszig S, Wiener-Kronish J, Miyazaki H, Vallas V, Mostov K*, et al.* (1997) *Pseudomonas aeruginosa*-mediated cytotoxicity and invasion correlate with distinct genotypes at the loci encoding exoenzyme S. *Infect Immun* 65(2):579-586.

169. Shim H, Chauhan S, Ryoo D, Bowers K, Thomas SM*, et al.* (2000) Rhizosphere competitiveness of trichloroethylene-degrading, poplar-colonizing recombinant bacteria. *Appl Environ Microbiol* 66(11):4673-4678.

170. Miller JH (1972) Experiments in molecular genetics. (Cold Spring Harbor Laboratory, Cold Spring Harbor, N.Y.).

171. Bassler BL (2002) Small talk. Cell-to-cell communication in bacteria. *Cell* 109(4):421-424.

172. Kaplan HB & Greenberg EP (1985) Diffusion of autoinducer is involved in regulation of the *Vibrio fischeri* luminescence system. *J Bacteriol* 163(3):1210-1214.

173. Bassler BL, Wright M, & Silverman MR (1994) Multiple signalling systems controlling expression of luminescence in *Vibrio harveyi*: sequence and function of genes encoding a second sensory pathway. *Mol Microbiol* 13(2):273-286.

174. Bansal T, Jesudhasan P, Pillai S, Wood TK, & Jayaraman A (2008) Temporal regulation of enterohemorrhagic *Escherichia coli* virulence mediated by autoinducer-2. *Applied Microbiol Biotechnol* 78:811-819.

175. Englert DL, Manson MD, & Jayaraman A (2009) Flow-Based Microfluidic Device for Quantifying Bacterial Chemotaxis in Stable, Competing Gradients. *Appl Environ Microbiol* 75:4557-4564.

176. Englert DL, Jayaraman A, & Manson MD (2009) Microfluidic techniques for the analysis of bacterial chemotaxis. *Methods Mol. Biol.* 571:1-23.

177. Taga ME, Semmelhack JL, & Bassler BL (2001) The LuxS-dependent autoinducer AI-2 controls the expression of an ABC transporter that functions in AI-2 uptake in *Salmonella typhimurium*. *Mol. Microbiol.* 42(3):777-793.

178. Adler J (1973) A method for measuring chemotaxis and use of the method to determine optimum conditions for chemotaxis by *Escherichia coli*. *J. Gen. Microbiol.* 74:77-91.

179. Mesibov R, Ordal GW, & Adler J (1973) The range of attractant concentrations for bacterial chemotaxis and the threshold and size of response over this range. Weber law and related phenomena. *J. Gen. Physiol.* 62(2):203-223.

180. Zhang Y, Gardina PJ, Kuebler AS, Kang HS, Christopher JA, *et al.* (1999) Model of maltose-binding protein/chemoreceptor complex supports intrasubunit signaling mechanism. *Proc. Natl. Acad. Sci. USA* 96(3):939-944.

181. Englert DL, Manson MD, & Jayaraman A (2009) Flow-based microfluidic device for quantifying bacterial chemotaxis in stable, competing gradients. *Appl. Environ. Microbiol.* 75:4557-4564.

182. Mao H, Cremer PS, & Manson MD (2003) A sensitive, versatile microfluidic assay for bacterial chemotaxis. *Proc. Natl. Acad. Sci. USA* 100(9):5449-5454.

183. Taga ME, Semmelhack JL, & Bassler BL (2001) The LuxS-dependent autoinducer AI-2 controls the expression of an ABC transporter that functions in AI-2 uptake in *Salmonella typhimurium*. *Mol Microbiol* 42(3):777-793.

184. Zhang Y, Gardina PJ, Kuebler AS, Kang HS, Christopher JA, *et al.* (1999) Model of maltose-binding protein/chemoreceptor complex supports intrasubunit signaling mechanism. *Proc Nat Acad Sci USA* 96(3):939-944.

185. Miller ST, Xavier KB, Campagna SR, Taga ME, Semmelhack MF*, et al.* (2004) Crystal structure of *Salmonella typhimurium* AI-2 receptor LsrB in complex with R-THMF.

186. Tajima H, Imada K, Sakuma M, Sumii M, Nara T*, et al.* (2005) Crystal structure of the ligand binding domain of the bacterial serine chemoreceptor Tsr. (http://www.pdb.org/pdb/explore/explore.do?structureId=2D4U).

187. Christopher JA (1988) SPOCK, The structural properties observation and calculation kit (The Center for Macromolecular Design, Texas A&M University College Station, TX.).

188. Pearlman DA, Case DA, Caldwell JW, Ross WS, Cheatham TE, III*, et al.* (1995) AMBER 4.1University of California, San Francisco).

189. Taga ME, Miller ST, & Bassler BL (2003) Lsr-mediated transport and processing of AI-2 in *Salmonella typhimurium*. *Mol Microbiol* 50(4):1411-1427.

190. Alexander RP & Zhulin IB (2007) Evolutionary genomics reveals conserved structural determinants of signaling and adaptation in microbial chemoreceptors. *Proc Natl Acad Sci USA* 104:2885-2890.

191. Taga ME, Miller ST, & Bassler BL (2003) Lsr-mediated transport and processing of AI-2 in *Salmonella typhimurium*. *Mol. Microbiol.* 50(4):1411-1427.

192. Hazelbauer GL & Adler J (1971) Role of the galactose binding protein in chemotaxis of *Escherichia coli* toward galactose. *Nat. New Biol.* 230(12):101-104.

193. Aksamit RR & Koshland DE, Jr. (1974) Identification of the ribose binding protein as the receptor for ribose chemotaxis in *Salmonella typhimurium*. *Biochemistry* 13(22):4473-4478.

194. Manson MD, Blank V, Brade G, & Higgins CF (1986) Peptide chemotaxis in *E. coli* involves the Tap signal transducer and the dipeptide permease. *Nature* 321(6067):253-256.

195. Zhu J & Pei D (2008) A LuxP-based fluorescent sensor for bacterial autoinducer II. *ACS Chem. Biol.* 3(2):110-119.

196. Neumann S, Hansen CH, Wingreen NS, & Sourjik V (2010) Differences in signalling by directly and indirectly binding ligands in bacterial chemotaxis. *EMBO J*. 29(20):3484-3495.

197. Bassler BL (2002) Small talk: Cell-to-cell communication in bacteria. *Cell* 109(4):421-424.

198. Gonzalez Barrios AF, Zuo R, Hashimoto Y, Yang L, Bentley WE*, et al.* (2006) Autoinducer 2 controls biofilm formation in *Escherichia coli* through a novel motility quorum-sensing regulator (MqsR, B3022). *J. Bacteriol.* 188(1):305-316.

199. Parkinson JS & Houts SE (1982) Isolation and behavior of *Escherichia coli* deletion mutants lacking chemotaxis functions. *J Bacteriol* 151(1):106-113.

200. Englert DL, Jayaraman A, & Manson MD (2009) Microfluidic techniques for the analysis of bacterial chemotaxis. *Methods Mol Biol* 571:1-23.

201. Tso WW & Adler J (1974) Negative chemotaxis in *Escherichia coli*. *J Bacteriol* 118(2):560-576.

202. Mao H, Cremer PS, & Manson MD (2003) A sensitive, versatile microfluidic assay for bacterial chemotaxis. *Proc Natl Acad Sci U S A* 100(9):5449-5454.

203. Parkinson JS & Houts SE (1982) Isolation and behavior of *Escherichia coli* deletion mutants lacking chemotaxis functions. *J. Bacteriol.* 151(1):106-113.

204. Baba T, Ara T, Hasegawa M, Takai Y, Okumura Y*, et al.* (2006) Construction of *Escherichia coli* K-12 in-frame, single-gene knockout mutants: the Keio collection. *Mol. Syst. Biol.* 2:2006-2008.

205. Hansen MC, Palmer RJ, Jr., Udsen C, White DC, & Molin S (2001) Assessment of GFP fluorescence in cells of *Streptococcus gordonii* under conditions of low pH and low oxygen concentration. *Microbiol* 147(5):1383-1391.

206. Kitagawa M, Ara T, Arifuzzaman M, Ioka-Nakamichi T, Inamoto E*, et al.* (2005) Complete set of ORF clones of *Escherichia coli* ASKA library (a complete set of *E. coli* K-12 ORF archive): unique resources for biological research. *DNA Res.* 12(5):291-299.

207. Callahan AM & Parkinson JS (1985) Genetics of methyl-accepting chemotaxis proteins in *Escherichia coli*: *cheD* mutations affect the structure and function of the Tsr transducer. *J. Bacteriol.* 161(1):96-104.

208. Maeda T, Sanchez-Torres V, & Wood TK (2008) Metabolic engineering to enhance bacterial hydrogen production. *Microbial. Biotechnol.* 1(1):30-39.

209. Slocum MK & Parkinson JS (1983) Genetics of methyl-accepting chemotaxis proteins in *Escherichia coli*: organization of the Tar region. *J. Bacteriol.* 155(2):565-577.

210. Carter P (1986) Site-directed mutagenesis. *Biochem J* 237(1):1-7.

211. Hall-Stoodley L & Stoodley P (2009) Evolving concepts in biofilm infections. *Cell Microbiol* 11(7):1034-1043.

212. Beloin C, Roux A, & Ghigo JM (2008) *Escherichia coli* biofilms. Bacterial biofilms. *Curr top microbiol immunol,* ed Romeo T (Springer Berlin), Vol 322, pp 249-289.

213. Hall-Stoodley L, Costerton JW, & Stoodley P (2004) Bacterial biofilms: from the natural environment to infectious diseases. *Nat Rev Micro* 2(2):95-108.

214. Burmølle M, Thomsen TR, Fazli M, Dige I, Christensen L*, et al.* (2010) Biofilms in chronic infections – a matter of opportunity – monospecies biofilms in multispecies infections. *FEMS Immunol Med Microbiol* 59(3):324-336.

215. Kolenbrander PE, Palmer RJ, Periasamy S, & Jakubovics NS (2010) Oral multispecies biofilm development and the key role of cell–cell distance. *Nat Rev Micro* 8(7):471-480.

216. Camp JG, Kanther M, Semova I, & Rawls JF (2009) Patterns and scales in gastrointestinal microbial ecology. *Gastroenterol* 136(6):1989-2002.

217. Marsh PD (1994) Microbial ecology of dental plaque and its significance in health and disease. *Adv Dental Res* 8(2):263-271.

218. Kirisits MJ & Parsek MR (2006) Does *Pseudomonas aeruginosa* use intercellular signalling to build biofilm communities? *Cell Microbiol* 8(12):1841-1849.

219. Hentzer M, Eberl L, Nielsen J, & Givskov M (2003) Quorum sensing: a novel target for the treatment of biofilm infections. *BioDrugs* 17(4):241-250.

220. Ren D & Wood TK (2004) (5Z)-4-bromo-5-(bromomethylene)-3-butyl-2(5H)-furanone reduces corrosion from Desulfotomaculum orientis. *Environ Microbiol* 6(5):535-540.

221. Rui L, Reardon KF, & Wood TK (2005) Protein engineering of toluene ortho-monooxygenase of *Burkholderia cepacia* G4 for regiospecific hydroxylation of indole to form various indigoid compounds. *Appl Microbiol Biotechnol* 66(4):422-429.

222. Kjelleberg S & Molin S (2002) Is there a role for quorum sensing signals in bacterial biofilms? *Current Opin Microbiol* 5(3):254-258.

223. Parsek MR & Greenberg EP (2005) Sociomicrobiology: the connections between quorum sensing and biofilms. *Trends Microbiol* 13(1):27-33.

224. Shirtliff ME, Mader JT, & Camper AK (2002) Molecular interactions in biofilms. *Chem Biol* 9(8):859-871.

225. Rochex A, Godon J-J, Bernet N, & Escudié R (2008) Role of shear stress on composition, diversity and dynamics of biofilm bacterial communities. *Water Res* 42(20):4915-4922.

226. Sternberg C & Tolker-Nielsen T (2006) Growing and analyzing biofilms in flow cells. *Curr Prot Microbiol*, (John Wiley & Sons, Inc.,USA).

227. Ensley BD, Ratzkin BJ, Osslund TD, Simon MJ, Wackett LP*, et al.* (1983) Expression of naphthalene oxidation genes in *Escherichia coli* results in the biosynthesis of indigo. *Science* 222(4620):167-169.

228. Fishman A, Tao Y, Rui L, & Wood TK (2005) Controlling the regiospecific oxidation of aromatics via active site engineering of toluene para-monooxygenase of *Ralstonia pickettii* PKO1. *J Biol Chem* 280(1):506-514.

229. Tao Y, Fishman A, Bentley WE, & Wood TK (2004) Altering toluene 4-monooxygenase by active-site engineering for the synthesis of 3-methoxycatechol, methoxyhydroquinone, and methylhydroquinone. *J Bacteriol* 186(14):4705-4713.

230. Jagura-Burdzy G & Hulanicka D (1981) Use of gene fusions to study expression of cysB, the regulatory gene of the cysteine regulon. *J Bacteriol* 147(3):744-751.

231. Eaton R & Chapman P (1995) Formation of indigo and related compounds from indolecarboxylic acids by aromatic acid-degrading bacteria: chromogenic reactions for cloning genes encoding dioxygenases that act on aromatic acids. *J Bacteriol* 177(23):6983-6988.

232. Canada KA, Iwashita S, Shim H, & Wood TK (2002) Directed evolution of toluene ortho-monooxygenase for enhanced 1-naphthol synthesis and chlorinated ethene degradation. *J Bacteriol* 184(2):344-349.

233. Snaith RD (1984) Recombinant DNA techniques. *Biochem Ed* 12(4):187-187.

234. Kim J, Hegde M, & Jayaraman A (2010) Co-culture of epithelial cells and bacteria for investigating host-pathogen interactions. *Lab Chip* 10(1):43-50.

235. Sauer K, Rickard AH, & Davies DG (2007) Biofilms and biocomplexity. *Microbe* 2:347-353.

236. Beech IB & Sunner J (2004) Biocorrosion: towards understanding interactions between biofilms and metals. *Curr Opin Biotechnol* 15(3):181-186.

237. Dobretsov S, Teplitski M, & Paul V (2009) Mini-review: quorum sensing in the marine environment and its relationship to biofouling. *Biofouling* 25(5):413 - 427.

238. Wood TK, Hong SH, & Ma Q (2011) Engineering biofilm formation and dispersal. *Trends Biotechnol* 29(2):87-94.

239. Brenner K, You L, & Arnold FH (2008) Engineering microbial consortia: a new frontier in synthetic biology. *Trends Biotechnol* 26(9):483-489.

240. Prüß BM, Besemann C, Denton A, & Wolfe AJ (2006) A complex transcription network controls the early stages of biofilm development by *Escherichia coli*. *J Bacteriol* 188(11):3731-3739.

241. Jayaraman A, Mansfeld FB, & Wood TK (1999) Inhibiting sulfate-reducing bacteria in biofilms by expressing the antimicrobial peptides indolicidin and bactenecin. *J Ind Microbiol Biotechnol* 22:167-175.

242. Lee J, Maeda T, Hong SH, & Wood TK (2009) Reconfiguring the quorum-sensing regulator SdiA of *Escherichia coli* to control biofilm formation. *Appl Environ Microbiol* 75:1703-1716.

243. Hong SH, Wang X, & Wood TK (2010) Controlling biofilm formation, prophage excision, and cell death by rewiring global regulator H-NS of *Escherichia coli*. *Microbial Biotechnol* 3:344-356.

244. Lu TK & Collins JJ (2007) Dispersing biofilms with engineered enzymatic bacteriophage. *Proc Natl Acad Sci U S A* 104 11197-11202.

245. Hong SH, Lee J, & Wood TK (2010) Engineering global regulator Hha of *Escherichia coli* to control biofilm dispersal. *Microbial Biotechnol* 3(6):717-728.

246. Ma Q, Yang Z, Pu M, Peti W, & Wood TK (2011) Engineering a novel c-di-GMP-binding protein for biofilm dispersal. *Environ Microbiol* 13(3):631-642.

247. Fu P (2006) A perspective of synthetic biology: assembling building blocks for novel functions. *Biotechnol J* 1(6):690-699.

248. Purnick PEM & Weiss R (2009) The second wave of synthetic biology: from modules to systems. *Nat Rev Mol Cell Biol* 10(6):410-422.

249. Hooshangi S & Bentley WE (2008) From unicellular properties to multicellular behavior: bacteria quorum sensing circuitry and applications. *Curr Opin Biotechnol* 19(6):550-555.

250. Choudhary S & Schmidt-Dannert C (2010) Applications of quorum sensing in biotechnology. *Appl Microbiol Biotechnol* 86(5):1267-1279.

251. Ryan RP & Maxwell Dow J (2008) Diffusible signals and interspecies communication in bacteria. *Microbiology* 154(7):1845-1858.

252. Danino T, Mondragón-Palomino O, Tsimring L, & Hasty J (2010) A synchronized quorum of genetic clocks. *Nature* 463(7279):326-330.

253. You L, Cox RS, Weiss R, & Arnold FH (2004) Programmed population control by cell-cell communication and regulated killing. *Nature* 428(6985):868-871.

254. Williams P & Cámara M (2009) Quorum sensing and environmental adaptation in *Pseudomonas aeruginosa*: a tale of regulatory networks and multifunctional signal molecules. *Curr Opin Microbiol* 12(2):182-191.

255. Pesci EC, Pearson JP, Seed PC, & Iglewski BH (1997) Regulation of *las* and *rhl* quorum sensing in *Pseudomonas aeruginosa*. *J Bacteriol* 179:3127–3132.

256. Brenner K, Karig DK, Weiss R, & Arnold FH (2007) Engineered bidirectional communication mediates a consensus in a microbial biofilm consortium. *Proc Natl Acad Sci U S A* 104(44):17300-17304.

257. Balagadde FK, Song H, Ozaki J, Collins CH, Barnet M*, et al.* (2008) A synthetic *Escherichia coli* predator-prey ecosystem. *Mol Syst Biol* 4:187.

258. Kambam PKR, Henson MA, & Sun L (2008) Design and mathematical modelling of a synthetic symbiotic ecosystem. *IET Syst Biol* 2(1):33-38.

259. Brenner K & Arnold FH (2011) Self-organization, layered structure, and aggregation enhance persistence of a synthetic biofilm consortium. *PLoS ONE* 6(2):e16791.

260. Baba T, Ara T, Hasegawa M, Takai Y, Okumura Y*, et al.* (2006) Construction of *Escherichia coli* K-12 in-frame, single-gene knockout mutants: the Keio collection. *Mol Syst Biol* 2:2006.0008.

261. García-Contreras R, Zhang X-S, Kim Y, & Wood TK (2008) Protein translation and cell death: the role of rare tRNAs in biofilm formation and in activating dormant phage killer genes. *PLoS ONE* 3(6):e2394.

262. Hansen MC, Palmer RJ, Jr, Udsen C, White DC, & Molin S (2001) Assessment of GFP fluorescence in cells of *Streptococcus gordonii* under conditions of low pH and low oxygen concentration. *Microbiology* 147:1383-1391.

263. Seed P, Passador L, & Iglewski B (1995) Activation of the *Pseudomonas aeruginosa lasI* gene by LasR and the *Pseudomonas* autoinducer PAI: an autoinduction regulatory hierarchy. *J Bacteriol* 177(3):654-659.

264. Kitagawa M, Ara T, Arifuzzaman M, Ioka-Nakamichi T, Inamoto E*, et al.* (2005) Complete set of ORF clones of *Escherichia coli* ASKA library (a complete set of *E. coli* K-12 ORF archive): unique resources for biological research. *DNA Res* 12(5):291-299.

265. Pearson JP, Gray KM, Passador L, Tucker KD, Eberhard A*, et al.* (1994) Structure of the autoinducer required for expression of *Pseudomonas aeruginosa* virulence genes. *Proc Natl Acad Sci U S A* 91(1):197-201.

266. Charlton TS, De Nys R, Netting A, Kumar N, Hentzer M*, et al.* (2000) A novel and sensitive method for the quantification of *N*-3-oxoacyl homoserine lactones using gas chromatography–mass spectrometry: application to a model bacterial biofilm. *Environ Microbiol* 2(5):530-541.

267. Flickinger ST, Copeland MF, Downes EM, Braasch AT, Tuson HH*, et al.* (2011) Quorum sensing between *Pseudomonas aeruginosa* biofilms accelerates cell growth. *J Am Chem Soc* 133(15):5966–5975.

268. Pearson JP, Van Delden C, & Iglewski BH (1999) Active efflux and diffusion are involved in transport of *Pseudomonas aeruginosa* cell-to-cell signals. *J Bacteriol* 181(4):1203-1210.

269. Kaplan JB (2010) Biofilm dispersal: mechanisms, clinical Implications, and potential therapeutic uses. *J Dent Res* 89:205-218.

270. del Pozo JL & Patel R (2007) The challenge of treating biofilm-associated bacterial infections. *Clin Pharmacol Ther* 82(2):204-209.

271. Bardouniotis E, Huddleston W, Ceri H, & Olson ME (2001) Characterization of biofilm growth and biocide susceptibility testing of *Mycobacterium phlei* using the MBEC™ assay system. *FEMS Microbiol Lett* 203(2):263-267.

272. Boles BR & Horswill AR (2008) *agr*-mediated dispersal of *Staphylococcus aureus* biofilms. *PLoS Pathog* 4(4):e1000052.

273. Sauer K, Cullen MC, Rickard AH, Zeef LAH, Davies DG*, et al.* (2004) Characterization of nutrient-induced dispersion in *Pseudomonas aeruginosa* PAO1 biofilm. *J Bacteriol* 186:7312-7326.

274. Boles BR, Thoendel M, & Singh PK (2005) Rhamnolipids mediate detachment of *Pseudomonas aeruginosa* from biofilms. *Mol Microbiol* 57(5):1210-1223.

275. Davies DG & Marques CNH (2009) A fatty acid messenger is responsible for inducing dispersion in microbial biofilms. *J Bacteriol* 191:1393-1403.

276. Kolodkin-Gal I, Romero D, Cao S, Clardy J, Kolter R*, et al.* (2010) D-Amino acids trigger biofilm disassembly. *Science* 328(5978):627-629.

277. Lee J-H, Kaplan J, & Lee W (2008) Microfluidic devices for studying growth and detachment of *Staphylococcus epidermidis* biofilms. *Biomed Microdevices* 10(4):489-498.

278. Sambrook J, Fritsch EF, & Maniatis T (1989) Molecular cloning, a laboratory manual, 2nd ed. (Cold Spring Harbor Laboratory Press, Cold Spring Harbor, NY).

279. Heydorn A, Nielsen AT, Hentzer M, Sternberg C, Givskov M*, et al.* (2000) Quantification of biofilm structures by the novel computer program COMSTAT. *Microbiol* 146:2395-2407.

280. Erickson DL, Endersby R, Kirkham A, Stuber K, Vollman DD*, et al.* (2002) *Pseudomonas aeruginosa* quorum-sensing systems may control virulence factor expression in the lungs of patients with cystic fibrosis. *Infect Immun* 70(4):1783-1790.

281. Wood TK & Peretti SW (1991) Effect of chemically-induced, cloned-gene expression on protein synthesis in *E. coli*. *Biotechnol Bioeng* 38(4):397-412.

282. Mitchell P (2001) Microfluidics--downsizing large-scale biology. *Nat Biotechnol* 19(8):717-721.

283. Weibel DB, Diluzio WR, & Whitesides GM (2007) Microfabrication meets microbiology. *Nat Rev Microbiol* 5(3):209-218.

APPENDIX

Table I. Complete list of differentially-expressed genes above the statistically significant cut-off fold change of 4.0 (based on the standard deviation of the fold changes of all the genes) in suspension cells of PA14 grown in serum-RPMI medium at 37 ^{o}C for 7 h with and without 50 μM NE. Complete data for the 50 μM DNA microarrays are available using GEO series accession number GSE 13326.

Locus tag	Gene name	Alternate Gene Name	NE vs. control (50 μM)	Descriptions
PA0030			4.0	hypothetical protein
PA0128		*phnA*	4.0	conserved hypothetical protein
PA0322			6.1	probable transporter
PA0439		*dypB*	4.0	probable oxidoreductase
PA0443			7.5	probable transporter
PA0447	*gcdH*		4.0	glutaryl-CoA dehydrogenase
PA0510		*nirE*	6.1	probable uroporphyrin-III c-methyltransferase
PA0512		*nirH*	6.5	conserved hypothetical protein
PA0513		*nirG*	10.6	probable transcriptional regulator
PA0514	*nirL*		9.2	heme d1 biosynthesis protein NirL
PA0515		*nirD*	11.3	probable transcriptional regulator
PA0516	*nirF*		6.1	heme d1 biosynthesis protein NirF
PA0517	*nirC*		14.9	probable c-type cytochrome precursor
PA0518	*nirM*		12.1	cytochrome c-551 precursor
PA0519	*nirS*		16.0	nitrite reductase precursor
PA0523	*norC*		45.3	nitric-oxide reductase subunit C
PA0524	*norB*		39.4	nitric-oxide reductase subunit B
PA0525		*norD*	4.0	probable dinitrification protein NorD
PA0526			6.5	hypothetical protein
PA0672	*hemO*	*pigA*	-5.3	heme oxygenase

PA0707	*toxR*	*regA*	-7.5	transcriptional regulator ToxR
PA0713			4.9	hypothetical protein
PA0714			4.6	hypothetical protein
PA0876			4.0	probable transcriptional regulator
PA0880			5.7	probable ring-cleaving dioxygenase
PA0884		*dctP*	4.0	probable C4-dicarboxylate-binding periplasmic protein
PA0918			4.6	cytochrome b561
PA0985			-9.2	probable colicin-like toxin
PA0993	*cupC2*		5.3	chaperone CupC2
PA1123			8.0	hypothetical protein
PA1134			-5.7	hypothetical protein
PA1148	*toxA*	*eta*	-8.0	exotoxin A precursor
PA1172	*napC*		13.9	cytochrome c-type protein NapC
PA1173	*napB*		16.0	cytochrome c-type protein NapB precursor
PA1174	*napA*		9.8	periplasmic nitrate reductase protein NapA
PA1212			6.1	probable major facilitator superfamily (MFS) transporter
PA1216			7.5	hypothetical protein
PA1217			5.7	probable 2-isopropylmalate synthase
PA1218			4.6	hypothetical protein
PA1236			8.0	probable major facilitator superfamily (MFS) transporter
PA1246	*aprD*		-4.0	alkaline protease secretion protein AprD
PA1254			4.6	probable dihydrodipicolinate synthetase
PA1300			-9.8	probable sigma-70 factor, ECF subfamily
PA1301			-5.3	probable transmembrane sensor
PA1485			4.0	probable amino acid permease
PA1540			4.0	conserved hypothetical protein
PA1542			4.6	hypothetical protein
PA1550			6.1	hypothetical protein
PA1551		*fixG*	7.0	probable ferredoxin
PA1555		*ccoP*	7.5	probable cytochrome c
PA1556		*ccoO*	5.7	probable cytochrome c oxidase subunit

PA1601			4.0	probable aldehyde dehydrogenase
PA1632	*kdpF*		4.0	KdpF protein
PA1740			4.9	hypothetical protein
PA1746			4.9	hypothetical protein
PA1879			4.0	hypothetical protein
PA1897			5.3	hypothetical protein
PA1919	*nrdG*		4.3	class III (anaerobic) ribonucleoside-triphosphate reductase activating protein, 'activase', NrdG
PA1984		*exaC1*	-10.6	probable aldehyde dehydrogenase
PA2033			-10.6	hypothetical protein
PA2034			-10.6	hypothetical protein
PA2116			-5.7	conserved hypothetical protein
PA2147	*katE*		9.8	catalase HPII
PA2169			5.3	hypothetical protein
PA2171			6.5	hypothetical protein
PA2172			8.0	hypothetical protein
PA2173			4.3	hypothetical protein
PA2262		*kguT*	7.0	probable 2-ketogluconate transporter
PA2329			4.6	probable ATP-binding component of ABC transporter
PA2330			4.3	hypothetical protein
PA2331			9.2	hypothetical protein
PA2377			-8.6	hypothetical protein
PA2382	*lldA*		-7.0	L-lactate dehydrogenase
PA2383			-4.6	probable transcriptional regulator
PA2384			-4.3	hypothetical protein
PA2385	*pvdQ*		-13.9	PvdQ
PA2386	*pvdA*		-9.8	L-ornithine N5-oxygenase
PA2389			-7.0	conserved hypothetical protein
PA2390			-6.1	probable ATP-binding/permease fusion ABC transporter
PA2391	*opmQ*		-5.3	probable outer membrane protein precursor
PA2392	*pvdP*		-10.6	PvdP

PA2393			-13.9	probable dipeptidase precursor
PA2394	*pvdN*		-14.9	PvdN
PA2395	*pvdO*		-14.9	PvdO
PA2396	*pvdF*		-8.6	pyoverdine synthetase F
PA2397	*pvdE*		-12.1	pyoverdine biosynthesis protein PvdE
PA2398	*fpvA*		-9.2	ferripyoverdine receptor
PA2399	*pvdD*		-8.6	pyoverdine synthetase D
PA2400	*pvdJ*	*PA2401*	-7.5	PvdJ
PA2402			-8.0	probable non-ribosomal peptide synthetase
PA2411			-7.0	probable thioesterase
PA2412			-6.1	conserved hypothetical protein
PA2413	*pvdH*		-13.0	L-2,4-diaminobutyrate:2-ketoglutarate 4-aminotransferase
PA2424	*pvdL*		-9.8	PvdL
PA2425	*pvdG*		-12.1	PvdG
PA2426	*pvdS*		-7.5	sigma factor PvdS
PA2427			-9.8	hypothetical protein
PA2444	*glyA2*		-11.3	serine hydroxymethyltransferase
PA2445	*gcvP2*		-10.6	glycine cleavage system protein P2
PA2446	*gcvH2*		-11.3	glycine cleavage system protein H2
PA2451			-6.5	hypothetical protein
PA2452			-9.2	hypothetical protein
PA2563			4.3	probable sulfate transporter
PA2567			4.3	hypothetical protein
PA2570	*lecA*	*pa1L*	4.9	LecA
PA2664	*fhp*		4.0	Flavohemoprotein
PA2924	*hisQ*		4.3	histidine transport system permease HisQ
PA3032	*snr1*		4.3	cytochrome c Snr1
PA3218			8.0	hypothetical protein
PA3234		*yjcG*	4.3	probable sodium:solute symporter
PA3235		*yjcH*	6.1	conserved hypothetical protein
PA3391	*nosR*		18.4	regulatory protein NosR

PA3392	*nosZ*		4.0	nitrous-oxide reductase precursor
PA3405	*hasE*		-6.1	metalloprotease secretion protein
PA3406	*hasD*		-4.3	transport protein HasD
PA3407	*hasAp*		-42.2	heme acquisition protein HasAp
PA3408	*hasR*		-16.0	Haem uptake outer membrane receptor HasR precursor
PA3442		*ycbE*	5.3	probable ATP-binding component of ABC transporter
PA3719			4.3	hypothetical protein
PA3721			7.0	probable transcriptional regulator
PA3775			4.9	hypothetical protein
PA3784			9.2	hypothetical protein
PA3785			13.9	conserved hypothetical protein
PA3789			11.3	hypothetical protein
PA3790	*oprC*		4.6	Putative copper transport outer membrane porin precursor
PA3870	*moaA1*		34.3	molybdopterin biosynthetic protein A1
PA3871		*nifM*	14.9	probable peptidyl-prolyl cis-trans isomerase, PpiC-type
PA3872	*narI*		13.0	respiratory nitrate reductase gamma chain
PA3873	*narJ*		13.0	respiratory nitrate reductase delta chain
PA3874	*narH*		24.3	respiratory nitrate reductase beta chain
PA3875	*narG*		26.0	respiratory nitrate reductase alpha chain
PA3876	*narK2*		32.0	nitrite extrusion protein 2
PA3877	*narK1*		21.1	nitrite extrusion protein 1
PA3911		*yhbT*	14.9	conserved hypothetical protein
PA3912		*yhbV*	27.9	conserved hypothetical protein
PA3913		*yhbU*	39.4	probable protease
PA3914	*moeA1*		207.9	molybdenum cofactor biosynthetic protein A1
PA3915	*moaB1*		64.0	molybdopterin biosynthetic protein B1
PA3916	*moaE*		5.3	molybdopterin converting factor, large subunit
PA3917	*moaD*		5.7	molybdopterin converting factor, small subunit
PA3918	*moaC*		5.7	molybdopterin biosynthetic protein C
PA4038			4.3	hypothetical protein
PA4072			11.3	probable amino acid permease

PA4078			4.3	probable nonribosomal peptide synthetase
PA4079			4.6	probable dehydrogenase
PA4080		*rcsB*	4.6	probable response regulator
PA4081	*cupB6*		4.0	fimbrial subunit CupB6
PA4084	*cupB3*	*htrE*	11.3	usher CupB3
PA4127	*hpcG*	*hpaH*	4.6	2-oxo-hept-3-ene-1,7-dioate hydratase
PA4129			5.3	hypothetical protein
PA4130			7.0	probable sulfite or nitrite reductase
PA4131			12.1	probable iron-sulfur protein
PA4132			7.5	conserved hypothetical protein
PA4133		*ccoN*	22.6	cytochrome c oxidase subunit (cbb3-type)
PA4134			22.6	hypothetical protein
PA4137		*opdL*	6.1	probable porin
PA4152		*acoC*	8.6	probable hydrolase
PA4236	*katA*	*catA*	4.6	Catalase
PA4351			6.5	probable acyltransferase
PA4357		*yhgG*	4.9	conserved hypothetical protein
PA4467			-14.9	hypothetical protein
PA4468	*sodM*	*sodA*	-12.1	superoxide dismutase
PA4469			-13.0	hypothetical protein
PA4470	*fumC1*		-16.0	fumarate hydratase
PA4471		*fagA*	-13.0	hypothetical protein
PA4570			-7.0	hypothetical protein
PA4587	*ccpR*		8.6	cytochrome c551 peroxidase precursor
PA4635		*mgtC*	4.3	conserved hypothetical protein
PA4652			4.0	hypothetical protein
PA4810	*fdnI*	*fdhI*	14.9	nitrate-inducible formate dehydrogenase, gamma subunit
PA4811	*fdnH*	*fdhH*	52.0	nitrate-inducible formate dehydrogenase, beta subunit
PA4812	*fdnG*	*fdhG*	12.1	formate dehydrogenase-O, major subunit
PA4818			5.7	conserved hypothetical protein

PA4880			6.1	probable bacterioferritin
PA4895			-4.9	probable transmembrane sensor
PA4896			-4.9	probable sigma-70 factor, ECF subfamily
PA5053	*hslV*		5.3	heat shock protein HslV
PA5054	*hslU*		4.0	heat shock protein HslU
PA5150			-4.3	probable short-chain dehydrogenase
PA5383		*yeiH*	5.7	conserved hypothetical protein
PA5388			5.3	hypothetical protein
PA5415	*glyA1*		-4.3	serine hydroxymethyltransferase
PA5427	*adhA*		4.3	alcohol dehydrogenase
PA5548			4.6	probable major facilitator superfamily (MFS) transporter
PA5566			4.6	hypothetical protein

Table II. Complete list of differentially-expressed genes above the statistically significant cut-off fold change of 2.0 (based on the standard deviation of the fold changes of all the genes) in suspension cells of PA14 grown in serum-RPMI medium at 37 ^{o}C for 7 h with and without 500 μM NE. Complete data for the 50 μM DNA microarrays are available using GEO series accession number GSE 13326.

Locus tag	Gene name	Alternate gene name	NE vs. control (500 μM)	Description
PA0026	*plcB*		4	phospholipase C
PA0044	*exoT*		2.1	Exoenzyme T
PA0491			2.0	probable transcriptional regulator
PA0501	*bioF*		3.0	8-amino-7-oxononanoate synthase
PA0502		*bioH*	3.7	probable biotin biosynthesis protein bioH
PA0503		*bioC*	2.1	probable biotin synthesis protein BioC
PA0508			4.6	probable acyl-CoA dehydrogenase
PA0509	*nirN*		2.8	probable c-type cytochrome
PA0510		*nirE*	3.0	probable uroporphyrin-III c-methyltransferase
PA0512		*nirH*	2.0	conserved hypothetical protein
PA0513		*nirG*	3.5	probable transcriptional regulator
PA0514	*nirL*		3.0	heme d1 biosynthesis protein NirL
PA0515		*nirD*	4.3	probable transcriptional regulator
PA0516	*nirF*		2.0	heme d1 biosynthesis protein NirF
PA0517	*nirC*		2.5	probable c-type cytochrome precursor
PA0518	*nirM*		2.3	cytochrome c-551 precursor
PA0519	*nirS*		4.0	nitrite reductase precursor
PA0523	*norC*		3.7	nitric-oxide reductase subunit C
PA0524	*norB*		4.0	nitric-oxide reductase subunit B
PA0527	*dnr*		2.0	transcriptional regulator Dnr

PA0537			2.0	conserved hypothetical protein
PA0550		*ygbM*	2.0	conserved hypothetical protein
PA0584	*cca*		2.0	tRNA nucleotidyl transferase
PA0593	*pdxA*		2.0	pyridoxal phosphate biosynthetic protein PdxA
PA0639			2.0	conserved hypothetical protein
PA0659			2.0	hypothetical protein
PA0664			2.0	hypothetical protein
PA0713			2.0	hypothetical protein
PA0884		*dctP*	2.0	probable C4-dicarboxylate-binding periplasmic protein
PA0927	*ldhA*	*ldhD*	2.0	D-lactate dehydrogenase (fermentative)
PA0949	*wrbA*		2.0	Trp repressor binding protein WrbA
PA0950			2.0	probable arsenate reductase
PA0997	*pqsB*		2.6	Beta-keto-acyl carrier protein synthase
PA1000	*pqsE*		4.3	Quinolone signal response protein
PA1003	*mvfR*		3	Transcriptional regulator MvfR
PA1029			2.0	hypothetical protein
PA1058		*phaF*	2.0	conserved hypothetical protein
PA1070	*braG*		-8.6	branched-chain amino acid transport protein BraG
PA1071	*braF*		-17.2	branched-chain amino acid transport protein BraF
PA1072	*braE*		-14.9	branched-chain amino acid transport protein BraE
PA1073	*braD*		-14.9	branched-chain amino acid transport protein BraD
PA1074	*braC*		-8.6	branched-chain amino acid transport protein BraC
PA1075			-8.6	hypothetical protein
PA1076			-17.2	hypothetical protein
PA1077	*flgB*		-27.9	flagellar basal-body rod protein FlgB
PA1078	*flgC*		2.6	flagellar basal-body rod protein FlgC
PA1079	*flgD*		2.3	flagellar basal-body rod modification protein FlgD
PA1082	*flgG*		2.0	flagellar basal-body rod protein FlgG

PA1083	*flgH*		-4.6	flagellar L-ring protein precursor FlgH
PA1084	*flgI*		-4.6	flagellar P-ring protein precursor FlgI
PA1085	*flgJ*		-4.6	flagellar protein FlgJ
PA1087	*flgL*	*Flak*	2.1	flagellar hook-associated protein type 3 FlgL
PA1092	*fliC*		2.3	flagellin type B
PA1094	*fliD*		2.0	flagellar capping protein FliD
PA1095		*fliS*	2.3	hypothetical protein
PA1097	*fleQ*		2.5	transcriptional regulator FleQ
PA1098	*fleS*		2.3	two-component sensor
PA1099	*fleR*		4.3	two-component response regulator
PA1101	*fliF*		2.1	Flagella M-ring outer membrane protein precursor
PA1103		*fliH*	2.8	probable flagellar assembly protein
PA1130	*rhlC*		2.8	Rhamnosyltransferase 2
PA1133			2.0	hypothetical protein
PA1138			2.0	probable transcriptional regulator
PA1162	*dapE*		2.0	succinyl-diaminopimelate desuccinylase
PA1174	*napA*		2.0	periplasmic nitrate reductase protein NapA
PA1176	*napF*		2.0	ferredoxin protein NapF
PA1177	*napE*		2.0	periplasmic nitrate reductase protein NapE
PA1190		*yohC*	2.0	conserved hypothetical protein
PA1247	*aprE*		-2.6	Alkaline protease secretion protein AprE
PA1249	*aprA*		-2.1	Alkaline metalloproteinase precursor
PA1313			2.0	probable major facilitator superfamily (MFS) transporter
PA1359			2.0	probable transcriptional regulator
PA1376	*aceK*		2.0	isocitrate dehydrogenase kinase/phosphatase
PA1416			2.0	conserved hypothetical protein
PA1428		*yjaB*	2.0	conserved hypothetical protein
PA1455	*fliA*	*rpoF*	2.0	sigma factor FliA

PA1474			2.0	hypothetical protein
PA1485			2.0	probable amino acid permease
PA1498	*pykF*	*pyk-I*	2.0	pyruvate kinase I
PA1533			2.0	conserved hypothetical protein
PA1541			2.0	probable drug efflux transporter
PA1614	*gpsA*	*gpdA*	2.0	glycerol-3-phosphate dehydrogenase, biosynthetic
PA1651			2.0	probable transporter
PA1654			2.0	probable aminotransferase
PA1670	*stp1*		2.0	serine/threonine phosphoprotein phosphatase Stp1
PA1679			2.0	hypothetical protein
PA1680			2.0	hypothetical protein
PA1681	*aroC*		2.0	chorismate synthase
PA1690	*pscU*		2.0	translocation protein in type III secretion
PA1691	*pscT*		-4.3	translocation protein in type III secretion
PA1692		*pscS*	-2.5	probable translocation protein in type III secretion
PA1693	*pscR*		-2.5	translocation protein in type III secretion
PA1694	*pscQ*		-2.1	translocation protein in type III secretion
PA1695	*pscP*		2.0	translocation protein in type III secretion
PA1696	*pscO*		2.0	translocation protein in type III secretion
PA1697		*pscN*	-2.1	ATP synthase in type III secretion system
PA1698	*popN*		-2.0	Type III secretion outer membrane protein PopN precursor
PA1699		*pcr1*	2.8	conserved hypothetical protein in type III secretion
PA1700		*pcr2*	2.3	conserved hypothetical protein in type III secretion
PA1705	*pcrG*		-2.5	regulator in type III secretion
PA1708	*popB*	*pepB*	2.6	translocator protein PopB
PA1709	*popD*	*pepD*	4.6	Translocator outer membrane protein PopD precursor
PA1710	*exsC*		2.1	Exoenzyme S synthesis protein C precursor.
PA1711	*exsE*		3.7	ExsE

PA1712	*exsB*		3.7	Exoenzyme S synthesis protein B
PA1713	*exsA*		2.1	transcriptional regulator ExsA
PA1714	*exsD*		3.0	ExsD
PA1715	*pscB*		3.5	type III export apparatus protein
PA1718	*pscE*		-2.1	type III export protein PscE
PA1720	*pscG*		-2.0	type III export protein PscG
PA1723	*pscJ*		3.3	type III export protein PscJ
PA1724	*pscK*		3.3	type III export protein PscK
PA1725	*pscL*		4.6	type III export protein PscL
PA1726	*bglX*		2.1	periplasmic beta-glucosidase
PA1727			2.6	conserved hypothetical protein
PA1728			3.0	hypothetical protein
PA1729			3.7	conserved hypothetical protein
PA1790			2.0	hypothetical protein
PA1795	*cysS*		2.0	cysteinyl-tRNA synthetase
PA1814			-11.3	hypothetical protein
PA1819		*yjdE*	2.0	probable amino acid permease
PA1871	*lasA*		6.5	LasA protease precursor
PA1898	*qscR*		2.5	Quorum-sensing control repressor
PA1901	*phzC2*		2.5	Phenazine biosynthesis protein PhzC
PA1902	*phzD2*		2	Phenazine biosynthesis protein PhzD
PA1903	*phzE2*		2.3	Phenazine biosynthesis protein PhzE
PA1904	*phzF2*		3.3	Probable phenazine biosynthesis protein
PA1909			2.0	hypothetical protein
PA1919	*nrdG*		-13.0	class III (anaerobic) ribonucleoside-triphosphate reductase activating protein, 'activase', NrdG
PA1949	*rbsR*		2.0	ribose operon repressor RbsR
PA2007	*maiA*		2.0	maleylacetoacetate isomerase

PA2031			2.0	hypothetical protein
PA2055			2.0	probable major facilitator superfamily (MFS) transporter
PA2066			-11.3	hypothetical protein
PA2156		*ybhP*	2.0	conserved hypothetical protein
PA2167			2.0	hypothetical protein
PA2249	*bkdB*		2.0	branched-chain alpha-keto acid dehydrogenase (lipoamide component)
PA2285			2.0	hypothetical protein
PA2290	*gcd*		2.0	glucose dehydrogenase
PA2338		*mtlE*	2.0	probable binding protein component of ABC maltose/mannitol transporter
PA2380			2.0	hypothetical protein
PA2399	*pvdD*		2.3	Pyoverdine synthetase D
PA2426	*pvdS*		-2.1	Sigma factor PvdS
PA2499		*ykoA*	2.0	probable deaminase
PA2510	*catR*		2.0	transcriptional regulator CatR
PA2586	*gacA*		2.0	response regulator GacA
PA2663			2.0	hypothetical protein
PA2681			-19.7	probable transcriptional regulator
PA2688	*pfeA*		2.0	Ferric enterobactin receptor, outer membrane protein PfeA precursor
PA2737			2.0	conserved hypothetical protein
PA2741	*rplT*		-3.7	50S ribosomal protein L20
PA2742	*rpmI*		-4.6	50S ribosomal protein L35
PA2743	*infC*		-4.0	translation initiation factor IF-3
PA2761			-4.0	hypothetical protein
PA2767			2.0	probable enoyl-CoA hydratase/isomerase
PA2802			2.0	probable transcriptional regulator
PA2853	*oprI*		-3.3	Outer membrane lipoprotein OprI precursor
PA2857			2.0	probable ATP-binding component of ABC transporter
PA2883			-2.8	hypothetical protein

PA2900			-12.1	probable outer membrane protein precursor
PA2939		*pepB*	-3.0	probable aminopeptidase
PA2960	*pilZ*		-2.8	type 4 fimbrial biogenesis protein PilZ
PA3083	*pepN*		2.0	aminopeptidase N
PA3095	*xcpZ*		3.7	general secretion pathway protein M
PA3097	*xcpX*		2.6	general secretion pathway protein K
PA3099	*xcpV*		2.8	general secretion pathway protein I
PA3100	*xcpU*		2.8	General secretion pathway outer membrane protein H precursor
PA3101	*xcpT*		2.5	general secretion pathway protein G
PA3102	*xcpS*		2.8	general secretion pathway protein F
PA3103	*xcpR*		2.0	general secretion pathway protein E
PA3115	*fimV*		2.1	Motility protein FimV
PA3129		*yohI*	2.0	conserved hypothetical protein
PA3131		*edaB*	2.0	probable aldolase
PA3140			2.0	hypothetical protein
PA3196			2.0	hypothetical protein
PA3198		*ypuG*	2.0	conserved hypothetical protein
PA3207			2.0	hypothetical protein
PA3209		*ykgJ*	2.0	conserved hypothetical protein
PA3212			2.0	probable ATP-binding component of ABC transporter
PA3222			2.0	hypothetical protein
PA3225			2.0	probable transcriptional regulator
PA3227	*ppiA*	*cypH*	2.0	peptidyl-prolyl cis-trans isomerase A
PA3303			2.0	probable major facilitator superfamily (MFS) transporter
PA3364	*amiC*		2.0	aliphatic amidase expression-regulating protein
PA3369			2.0	hypothetical protein
PA3407	*hasAp*		2.3	heme acquisition protein HasAp
PA3462			2.0	probable sensor/response regulator hybrid

PA3469		*ywjB*	2.0	conserved hypothetical protein
PA3511			-10.6	probable short-chain dehydrogenase
PA3533		*ydhD*	2.0	conserved hypothetical protein
PA3540	*algD*		2.5	GDP-mannose 6-dehydrogenase AlgD
PA3541	*alg8*		2.5	alginate biosynthesis protein Alg8
PA3542	*alg44*		-2.6	alginate biosynthesis protein Alg44
PA3543	*algK*		-2.8	alginate biosynthetic protein AlgK precursor
PA3544	*algE*	*alg76*	2.0	Alginate production outer membrane protein AlgE precursor
PA3545	*algG*		3.3	alginate-c5-mannuronan-epimerase AlgG
PA3546	*algX*		2.1	alginate biosynthesis protein AlgX
PA3560	*fruA*		3.5	phosphotransferase system, fructose-specific IIBC component
PA3561	*fruK*		2.5	1-phosphofructokinase
PA3562		*fruI*	2.5	probable phosphotransferase system enzyme I
PA3563	*fruR*		3.7	fructose transport system repressor FruR
PA3564		*yjjV*	3.5	conserved hypothetical protein
PA3566		*ycnE*	2.8	conserved hypothetical protein
PA3567			3.3	probable oxidoreductase
PA3585	*glpM*		2.5	membrane protein GlpM
PA3586			2.0	probable hydrolase
PA3590			2.0	probable hydroxyacyl-CoA dehydrogenase
PA3628		*yeiG*	2.0	probable esterase
PA3629	*adhC*		2.0	alcohol dehydrogenase class III
PA3639	*accA*		2.0	acetyl-coenzyme A carboxylase carboxyl transferase (alpha subunit)
PA3686	*adk*		2.0	adenylate kinase
PA3699			2.0	probable transcriptional regulator
PA3715			2.0	hypothetical protein
PA3724	*lasB*		2	Elastase LasB
PA3730			2.0	hypothetical protein

PA3742	*rplS*		-16.0	50S ribosomal protein L19
PA3753		*fbp*	2.0	conserved hypothetical protein
PA3754		*yeaB*	2.0	hypothetical protein
PA3772			2.0	hypothetical protein
PA3779			2.0	hypothetical protein
PA3785			2.0	conserved hypothetical protein
PA3787			2.0	conserved hypothetical protein
PA3820	*secF*		2.0	secretion protein SecF
PA3827		*yjgQ*	2.0	conserved hypothetical protein
PA3832	*holC*		2.0	DNA polymerase III, chi subunit
PA3910			2.3	hypothetical protein
PA3912		*yhbV*	7.5	conserved hypothetical protein
PA3913		*yhbU*	5.7	probable protease
PA3914	*moeA1*		4.9	molybdenum cofactor biosynthetic protein A1
PA3915	*moaB1*		2.6	molybdopterin biosynthetic protein B1
PA3916	*moaE*		3.3	molybdopterin converting factor, large subunit
PA3917	*moaD*		24.3	molybdopterin converting factor, small subunit
PA3918	*moaC*		-2.0	molybdopterin biosynthetic protein C
PA3974	*ladS*		2.0	Lost Adherence Sensor, LadS
PA4015			2.0	conserved hypothetical protein
PA4091	*hpaA*		2.0	4-hydroxyphenylacetate 3-monooxygenase large chain
PA4121			2.3	conserved hypothetical protein
PA4122			2.5	conserved hypothetical protein
PA4123	*hpcC*	*hpaE*	2.3	5-carboxy-2-hydroxymuconate semialdehyde dehydrogenase
PA4124	*hpcB*	*hpaD*	2.8	homoprotocatechuate 2,3-dioxygenase
PA4125	*hpcD*		2.5	5-carboxymethyl-2-hydroxymuconate isomerase
PA4134			2.0	hypothetical protein
PA4161	*fepG*		2.0	ferric enterobactin transport protein FepG

PA4168	*fpvB*		2.0	Second ferric pyoverdine receptor FpvB
PA4198			2.0	probable AMP-binding enzyme
PA4221	*fptA*		2.5	Fe(III)-pyochelin outer membrane receptor precursor
PA4333		*fumA*	2.0	probable fumarase
PA4415	*mraY*		2.0	phospho-N-acetylmuramoyl-pentapeptide-transferase
PA4418	*ftsI*	*pbpB*	2.0	penicillin-binding protein 3
PA4434			2.0	probable oxidoreductase
PA4438		*yhcM*	2.0	conserved hypothetical protein
PA4460		*yhbN*	-2.1	conserved hypothetical protein
PA4461		*yhbG*	-2.1	probable ATP-binding component of ABC transporter
PA4466			-2.1	probable phosphoryl carrier protein
PA4467			-2.5	hypothetical protein
PA4468	*sodM*	*Soda*	-7.5	superoxide dismutase
PA4469			-4.3	hypothetical protein
PA4470	*fumC1*		-4.9	fumarate hydratase
PA4471		*fagA*	-2.8	hypothetical protein
PA4481	*mreB*	*rodY*	2.0	rod shape-determining protein MreB
PA4482	*gatC*		2.0	Glu-tRNA(Gln) amidotransferase subunit C
PA4483	*gatA*		2.0	Glu-tRNA(Gln) amidotransferase subunit A
PA4527	*pilC*		2.8	Still frameshift fimbrial biogenesis protein PilC
PA4528	*pilD*		3	Type 4 prepilin peptidase PilD
PA4544	*rluD*	*yfiI*	2.0	pseudouridine synthase
PA4548		*yfiT*	2.0	probable D-amino acid oxidase
PA4576			2.0	probable ATP-dependent protease
PA4746		*yhbC*	2.0	conserved hypothetical protein
PA4751	*ftsH*	*tolZ*	2.0	cell division protein FtsH
PA4846	*aroQ1*	*aroD1*	2.0	3-dehydroquinate dehydratase
PA4917			-13.9	hypothetical protein

PA4973	*thiC*		3.5	thiamin biosynthesis protein ThiC
PA4974		*opmH*	3.0	probable outer membrane protein precursor
PA4976	*aruH*		2.3	Arginine:Pyruvate Transaminas, AruH
PA4977	*aruI*		2.0	2-ketoarginine decarboxylase, AruI
PA4982			2.0	probable two-component sensor
PA5002			2.5	hypothetical protein
PA5010	*waaG*	*rfaG*	2.1	UDP-glucose:(heptosyl) LPS alpha 1,3-glucosyltransferase WaaG
PA5011	*waaC*	*rfaC*	2.8	heptosyltransferase I
PA5018	*msrA*	*pmsR*	2.0	peptide methionine sulfoxide reductase
PA5019		*yhiR*	2.8	conserved hypothetical protein
PA5024		*ytnM*	2.0	conserved hypothetical protein
PA5028			2.0	conserved hypothetical protein
PA5067	*hisE*		2.0	phosphoribosyl-ATP pyrophosphohydrolase
PA5071			2.3	conserved hypothetical protein
PA5241	*ppx*	*gppA*	2.1	Exopolyphosphatase
PA5242	*ppk*		3.0	polyphosphate kinase
PA5245		*yhbL*	5.7	conserved hypothetical protein
PA5247		*yaiI*	3.0	conserved hypothetical protein
PA5250			2.5	conserved hypothetical protein
PA5253	*algP*	*algR3*	2.6	alginate regulatory protein AlgP
PA5258		*hemX*	2.1	hypothetical protein
PA5260	*hemC*	*popE*	2.0	porphobilinogen deaminase
PA5260	*hemC*	*popE*	2.0	porphobilinogen deaminase
PA5261	*algR*		4.9	alginate biosynthesis regulatory protein AlgR
PA5262	*algZ*	*fimS*	3.7	alginate biosynthesis protein AlgZ/FimS
PA5279			2.6	conserved hypothetical protein
PA5281		*yigB*	2.3	probable hydrolase
PA5285			5.3	hypothetical protein

PA5286		*yjbQ*	4.3	conserved hypothetical protein
PA5287	*amtB*		2.3	ammonium transporter AmtB
PA5289			2.5	hypothetical protein
PA5292	*pchP*		2.0	phosphorylcholine phosphatase
PA5292	*pchP*		2.0	phosphorylcholine phosphatase
PA5293			3.0	probable transcriptional regulator
PA5296	*rep*		4.3	ATP-dependent DNA helicase Rep
PA5297	*poxB*		2.5	pyruvate dehydrogenase (cytochrome)
PA5320	*coaC*	*coaB*	3.3	Phosphopantothenoylcysteine synthase/(R)-4'-phospho-N-pantothenoylcysteine decarboxylase
PA5321	*dut*		4.3	deoxyuridine 5'-triphosphate nucleotidohydrolase
PA5327			2.1	probable oxidoreductase
PA5329			3.5	conserved hypothetical protein
PA5336	*gmk*		2.6	guanylate kinase
PA5342			2.1	probable transcriptional regulator
PA5347			2.1	hypothetical protein
PA5348			2.0	probable DNA-binding protein
PA5348			2.0	probable DNA-binding protein
PA5350	*rubA2*		2.5	Rubredoxin 2
PA5351	*rubA1*		3.3	Rubredoxin 1
PA5352		*glcG*	2.5	conserved hypothetical protein
PA5353	*glcF*		2.5	glycolate oxidase subunit GlcF
PA5355	*glcD*		3.0	glycolate oxidase subunit GlcD
PA5357		*ubiC*	2.8	hypothetical protein
PA5358	*ubiA*		2.6	4-hydroxybenzoate-octaprenyl transferase
PA5365	*phoU*		3.5	phosphate uptake regulatory protein PhoU
PA5366	*pstB*		2.0	ATP-binding component of ABC phosphate transporter
PA5366	*pstB*		2.0	ATP-binding component of ABC phosphate transporter

PA5367	*pstA*		3.5	membrane protein component of ABC phosphate transporter
PA5378			2.3	hypothetical protein
PA5383		*yeiH*	3.3	conserved hypothetical protein
PA5394	*cls*		2.6	cardiolipin synthase
PA5398	*dgcA*		3.3	DgcA, Dimethylglycine catabolism
PA5405			2.5	hypothetical protein
PA5407			2.0	hypothetical protein
PA5559	*atpE*	*papH*	3.5	atp synthase C chain
PA5565	*gidA*		2.1	glucose-inhibited division protein A
PA5566			2.5	hypothetical protein
PA5569	*rnpA*		2.3	ribonuclease P protein component

Table III. Complete list of common genes differentially-expressed above the statistically significant cut-off fold change of 4.0-fold (for the 50 μM NE array) and 2.0-fold (for the 500 μM NE array) in suspension cells of PA14 grown in serum-RPMI medium at 37 ^{o}C for 7 h with and without 50 μM NE.

Locus tag	Gene name	Alt. gene name	NE vs. control (50 μM)	NE vs. control (500 μM)	Description
PA0510		*nirE*	6.1	3.0	probable uroporphyrin-III c-methyltransferase
PA0512		*nirH*	6.5	2.0	conserved hypothetical protein
PA0513		*nirG*	10.6	3.5	probable transcriptional regulator
PA0514	*nirL*		9.2	3.0	heme d1 biosynthesis protein NirL
PA0515		*nirD*	11.3	4.3	probable transcriptional regulator
PA0516	*nirF*		6.1	2.0	heme d1 biosynthesis protein NirF
PA0517	*nirC*		14.9	2.5	probable c-type cytochrome precursor
PA0518	*nirM*		12.1	2.3	cytochrome c-551 precursor
PA0519	*nirS*		16.0	4.0	nitrite reductase precursor
PA0523	*norC*		45.3	3.7	nitric-oxide reductase subunit C
PA0524	*norB*		39.4	4.0	nitric-oxide reductase subunit B
PA0713			4.9	2.0	hypothetical protein
PA0884		*dctP*	4.0	2.0	probable C4-dicarboxylate-binding periplasmic protein
PA1174	*napA*		9.8	2.0	periplasmic nitrate reductase protein NapA
PA1485			4.0	2.0	probable amino acid permease
PA1919	*nrdG*		4.3	-13.0	class III (anaerobic) ribonucleoside-triphosphate reductase activating protein, 'activase', NrdG
PA2399	*pvdD*		-8.6	2.3	Pyoverdine synthetase D
PA2426	*pvdS*		-7.5	-2.1	Sigma factor PvdS
PA3407	*hasAp*		-42.2	2.3	heme acquisition protein HasAp
PA3785			13.9	2.0	conserved hypothetical protein
PA3912		*yhbV*	27.9	7.5	conserved hypothetical protein

PA3913		*yhbU*	39.4	5.7	probable protease
PA3914	*moeA1*		207.9	4.9	molybdenum cofactor biosynthetic protein A1
PA3915	*moaB1*		64.0	2.6	molybdopterin biosynthetic protein B1
PA3916	*moaE*		5.3	3.3	molybdopterin converting factor, large subunit
PA3917	*moaD*		5.7	24.3	molybdopterin converting factor, small subunit
PA3918	*moaC*		5.7	-2.0	molybdopterin biosynthetic protein C
PA4134			22.6	2.0	hypothetical protein
PA4467			-14.9	-2.5	hypothetical protein
PA4468	*sodM*	*sodA*	-12.1	-7.5	superoxide dismutase
PA4469			-13.0	-4.3	hypothetical protein
PA4470	*fumC1*		-16.0	-4.9	fumarate hydratase
PA4471		*fagA*	-13.0	-2.8	hypothetical protein

VITA

Name: Manjunath Narayan Hegde

Address: Department of Chemical Engineering

c/o Dr. Jayaraman and Dr. Wood

Texas A&M University

College Station, TX 77843-3122

Email Address: mjhegde@gmail.com

Education: Ph.D., Chemical Engineering, Texas A&M University

B.Eng., Chemical Engineering, R. V. College of Engineering,

Bangalore, India, 2006